VYSOKÉ UČENÍ TECHNICKÉ V BRNĚ

BRNO UNIVERSITY OF TECHNOLOGY

FAKULTA STROJNÍHO INŽENÝRSTVÍ
LETECKÝ ÚSTAV

FACULTY OF MECHANICAL ENGINEERING
INSTITUTE OF AEROSPACE ENGINEERING

NÁVRH TRUPU LETOUNU TL-4000

FUSELAGE DESIGN OF TL-4000 AIRCRAFT

DIPLOMOVÁ PRÁCE
MASTER'S THESIS

AUTOR PRÁCE — Bc. MICHAL HOLIŠ
AUTHOR

VEDOUCÍ PRÁCE — Ing. MICHAL MALIŠ, Ph.D.
SUPERVISOR

BRNO 2014

Vysoké učení technické v Brně, Fakulta strojního inženýrství

Letecký ústav
Akademický rok: 2013/2014

ZADÁNÍ DIPLOMOVÉ PRÁCE

student(ka): Bc. Michal Holiš

který/která studuje v **magisterském navazujícím studijním programu**

obor: **Stavba letadel (2301T039)**

Ředitel ústavu Vám v souladu se zákonem č.111/1998 o vysokých školách a se Studijním a zkušebním řádem VUT v Brně určuje následující téma diplomové práce:

Návrh trupu letounu TL-4000

v anglickém jazyce:

Fuselage design of TL-4000 aircraft

Stručná charakteristika problematiky úkolu:

Navrhněte trup celokompozitového letounuTL-4000 stavěného podle požadavků předpisu CS-23. Podrobněji se věnujte návrhu laminátu v zadní části trupu. Zpracujte požadavky předpisu, vypočítejte zatížení trupu. Zpracujte systémový model nosných části trupu s ohledem na upnutí k okolní konstrukci. Proveďte výpočet únosnosti a pevnostní kontrolu konstrukce.

Cíle diplomové práce:

1.Rozbor požadavků předpisu
2.Výpočet zatížení trupu
3.Systémový model nosných částí trupu
4.Pevnostní kontrolu konstrukce trupu

Seznam odborné literatury:

[1] CS-23, Normal, Utility, Aerobatic and Commuter Category Aeroplanes, EASA, 2003, 140 stran
[2] Niu,C.Y.M., Composite Airframe Structure, Hong Kong Conmilit Press Ltd., Brno, 2005, 664 stran,
[3] MIddleton, D.H., Composite MAterial in Aircraft Structure, Longman Singapore Publisher Ltd.,1990, 379 stran

Vedoucí diplomové práce: Ing. Michal Mališ, Ph.D.

Termín odevzdání diplomové práce je stanoven časovým plánem akademického roku 2013/2014.

V Brně, dne 15.11.2013

L.S.

doc. Ing. Jaroslav Juračka, Ph.D. Ředitel ústavu	prof. RNDr. Miroslav Doupovec, CSc., dr. h. c. Děkan fakulty

Abstrakt

Táto diplomová práca sa zaoberá návrhom kompozitového trupu štvormiestneho jednomotorového turistického letúnu TL-4000, ktorý spadá do kategórie CS-23 zo zameraním sa na zadnú časť. V tejto práci je vypracovaný návrh vnútornej konštrukcie s ohľadom na posádku a pasažierov. Z navrhnutej konštrukcie je vytvorený MKP model po ktorom nasleduje vypracovanie a vyhodnotenie skladby laminátových a sendvičových častí nosnej konštrukcie pomocou softvérov MSC.Patran/Nastran a ComPost pre vypočítané kombinácie vzdušného zaťaženia.

Kľúčové slová

TL-4000, trup, kompozitový materiál, metóda konečných prvkov, vzdušné zaťaženie, vnútorná konštrukcia

Abstract

This thesis deals with design of the composite fuselage for four seater single-engined tourist airplane TL-4000 within CS-23 regulations with focus on the rear part of the airplane. In this thesis there is created design of the internal structure with crew and passengers consideration. From internal structure design is FEM mesh created with following computation and analysis laminate and sandwich structure layout of the structure with MSC.Patran/Nastran and ComPost software for combinations of air loads.

Keywords

TL-4000, fuselage, composite material, finite element method, air loading, internal structure

Bibliographic citation

HOLIŠ, M. *Návrh trupu letounu TL-4000.* Brno: Vysoké učení technické v Brně, Fakulta strojního inženýrství, 2014. 122 s. Vedoucí diplomové práce Ing. Michal Mališ, Ph.D..

Affidavit

I declare that I have elaborated my master thesis on the theme of “Fuselage design of TL-4000 aircraft” independently, under the supervision of the master’s thesis supervisor and with the use of technical literature and other sources of information which are all quoted in the thesis and detailed in the list of literature at the end of the thesis.

In Brno 25.5.2014

.....

Michal Holiš

On the first place I would like to express my gratitude to my parents who were supporting me during whole my study period.

This way I would also like to express my gratitude to supervisor of my master thesis Ing. Michal Mališ, Ph.D for plenty practical advises regarding design and structural analysis and also for his endless sea of patience during consultations. My thanks also belong to Ing. František Vaněk for useful hints with air loads computation and Ing. Martin Weis for advices regarding use of the MSC.Patran software.

List of content

1. Introduction

TL-4000 aircraft is touring four seater single engined propeller aircraft within CS 23 category. It is designed as low wing composite aircraft with non retractable tricycle landing gear. The empennage layout is classic, fuselage-mounted. [1]

The goal of this thesis is to design fuselage of TL-4000 aircraft following the CS 23 regulations to withstand any loading that can occur during flight with focus on computation of air loads and structural analysis of the rear part.

For design of inner structure and mesh creating is used CATIA software and for structural analysis and laminate layout is used MSC.Patran/Nastran and ComPost software.

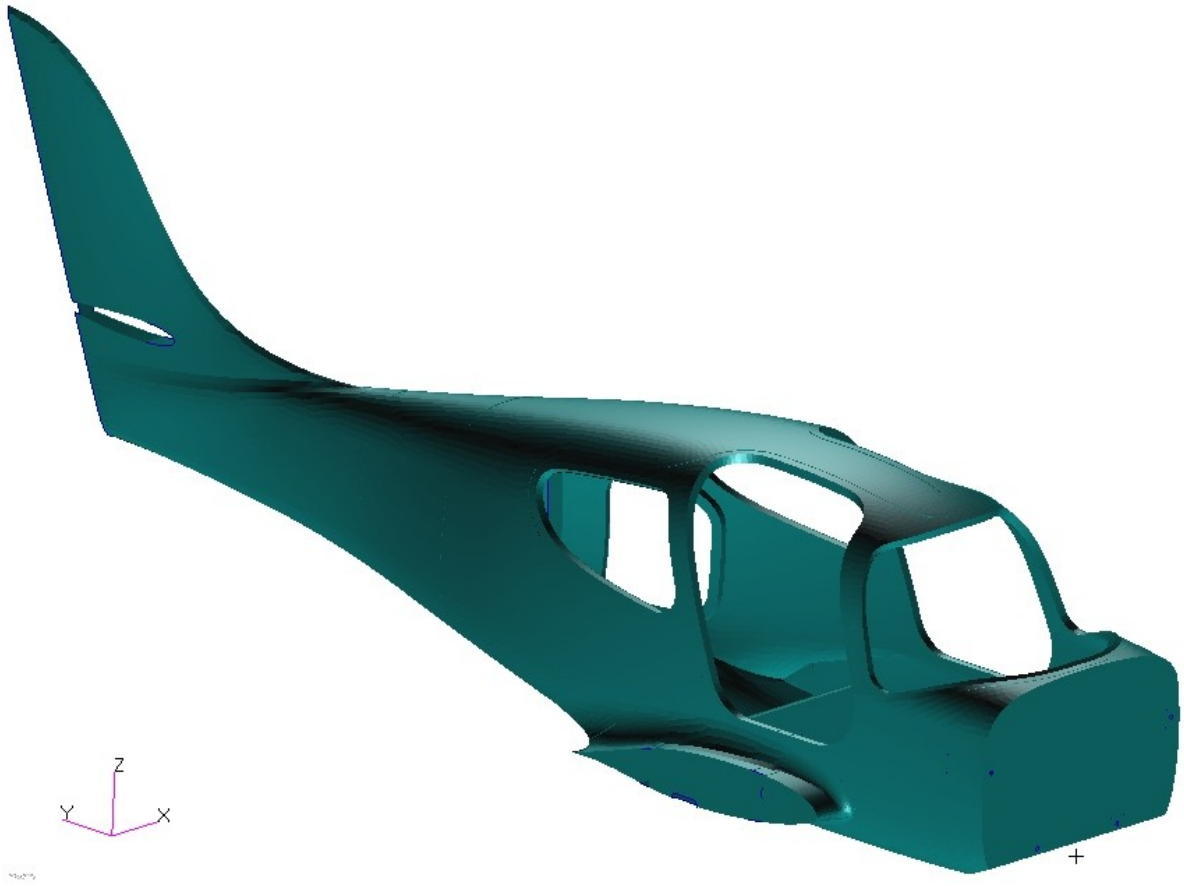

Fig. 1 Aircraft coordinate system

2. Flight envelope

2.1 Input data

Name	Sign	Value [metric]	Value [imperial]
Empty weight	m	900.00 kg	1984.13 lb
Maximum takeoff weight	m_{TOW}	1550.00 kg	3417.11 lb
Maximum payload	m_p	600.00 kg	1322.75 lb
Maximum fuel weight	m_f	240.00 kg	529.10 lb
Maximum permanent engine power	P_{max}	231 kW	
Estimated hrizontal flight speed	v_{Hmax}	380.00 km/h	205.18 kt
Maximum wing lift coefficient	c_{Lmax}	1.54	
Minimum lift coefficient (flight on back)	c_{Lmin}	1.23	
Mean aerodynamical chord	c_{mac}	1.19m	
Maximum lift coefficient with flaps	c_{Lflaps}	2.03	

Tab. 1 Estimated weight and performances [1]

2.2 Regulations [2]

General: Compliance with the strength requirements of this subpart must be shown at any

combination of airspeed and load factor on and within the boundaries of a flight envelope (similar to the one in sub-paragraph (d)) that represents the envelope of the flight loading conditions specified by the manoeuvring and gust criteria of sub-paragraphs (b) and (c) respectively.

b) *Manoeuvring envelope.* Except where limited by maximum (static) lift coefficients, the aeroplane is assumed to be subjected to symmetrical manoeuvres resulting in the following limit load factors:
   1. The positive manoeuvring load factor specified in CS 23.337 at speeds up to VD;
   2. The negative manoeuvring load factor specified in CS 23.337 at VC; and
   3. Factors varying linearly with speed from the specified value at VC to 0·0 at VD for the normal and commuter category, and -1·0 at VD for the aerobatic and utility categories.

c) *Gust envelope*
   1. The aeroplane is assumed to be subjected to symmetrical vertical gusts in level flight. The resulting limit load factors must correspond to the conditions determined as follows:
      i. Positive (up) and negative (down) gusts of 50 fps at VC must be considered at altitudes between sea level and 6096 m (20 000 ft). The gust velocity may be reduced linearly from 50 fps at 6096 m (20 000 ft) to 25 fps at 15240 m (50 000 ft); and
      ii. Positive and negative gusts of 25 fps at VD must be considered at altitudes between sea level and 6096 m (20 000 ft). The gust velocity may be reduced linearly from 25 fps at 6096 m (20,000 ft) to 12·5 fps at 15240 m (50,000 ft).

iii. In addition, for commuter category aeroplanes, positive (up) and negative (down) rough air gusts of 66 fps at VB must be considered at altitudes between sea level and 6096 m (20 000 ft). The gust velocity may be reduced linearly from 66 fps at 6096 m (20 000 ft) to 38 fps at 15240 m (50 000 ft).

2. The following assumptions must be made:
   i. The shape of gust is
   $$U = \frac{U_{de}}{2} . \left(1 - cos \frac{2.\pi.s}{25.\bar{C}}\right)$$
   ii. Gust load factors vary linearly with speed between v_C and v_D.

d) *High lift devices* If flaps or similar high lift devices are to be used for take-off, approach or landing, the aeroplane, with the flaps fully extended at v_F is assumed to be subjected to symmetrical manoeuvres and gusts within the range determined by:
   1. Manoeuvring, to a positive limit load factor of 2·0; and
   2. Positive and negative gust of (25 ft) per second acting normal to the flight path in level flight

2.3 Flight envelope for m_{TOW} [2]

2.3.1 Airspeeds

1) Design cruising speed v_c
   a. v_c in knots for normal, utility and commuter may not be less than
   $$v_c = 33 . \sqrt{\frac{W}{S}} = 167.38\ kt$$
   b. v_c need not be more than
   $$v_c = 0.9. v_{hmax} = 184.67\ kt$$
   c. From previous two points is chosen value for cruise speed
   $$v_c = 184.67. kt\ =\ 342.00\ km/h$$

2) Design dive speed:
   For normal and commuter category aeroplanes:
   $v_D = 1.4 . v_{cmin} = 233.80 . kt =\ 433.00\ km/h$

3) Design stall speed
   $$v_s = \sqrt{\frac{2.m.g}{\rho.S.c_{Lmax}}} = 70.19\ kt = 130.00\ km/h$$

4) Design manoeuvring speed for load factor $n_1 = 3.8$
   v_A may not be less than
   $v_A = v_s.\sqrt{n_1} = 136.61\ kt = 253.00\ km/h$

5) Stall speed for flight on back
   $$v_{sG} = \sqrt{\frac{2.m.g}{\rho.S.c_{Lmin}}} = 78.29\ kt = 145.00\ km/h$$

6) Manoeuvring speed for flight on back
   a. Maximum load factor for flight on back may not be less than
   $n_2 = -0.4 . n_1 = -1.52$
   b. Manoeuvring speed for flight on back
   $v_G = v_{sG} . \sqrt{n_2} = 96.11\ kt = 178.00\ km/h$

2.3.2 High lift devices airspeeds

1) Stall speed for flight with flaps fully extended:

$$v_{sF} = \sqrt{\frac{2.m.g}{\rho.S.c_{Lmin}}} = 31.51\frac{m}{s} = 113.00\ km/h$$

2) v_F must be assumed to be greater value of:

$1.4\ .v_S = 182.00\ km/h$

or

$1.8\ .v_{sF} = 203.40\ km/h$

As v_F is considered $v_F = 203.00\ km/h$

3) v_{AF} speed for load factor $n = 2$

$$v_{AF} = \sqrt{\frac{2.m.g.n}{\rho.S.c_{Lmin}}} = 44.57\frac{m}{s} = 160.00\ km/h$$

2.3.3 Gust loads

1) Gust load for cruise speed
   a. Aeroplane mass ratio

$$\mu g = \frac{2\left(\frac{W}{S}\right)}{\rho\ .c_{mac}\ .\alpha\ .g} = 32.59$$

   b. Gust alleviation factor

$$kg = \frac{0.88\ .\mu g}{5.3 + \mu g} = 0.76$$

   c. Gust load factor

$$n = 1 \pm \frac{kg\ .\rho\ .\ U_{de}\ .v_A}{2\left(\frac{W}{S}\right)} = 1 \pm 2.88$$

$$n_+ = 3.88$$

$$n_- = -1.88$$

2) Gust load for dive speed

The same constants μg and kg were used

   a. Gust load factor

$$n = 1 \pm \frac{kg\ .\rho\ .U_{de}\ .v_A}{2\left(\frac{W}{S}\right)} = 1 \pm 1.82$$

$$n_+ = 2.82$$

$$n_- = -0.82$$

3) Gust loading for extended flaps

Used the same constants as for cruise and dive speed, negative load factor is not taken into account in this point, because it's not usual to fly on back with extended flaps

$$n_+ = 1 + \frac{kg\ .\rho\ .\ U_{de}\ .v_A}{2\ .\left(\frac{W}{S}\right)} = 1.85$$

2.3.4 Flight envelope

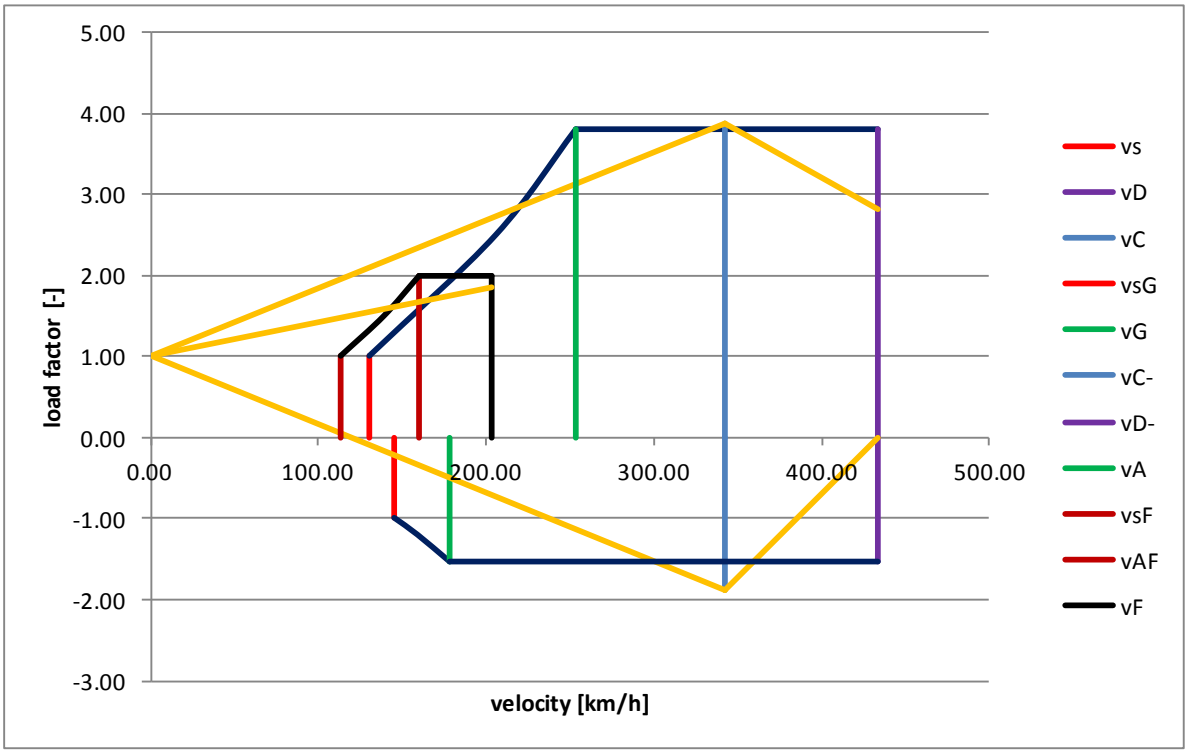

Fig. 2 Flight envelope for m_{TOW}

2.4 Flight envelope for m [2]

2.4.1 Airspeeds

7) Design cruising speed v_c
   Cruise speed remains the same:

$$v_c = 184.67\ kt\ =\ 342.00\ km/h$$

8) Design dive speed:
   Dive speed remains on the same value as in m_{TOW}:
   $v_D = 233.80\ kt =\ 433.00\ km/h$
9) Design stall speed

$$v_s = \sqrt{\frac{2\,.\,m\,.\,g}{\rho\,.\,S\,.\,c_{Lmax}}} = 53.46\ kt = 99.00\ km/h$$

10) Design manoeuvring speed for load factor $n_1 = 3.8$
    v_A may not be less than
    $v_A = v_s\,.\sqrt{n_1} = 103.67\ kt = 192.00\ km/h$
11) Stall speed for flight on back

$$v_{sG} = \sqrt{\frac{2\,.\,m\,.\,g}{\rho\,.\,S\,.\,c_{Lmin}}} = 59.40\ kt = 110.00\ km/h$$

12) Manoeuvring speed for flight on back
    a. Maximum load factor for flight on back may not be less than
    $n_2 = 0.4\,.\,n_1 = 1.52$

b. Manoeuvring speed for flight on back

$$v_G = v_{sG} \cdot \sqrt{n_2} = 72.89\ kt = 135.00\ km/h$$

2.4.2 High lift devices airspeeds

4) Stall speed for flight with flaps fully extended:

$$v_{sF} = \sqrt{\frac{2 \cdot m \cdot g}{\rho \cdot S \cdot c_{Lmin}}} = 24.01 \frac{m}{s} = 86.00\ km/h$$

5) v_F must be assumed to be greater value of:

$1.4\ v_s = 138.60\ km/h$

or

$1.8\ v_{sF} = 154.80\ km/h$

As v_F is considered $v_F = 154.00\ km/h$

6) v_{AF} speed for load factor $n = 2$

$$v_{AF} = \sqrt{\frac{2 \cdot m \cdot g \cdot n}{\rho \cdot S \cdot\ c_{Lmin}}} = 33.96 \frac{m}{s} = 122.00\ km/h$$

2.4.2 Gust loads

1) Gust load for cruise speed

a. Aeroplane mass ratio

$$\mu g = \frac{2 \cdot \left(\frac{W}{S}\right)}{\rho \cdot c_{mac} \cdot \alpha \cdot g} = 18.92$$

b. Gust alleviation factor

$$kg = \frac{0.88 \cdot \mu g}{5.3 + \mu g} = 0.69$$

c. Gust load factor

$$n = 1 \pm \frac{kg \cdot \rho \cdot\ U_{de} \cdot v_A}{2\left(\frac{W}{S}\right)} = 1 \pm 4.50$$

$$n_+ = 5.50$$

$$n_- = -3.50$$

2) Gust load for dive speed

The same constants μg and kg were used

a. Gust load factor

$$n = 1 \pm \frac{kg \cdot \rho \cdot\ U_{de} \cdot v_A}{2 \cdot \left(\frac{W}{S}\right)} = 1 \pm 2.85$$

$$n_+ = 3.85$$

$$n_- = -1.85$$

3) Gust loading for extended flaps

Used the same constants as for cruise and dive speed, negative load factor is not taken into account in this point, because it's not usual to fly on back with extended flaps

$$n_+ = 1 + \frac{kg \cdot \rho \cdot U_{de} \cdot\ v_A}{2 \cdot \left(\frac{W}{S}\right)} = 2.01$$

2.4.3 Flight envelope

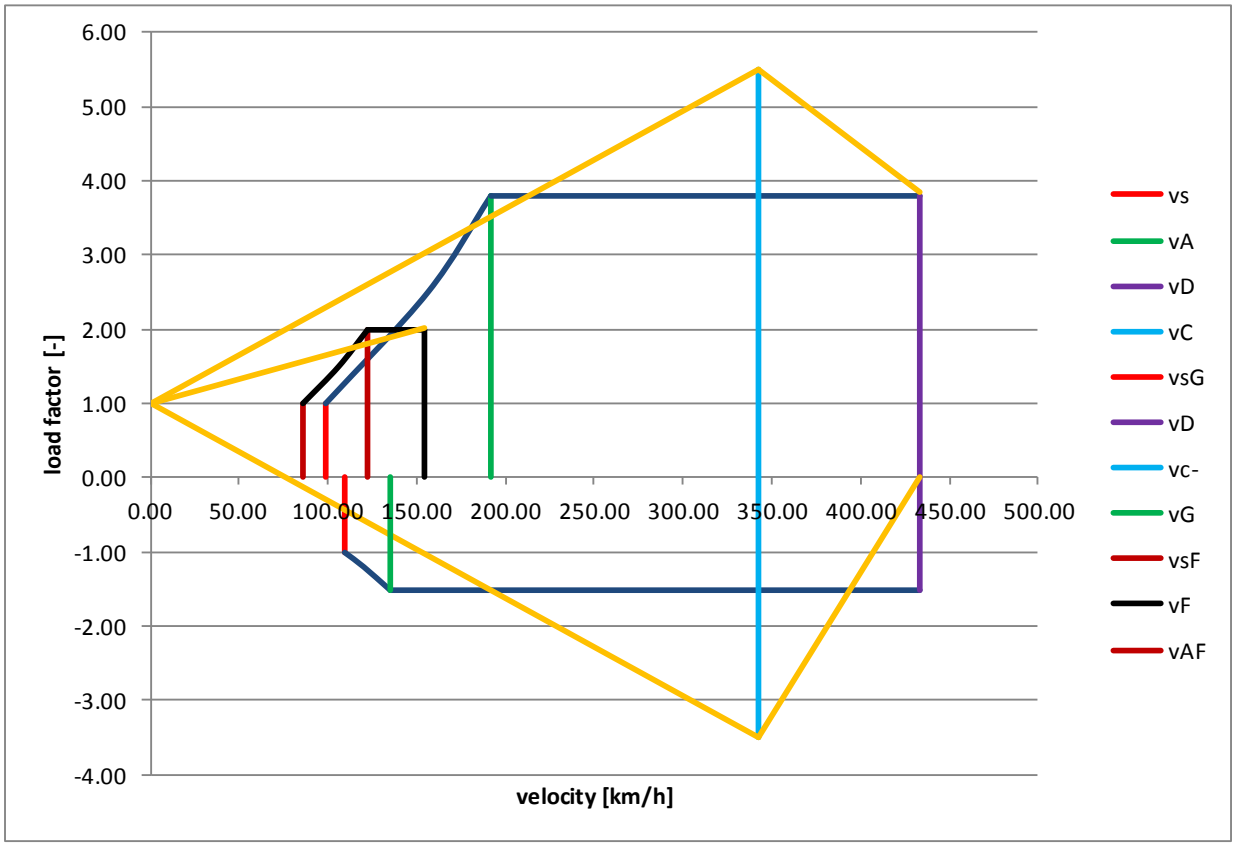

Fig. 3 Flight envelope for m

3. Horizontal tail loading

In this chapter there will be computed three main load cases which occur during all flight modes – trim, gust and manoeuvre loading.

Further load distribution will be computed just for maximum force that acts on the horizontal tail for case of unsymmetrical loading, but for load combination it is necessary to know also other forces acting on horizontal tail. These forces will be further applied in fuselage in combination with vertical tail forces.

3.1 Input data [3]

Name	Sign	Value [metric]
Maximum takeoff weight	m_{TOW}	$1550\ kg$
Empty weight	m	$900\ kg$
Wing area	S	$12.34\ m^2$
Maximum lift coefficient	c_{Lmax}	1.54
Density of air	ρ	$1.225\ kg/m^3$
Wing lift curve slope	$c_{l\alpha}$	$5.28\ 1/rad$
Mean aerodynamic chord	c_{MAC}	$1.19\ m$
Horizontal tail surface	S_{HT}	$2.39\ m^2$
Moment coefficient at zero lift	c_{m0}	-0.12
Horizontal tail estimated weight	m_{HT}	$20\ kg$
Gravitational acceleration	g	$9.81\ m/s^2$
Minimum lift coefficient	c_{Lmin}	-1.23
Lift coefficient with extended flaps	c_{Lflaps}	2.03
Wing span	b	$10.8\ m$
Horizontal tail arm	l_{HT}	$4.46\ m$
Fuselage thickness	$b_{fuselage}$	$1.3\ m$
Fuselage length	$l_{fuselage}$	$7.9\ m$

Tab. 2 Input data [3]

3.2 Trim loading computation

Trim force acts against yawn moment, which is created by moving of lift resultant force in every flight mode without yawning acceleration around lateral axis. Horizontal tail has to be designed for such trim loading that can appear in any point of envelope and any extension of flaps.

Trim force:

$$F_{HT,trim} = \frac{\frac{1}{2} \,.\, \rho \,.\, v^2 \,.\, S \,.\, c_{MAC} \,.\, c_{m0} + n \,.\, m \,.\, g \,.\, c_{MAC} \,.\, (\bar{x}_{cg} - \bar{x}_A)}{l_{vop}}$$

Computation of distance between centre of gravity and aerodynamic centre:

Centre of gravity is considered to vary between 15% and 35% of mean aerodynamic chord, aerodynamic centre is considered for configuration wing-fuselage. All the values are computed from leading edge of mean aerodynamic chord.

15% of MAC:

$x_{cg15} = 0.15 \,.\, c_{MAC} = 0.18\ m$

35% of MAC:

$x_{cg35} = 0.35 \,.\, c_{MAC} = 0.42\ m$

Aerodynamic centre for fuselage [4]:

$\Delta x_{A,fuselage} = -0.14\ m$

Aerodynamic centre of wing is considered in 25% of MAC

$x_{A,wing} = 0.25 \,.\, c_{MAC} = 0.30\ m$

Aerodynamic centre for combination wing-fuselage:

$x_A = x_{A,wing} + \Delta x_{A,fuselage} = 0.11\ m$

Relative values:

$\bar{x}_{cg15} = \frac{x_{cg15}}{c_{MAC}} = 0.15$

$\bar{x}_{cg35} = \frac{x_{cg35}}{c_{MAC}} = 0.35$

$\bar{x}_A = \frac{x_A}{c_{MAC}} = 0.1$

$l_{HT} = 4.64\ m$

v	$v\ [km/h]$	n	$m\ [kg]$	$x_T - x_A\ [-]$	$F_{HT,trim}\ [N]$
v_s	130.00	1.00	1550.00	0.05	-79.22
				0.25	701.38
	99.00		900.00	0.05	-45.80
				0.25	407.46
v_A	253.00	3.80	1550.00	0.05	-297.42
				0.25	2668.86
	192.00		900.00	0.05	-167.49
				0.25	1554.87
v_{C-}	342.00	-1.52	1550.00	0.05	-2335.36
				0.25	-3521.87
			900.00	0.05	-2200.41
				0.25	-2889.35
v_{D-}	433.00	3.80	1550.00	0.05	-2423.15
				0.25	543.13
			900.00	0.05	-2760.52
				0.25	-1038.17
v_{D0}	433.00	0.00	1550.00	0.05	-3227.66
				0.25	-3227.66
			900.00	0.05	-3227.66
				0.25	-3227.66
v_{D-}	433.00	-1.52	1550.00	0.05	-3549.46
				0.25	-4735.97
			900.00	0.05	-3414.51
				0.25	-4103.45
v_{sG}	145.00	-1.00	1550.00	0.05	-573.66
				0.25	-1354.26
	110.00		900.00	0.05	-331.23
				0.25	-784.48
v_G	178.00	-1.52	1550.00	0.05	-867.25
				0.25	-2053.76
	135.00		900.00	0.05	-500.60
				0.25	-1189.54
v_{sF}	113.00	1.00	1550.00	0.05	-8.11
				0.25	772.49
	86.00		900.00	0.05	-4.39
				0.25	448.86
v_{AF}	160.00	2.00	1550.00	0.05	-17.28
				0.25	1543.92
	122.00		900.00	0.05	-10.37
				0.25	896.13
v_F	203.00	2.00	1550.00	0.05	-285.99
				0.25	1275.20
			900.00	0.05	-463.56
				0.25	442.94

Tab. 3 Trim loading

3.3 Gust loading computation

Gust loading is computed as combination of trim loading and gust loading for load factor $n = 1$. As worst factors were considered peeks of manoeuvring envelope with combination of aircraft maximum and minimum weight and centre of gravity at its most forward and backward positions.

Trim loading was computed after formula in chapter 3.2 with load factor $n = 1$.

$$\Delta F_{HT,gust} = \frac{1}{2} \,.\, \rho \,.\, S_{HT} \,.\, a_{HT} \,.\, \left(1 - \frac{\delta\varepsilon}{\delta\alpha}\right) \,.\, v \,.\, U_{de} \,.\, kg$$

Where:

$$\frac{\delta\varepsilon}{\delta\alpha} = 1.75 \frac{c_{L\alpha}}{\pi \,.\, \left(\frac{b^2}{S}\right) \,.\, \left(\frac{\bar{l}_{HT}}{\eta}\right)^{\frac{1}{4}} \,.\, \left(1 + \left|\bar{h}_{HT}\right|\right)} = 0.25$$

$$a_{HT} = \frac{2 \,.\, \pi}{1 + \frac{3}{\left(\frac{b_{HT}^2}{S_{HT}}\right) \,.\, \cos(\chi_{HT})}} = 3.31 \frac{1}{rad}$$

$$\bar{l}_{HT} = \frac{2 \,.\, l_{HT}}{l_{fuselage}} = 1.13$$

$$\bar{h}_{HT} = \frac{2 \,.\, \left(\frac{\sin(c_{L\alpha})}{l_{HT}}\right)}{l_{fuselage}} = -0.05$$

$$F_{HT,gust} = F_{HT,trim,n=1} + \Delta F_{HT,gust}$$

v	weight configuration	$CG\ [\%c_{MAC}]$	$v\ value\ [m/s]$	$U\ [m/s]$	kg	$F_{HT,trim,n=1}\ [N$	$\Delta F_{HT,gust}\ [N]$	$F_{gust}\ [N]$
v_A	m_{TOW}	15.00	70.28	15.24	0.76	-924.31	2929.61	2005.30
		35.00				-269.45	2929.61	2660.16
	m	15.00	53.33		0.69	-457.01	2019.26	1562.25
		35.00				197.86	2019.26	2217.11
	m_{TOW}	15.00	70.28	-15.24	0.76	-924.31	-2929.61	-3853.93
		35.00				-269.45	-2929.61	-3199.06
	m	15.00	53.33		0.69	-457.01	-2019.26	-2476.26
		35.00				197.86	-2019.26	-1821.40
v_c	m_{TOW}	15.00	95.00	15.24	0.76	-1835.94	3960.19	2124.24
		35.00				-1181.08	3960.19	2779.11
	m	15.00			0.69	-1910.43	3596.80	1686.37
		35.00				-1530.18	3596.80	2066.62
	m_{TOW}	15.00		-15.24	0.76	-1835.94	-3960.19	-5796.13
		35.00				-1181.08	-3960.19	-5141.26
	m	15.00			0.69	-1910.43	-3596.80	-5507.23
		35.00				-1530.18	-3596.80	-5126.98
v_D	m_{TOW}	15.00	120.28	7.62	0.76	-3050.04	2506.96	-543.08
		35.00				-2395.18	2506.96	111.78
	m	15.00			0.69	-3124.53	2276.92	-847.60
		35.00				-2744.28	2276.92	-467.36
	m_{TOW}	15.00		-7.62	0.76	-3050.04	-2506.96	-5557.00
		35.00				-2395.18	-2506.96	-4902.14
	m	15.00			0.69	-3124.53	-2276.92	-5401.45
		35.00				-2744.28	-2276.92	-5021.20
v_F	m_{TOW}	15.00	56.39	7.62	0.76	-531.81	1175.32	643.51
		35.00				123.06	1175.32	1298.37
	m	15.00			0.69	-606.29	1067.47	461.18
		35.00				-226.05	1067.47	841.42
	m_{TOW}	15.00		-7.62	0.76	-531.81	-1175.32	-1707.13
		35.00				123.06	-1175.32	-1052.26
	m	15.00			0.69	-606.29	-1067.47	-1673.76
		35.00				-226.05	-1067.47	-1293.52

Tab. 4 Gust loading

3.4 Manoeuvring loads computation

Each horizontal surface and its supporting structure, and the main wing of a canard or tandem wing configuration, if that surface has pitch control, must be designed for manoeuvring loads imposed by the following conditions:

a) A sudden movement of the pitching control, at the speed VA to the maximum aft movement, and the maximum forward movement, as limited by the control stops, or pilot effort, whichever is critical.
b) A sudden aft movement of the pitching control at speeds above VA, followed by a forward movement of the pitching control resulting in the following combinations of normal and angular acceleration [2]

Due to lack of input data using CS 23 regulation would be problematic for speed v_A so there was chosen CS VLA regulation considering size of the aircraft.

At first load factor increment Δn was computed from the manoeuvring envelope:

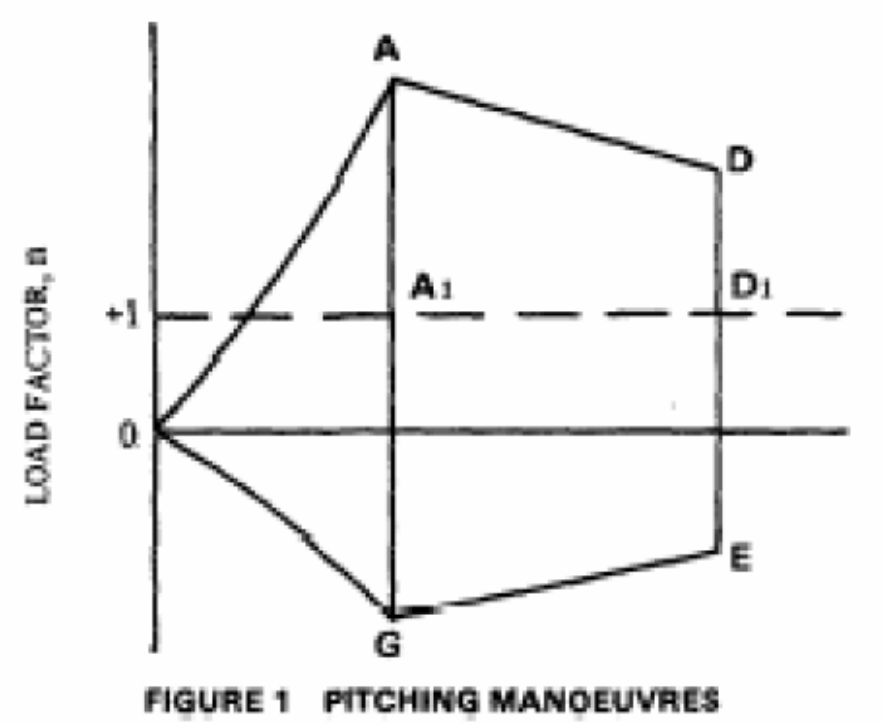

Fig. 4 Pitching manoeuvres load increment [5]

Speed	Initial Condition	Final Condition	Load Factor Increment
V_A	A_1	A	n1 – 1
	A	A_1	1 – n1
	A_1	G	n4 – 1
	G	A_1	1 – n4

Fig. 5 Pitching load factor increment manoeuvring speed [5]

Horizontal tail load increment ΔP:

$$\Delta P = \Delta n \,.\, m \,.\, g \left[\frac{X_{cg}}{l_t} - \frac{S_{HT}}{S} \,.\, \frac{a_{HT}}{a} \,.\, \left(1 - \frac{d\varepsilon}{d\alpha}\right) - \frac{\rho_0}{2} \,.\, (S_{HT} \,.\, a_{HT} \,.\, \frac{l_t}{m}\right]$$

speed	pitching	weight configuration	$CG\ [\%c_{MAC}]$	$\Delta n\ [-]$	$\Delta P\ [N]$
v_A	nose up (+n)	m_{TOW}	15.00	2.80	-3950.24
			35.00		-1929.28
		m	15.00		-2548.46
			35.00		-1361.73
	nose down (-n)	m_{TOW}	15.00	-2.80	3950.24
			35.00		1929.28
		m	15.00		2548.46
			35.00		1361.73
	nose up (+n)	m_{TOW}	15.00	2.52	-3555.22
			35.00		-1736.35
		m	15.00		-2293.61
			35.00		-1225.56
	nose down (-n)	m_{TOW}	15.00	-2.52	3555.22
			35.00		1736.35
		m	15.00		2293.61
			35.00		1225.56

Tab. 5 Pitching load increment manoeuvring speed

For the speeds above v_A was used formula from CS 23.423 to compute angular velocity:

$$\varepsilon = \frac{39}{v} \,.\, n \,.\, (n - 1.5)$$

$$\varepsilon = -\frac{39}{v} \,.\, n \,.\, (n - 1.5)$$

From this angular velocity is computed horizontal tail increment:

$$\Delta P = \frac{\varepsilon \,.\, J_z}{l_{HT}}$$

$I_z = 0.165 \,.\, l_{fuselage} = 1.3\ m$

$J_{z,m} = m \,.\, I_z^2 = 1529\ kg\,.m^2$

$J_{z,mTOW} = m_{TOW} \,.\, I_z^2 = 2633\ kg\,.m^2$

speed	pitching	Weight configuration	$CG\ [\%c_{MAC}]$	speed [kt]	$n\ [-]$	$\varepsilon\ [rad/s]$	$\Delta P\ [N]$
v_C	nose down (-n)	m_{TOW}	15.00	184.67	3.80	-1.85	-1061.59
			35.00				-1119.89
		m	15.00				-616.40
			35.00				-650.26
	nose up (+n)	m_{TOW}	15.00			1.85	1061.59
			35.00				1119.89
		m	15.00				616.40
			35.00				650.26
v_D	nose down (-n)	m_{TOW}	15.00	233.80	3.80	-1.46	-838.48
			35.00				-884.53
		m	15.00				-486.86
			35.00				-513.60
	nose up (+n)	m_{TOW}	15.00			1.46	838.48
			35.00				884.53
		m	15.00				486.86
			35.00				513.60

Tab. 6 Cruise and dive speed load factor increment

Resultant manoeuvring force is computed combination of trim force for load factor 1 and tail load increment:

$F_{HT,man} = F_{HT,trim,n=1} + \Delta P$

speed	pitching	F total [N]
v_A	nose up (+n)	-4884.77
		-2208.86
		-3011.98
		-1170.31
	nose down (-n)	3036.14
		1669.96
		2097.96
		1566.03
	nose up (+n)	-4488.72
		-2014.92
		-2756.48
		-1033.50
	nose down (-n)	2640.09
		1476.02
		1842.46
		1429.21

Tab. 7 Pitching load for manoeuvring speed

v_C	nose up (+n)	-774.36
		-61.19
		-1294.02
		-879.92
	nose down (-n)	-2897.53
		-2300.97
		-2526.83
		-2180.44
v_D	nose up (+n)	-3888.52
		-3279.71
		-3611.39
		-3257.88
	nose down (-n)	-2211.56
		-1510.65
		-2637.67
		-2230.68

Tab. 8 Pitching load for cruise and dive speed

4. Vertical tail loading

In this chapter will be computed forces acting on whole surface of the vertical tail, what is necessary for further computation of the load distribution along span of the vertical tail.

There will be considered just two load cases – for gust loading and manoeuvre loading. On the vertical tail could act also slipstream created by propeller, but this will not be considered even as trim load, because this load case is not significant at all and further will be considered that this force will be removed after manufacturing of the aircraft during removing of manufacturing disproportions.

4.1 Input data

Name	Sign	Value [metric]
Vertical tail surface	S_{VT}	$1.71\ m^2$
Vertical tail weight	m_{VT}	$15\ kg$
Vertical tail root chord	$c_{0,VT}$	$1.5\ m$
Vertical tail tip chord	$c_{k,VT}$	$0.58\ m$
Vertical tail span	b_{VT}	$1.65\ m$
Vertical tail mean aerodynamic chord	$c_{MAC,VT}$	$1.11\ m$
Vertical tail arm	l_{VT}	$4.57\ m$

Tab. 9 Input data for vertical tail loading

4.2 Gust loading computation

$$F_{VT,gust} = \frac{1}{2} . \rho . S_{VT} . a_{VT} . v . U . kg$$

Where vertical tail lift slope was estimated by graphs in [4]:

$$a_{VT} = 0.04\frac{1}{deg} = 2.41\frac{1}{rad}$$

gust load	velocity	$v\ [km/h]$	$U\ [m/s]$	kg	$F_{VT,gust}\ [N]$
m_{TOW}	v_C	342.00	15.24 -15.24	0.76	2761.98 -2761.98
m			15.24 -15.24	0.69	2508.54 -2508.54
m_{TOW}	v_D	433.00	7.62 -7.62	0.76	1748.45 -1748.45
m			7.62 -7.62	0.69	1588.01 -1588.01

Tab. 10 Gust loading for vertical tail

4.3 Manoeuvre loading

This computation is provided just for manoeuvring speed what is considered as speed with highest vertical tail loading.

There was three main flight conditions computed with: sideslip β, rudder deflection δ_{rudder} and their combination.

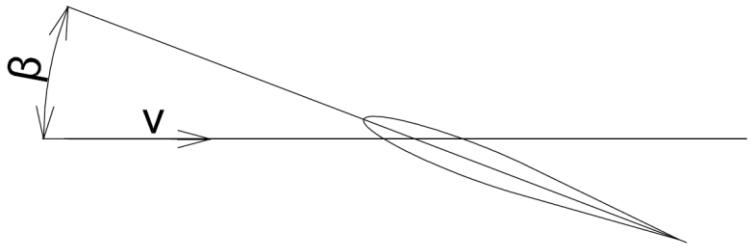

Fig. 6 Sideslip

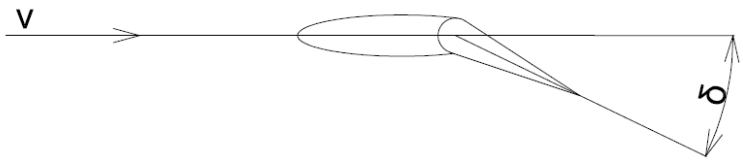

Fig. 7 Rudder deflection

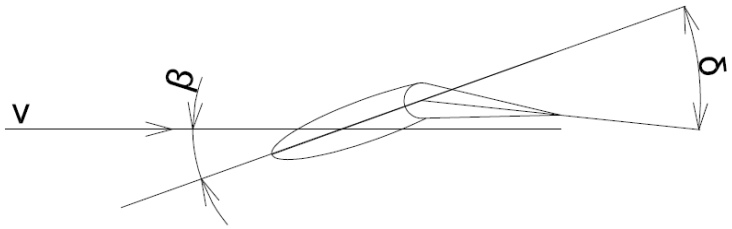

Fig. 8 Sideslip and rudder deflection

Then manoeuvring loading is computed after basic formula for computing lift of the wing:

$$F_{VT,man} = \frac{1}{2} \cdot \rho \cdot S_{VT} \cdot v^2 \cdot c_{L,VT}$$

Where $c_{L,VT}$ is lift coefficient created by vertical tail

$$c_{L,VT} = \alpha_{equivalent} \cdot a_{VT}$$

$\alpha_{equivalent}$ is equivalent angle of attack for given flight conditions

$$\alpha_{equivalent} = \beta - \delta_{equivalent}$$

$\delta_{equivalent}$ is equivalent rudder deflection based on efficiency of the rudder

$$\delta_{equivalent} = \frac{\delta\alpha}{\delta\delta} \cdot \delta_{rudder}$$

$\frac{\delta\alpha}{\delta\delta}$ is efficiency of the rudder, it was estimated to value 0.4, similar to other aircrafts with the same size although computed efficiency was 0.75 but this value can be considered only for deflection no more than seven degrees.

Weight configuration	$\beta\ [deg]$	δ_{rudder} $[deg]$	$\delta_{equivalent}$ $[deg]$	$\alpha_{equivalent}$ $[deg]$	$c_{L,VT}\ [-]$	v $[km/h]$	$F_{VT,man}\ [N]$
m_{TOW}	22.50	30.00	12.00	10.50	0.44		2281.27
	15.00	0.00	0.00	15.00	0.63	253.00	3258.96
	0.00	30.00	12.00	-12.00	0.50		2607.17
m	22.50	30.00	12.00	10.50	0.44		1313.83
	15.00	0.00	0.00	15.00	0.63	192.00	1876.90
	0.00	30.00	12.00	-12.00	0.50		1501.52

Tab. 11 vertical tail manoeuvre loading

Lowest value will not be further considered, because it has the same direction as highest loading, just value is smaller.

5. Horizontal tail load distribution

Computing of horizontal tail load distribution is primarily focused on resultant loading acting on the fuselage at horizontal tail root which is needed for further computation of bending and torsion moment acting from horizontal tail into the fuselage.

Load distribution along span of horizontal tail is required only for unsymmetrical loading for highest force value, which occurs during gusts.

5.1 Load distribution for gust

As a result of gust loading computation was considered just negative load case which is the highest horizontal tail loading.

$$F_{HT,gust} = -5796.13\ N$$

This loading was after CS 23 Appendix 1 divided by surface of the horizontal tail to get average surface loading.

$\overline{w}_{HT,gust} = -2425.16 \left[\frac{N}{m^2}\right]$

The horizontal tail was then divided to 15 sections and in each section was computed linear loading based on chord.

section no.	$\frac{b_{HT}}{2}$ $[m]$	c_{HT} $[m]$	q_{HT} $[N/m]$
15.00	1.92	0.50	575.59
14.00	1.79	0.51	595.36
13.00	1.66	0.53	615.12
12.00	1.54	0.55	634.89
11.00	1.41	0.56	654.66
10.00	1.28	0.58	674.43
9.00	1.15	0.60	694.20
8.00	1.02	0.61	713.96
7.00	0.90	0.63	733.73
6.00	0.77	0.65	753.50
5.00	0.64	0.67	773.27
4.00	0.51	0.68	793.03
3.00	0.38	0.70	812.80
2.00	0.26	0.72	832.57
1.00	0.13	0.73	852.34
0.00	0.00	0.75	872.10

Tab. 12 Horizontal tail linear loading distribution for gust

For gust loading is estimated that resultant force acts in 25% of the chord, so after CS 23 Appendix A was the values of $\rho 1$ and $\rho 2$ computed:

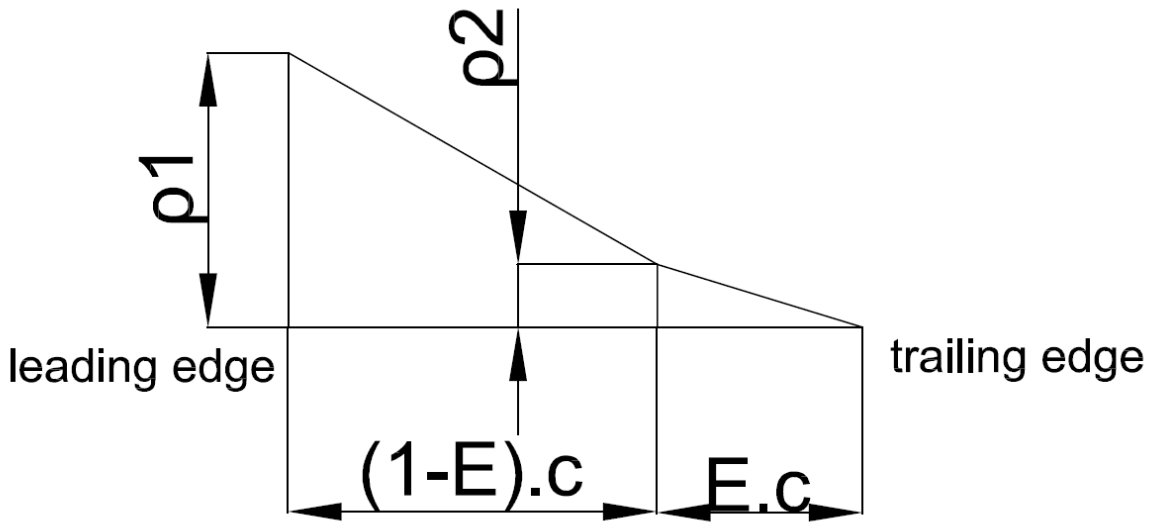

Fig. 9 load distribution along chord [2]

$$\rho 1 = 2 \,.\, \overline{w} \left(\frac{(2 - E - 3.\, d')}{1 - E} \right)$$

$$\rho 2 = 2 \,.\, \overline{w} \,(3 \,.\, d' + E - 1)$$

Where:

E is ratio of the elevator chord to total horizontal tail chord ($E = 0.4$)

d' is relative chord wise distance of resultant force created by lift. For gust $d' = 0.25$

From $\rho 1$ and $\rho 2$ were computed relative force proportions separately for stabilizer and elevator, which are the same for both load cases.

stabilizer	elevator
0.94	0.06

Tab. 13 Horizontal tail force proportions for gust

This force proportions were multiplied by q_{HT} to compute values of local loading for stabilizer q_{stab} and elevator q_{elev} separately.

Afterwards the force and bending moment acting in each section was computed by numerical integration.

$$T_{stab,i} = \frac{1}{2} \,.\, \left(q_{stab,i} + q_{stab,i-1}\right) \,.\, (b_{HT,i} - b_{HT,i-1})$$

$$M_{o,stab,i} = \frac{1}{2} \,.\, \left(T_{stab,i} + T_{stab,i-1}\right) \,.\, \left(b_{HT,i} - b_{HT,i-1}\right)$$

The same formulas were used to compute force and bending moment of the elevator.

$$T_{elev,i} = \frac{1}{2} \,.\, \left(q_{stab,i} + q_{stab,i-1}\right) \,.\, (b_{HT,i} - b_{HT,i-1})$$

$$M_{o,elev,i} = \frac{1}{2} \,.\, \left(T_{stab,i} + T_{stab,i-1}\right) \,.\, \left(b_{HT,i} - b_{HT,i-1}\right)$$

stabilizer			elevator		
$q_{stab,i}\ [N/m]$	$T_{stab,i}\ [N]$	$M_{o,stab,i}\ [N.m]$	$q_{elev,i}\ [N/m]$	$T_{elev,i}\ [N]$	$M_{o,elev,i}\ [N.m]$
-1128.43	0.00	0.00	-72.03	0.00	0.00
-1167.18	-146.92	-9.40	-74.50	-9.38	-0.60
-1205.93	-298.80	-37.93	-76.97	-19.07	-2.42
-1244.69	-455.64	-86.21	-79.45	-29.08	-5.50
-1283.44	-617.44	-154.89	-81.92	-39.41	-9.89
-1322.20	-784.20	-244.59	-84.40	-50.06	-15.61
-1360.95	-955.92	-355.96	-86.87	-61.02	-22.72
-1399.70	-1132.60	-489.63	-89.34	-72.29	-31.25
-1438.46	-1314.25	-646.23	-91.82	-83.89	-41.25
-1477.21	-1500.85	-826.39	-94.29	-95.80	-52.75
-1515.97	-1692.41	-1030.76	-96.76	-108.03	-65.79
-1554.72	-1888.94	-1259.97	-99.24	-120.57	-80.42
-1593.47	-2090.42	-1514.65	-101.71	-133.43	-96.68
-1632.23	-2296.87	-1795.43	-104.18	-146.61	-114.60
-1670.98	-2508.27	-2102.96	-106.66	-160.10	-134.23
-1709.74	-2724.64	-2437.87	-109.13	-173.91	-155.61

Tab. 14 Horizontal tail load distribution

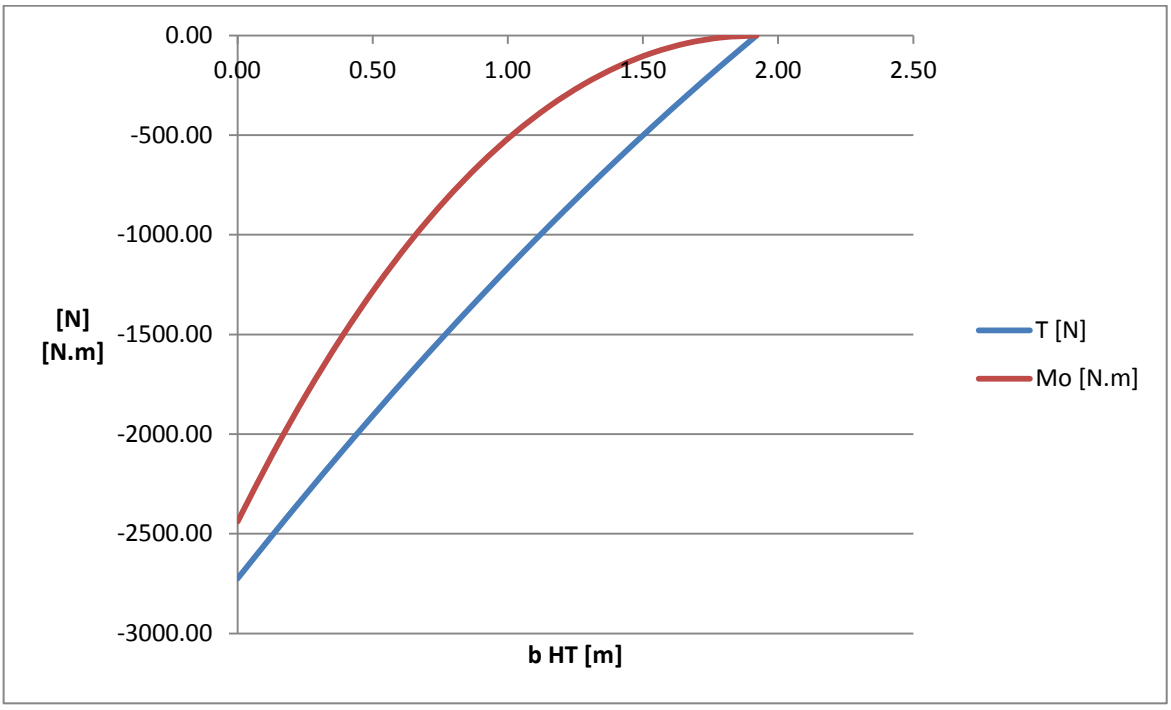

Fig. 10 Horizontal tail load distribution along stabilizer

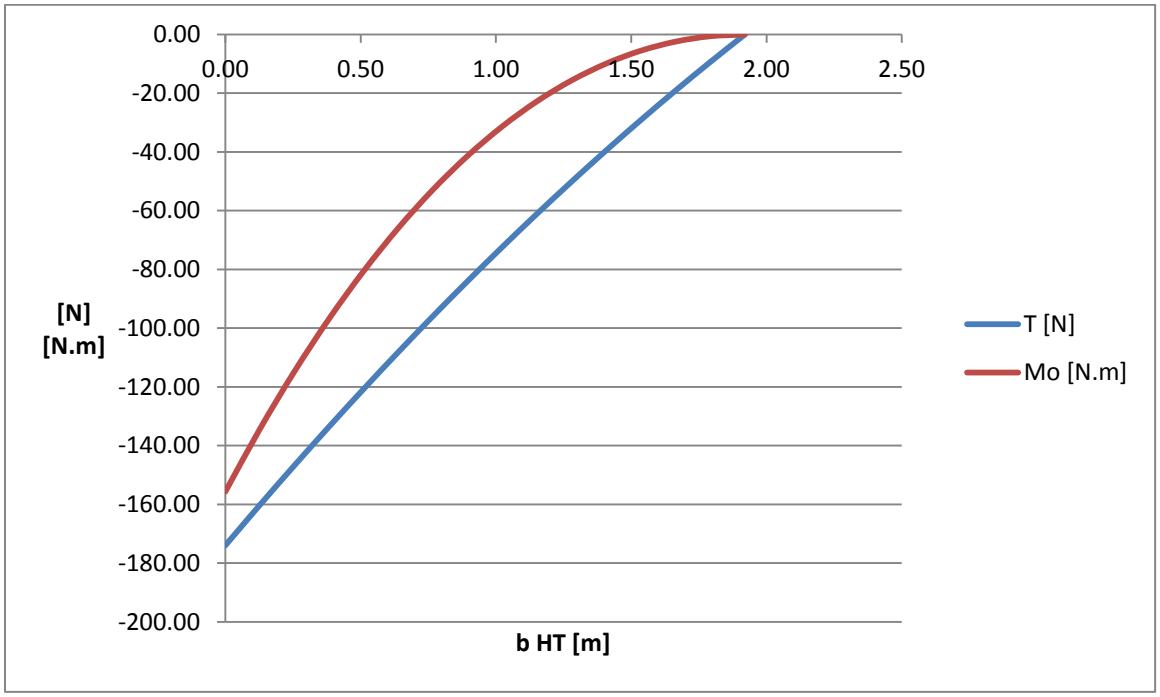

Fig. 11 Horizontal tail load distribution along elevator

For this fuselage design it is not absolutely necessary to compute force and moment acting on stabilizer and elevator separately, because for the purpose of structural design is needed force acting on whole horizontal tail surface.

6. Vertical tail load distribution

Computing of vertical tail load distribution is necessary for further load compensations which will be applied along span of the fin and also in places of hinges of the rudder. In that case it is necessary to compute distribution of force and bending moment along span of the fin and rudder.

As in previous chapter, also here is divided to fifteen cuts and depending on chord length is computed linear loading. Afterwards this loading is divided between fin and rudder and numerically integrated to force and moment that acts along fin and rudder span.

In this chapter, there is a difference that loads have to be divided between fin and rudder, because forces which act in hinges are computed from rudder force and moment.

6.1 Gust load distribution

At first surface loading was computed.

	maximum gust force $F_{VT,gust}[N]$	Surface loading $\bar{w}_{gust}\ [N/m^2]$
positive	2761.98	1615.19
negative	-2761.98	-1615.19

Tab. 15 Vertical tail surface loading for gust

Afterwards was computed linear loading distribution which is based on local chord length.

cut no.	b_{VT} $[m]$	c_{VT} $[m]$	q_{gust} $[N/m]$
15.00	1.65	0.58	936.81
14.00	1.54	0.64	1035.88
13.00	1.43	0.70	1134.94
12.00	1.32	0.76	1234.01
11.00	1.21	0.83	1333.07
10.00	1.10	0.89	1432.14
9.00	0.99	0.95	1531.20
8.00	0.88	1.01	1630.27
7.00	0.77	1.07	1729.33
6.00	0.66	1.13	1828.40
5.00	0.55	1.19	1927.46
4.00	0.44	1.25	2026.53
3.00	0.33	1.32	2125.59
2.00	0.22	1.38	2224.66
1.00	0.11	1.44	2323.72
0.00	0.00	1.50	2422.79

Tab. 16 Vertical tail linear loading distribution for gust

The distribution along chord was computed after CS 23 Appendix A

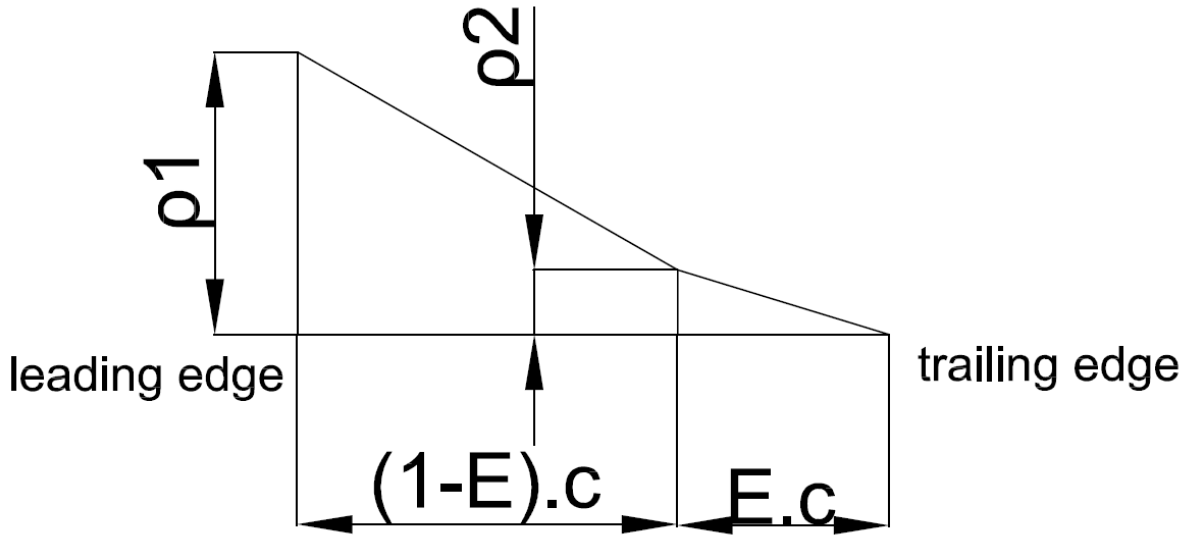

Fig. 12 Load distribution along chord

Where:

$$\rho 1 = 2 \,.\, \overline{w} \left(\frac{(2 - E - d')}{1 - E} \right)$$

$$\rho 2 = 2 \,.\, \overline{w} \,(3 \,.\, d' + E - 1)$$

Where:

E is ratio of the rudder chord to total horizontal tail chord ($E = 0.41$)

d' is relative chord wise distance of resultant force created by lift. For gust $d' = 0.25$

From $\rho 1$ and $\rho 2$ were computed relative force proportions separately for fin and rudder, which are the same for both load cases.

stabilizer	rudder)
0.93	0.07

Tab. 17 Vertical tail gust loading proportions

For further applying forces on fin in FEM model there was computed also point where acts force created by fin along chord length from leading edge in each cut.

cut no.	fin force acting point $[m]$	$q_{fin}\ [N/m]$	$T_{fin}\ [N]$	$M_{o,fin}\ [N.m]$	$q_{rud}\ [N/m]$	$T_{rud}\ [N]$	$M_{o,rud}\ [N.m]$
15.00	0.13	873.83	0.00	0.00	62.98	0.00	0.00
14.00	0.14	966.24	100.90	5.53	69.64	7.27	0.40
13.00	0.15	1058.64	211.93	22.69	76.30	15.27	1.64
12.00	0.16	1151.05	333.09	52.57	82.96	24.01	3.79
11.00	0.18	1243.45	464.39	96.30	89.62	33.47	6.94
10.00	0.19	1335.86	605.82	154.98	96.28	43.66	11.17
9.00	0.20	1428.26	757.39	229.73	102.94	54.59	16.56
8.00	0.22	1520.67	919.09	321.66	109.60	66.24	23.18
7.00	0.23	1613.07	1090.92	431.87	116.26	78.63	31.13
6.00	0.24	1705.48	1272.89	561.49	122.92	91.74	40.47
5.00	0.26	1797.88	1464.99	711.62	129.58	105.59	51.29
4.00	0.27	1890.29	1667.22	883.37	136.24	120.16	63.67
3.00	0.28	1982.69	1879.59	1077.85	142.90	135.47	77.69
2.00	0.30	2075.10	2102.09	1296.18	149.56	151.51	93.42
1.00	0.31	2167.50	2334.73	1539.46	156.22	168.27	110.96
0.00	0.32	2259.91	2577.50	1808.82	162.88	185.77	130.37

Tab. 18 Vertical tail Gust loading

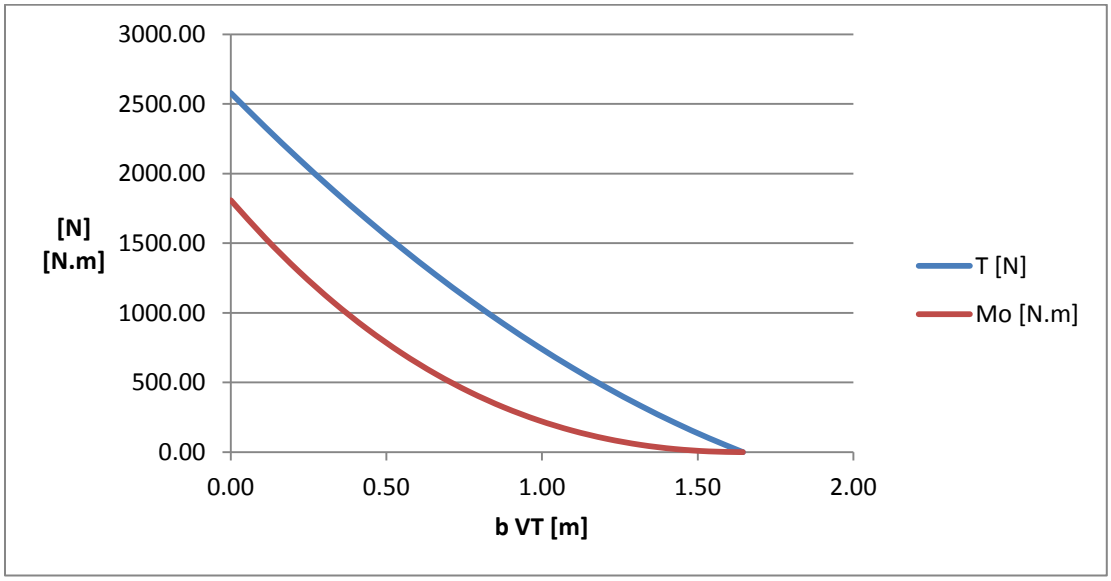

Fig. 13 Load distribution along fin without reaction forces

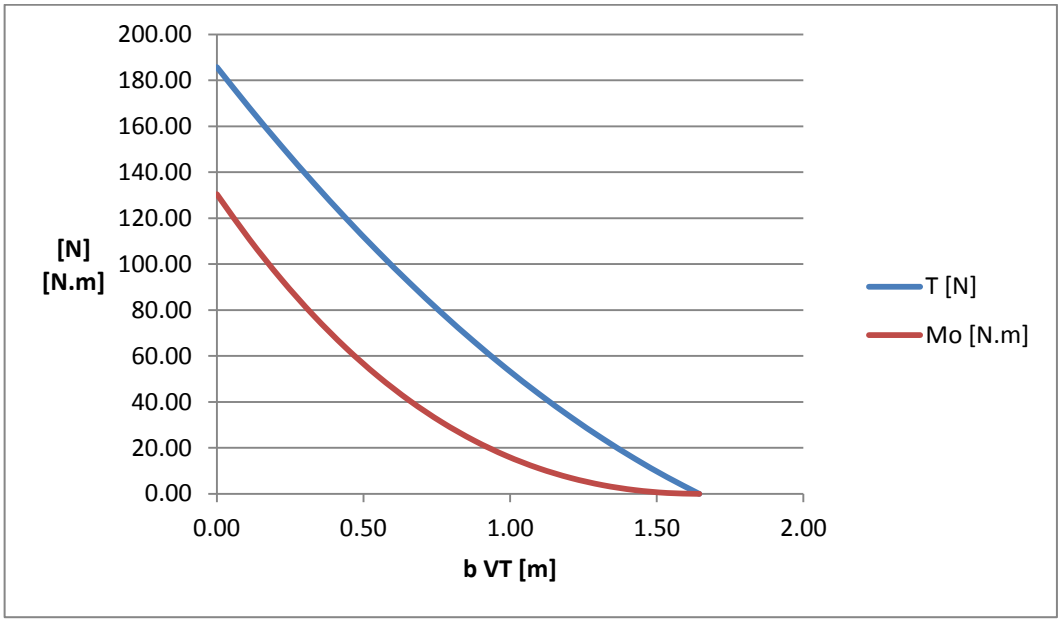

Fig. 14 Load distribution along rudder, without reaction forces

From rudder force and moment is computed force acting on rudder hinges which will be applied to the places where rudder will be attached to the fin. At first there was set the number of hinges to two.

$$a = \frac{\left(q_k \,.\, \frac{b_{VT}^2}{2} \,.+ (q_r - q_t) \,.\, \frac{b_{VT}^2}{6}\right)}{q_t \,.\, b_{VT} + (q_r - q_t) \,.\, \frac{b_{VT}}{2}} = 0.7\ m$$

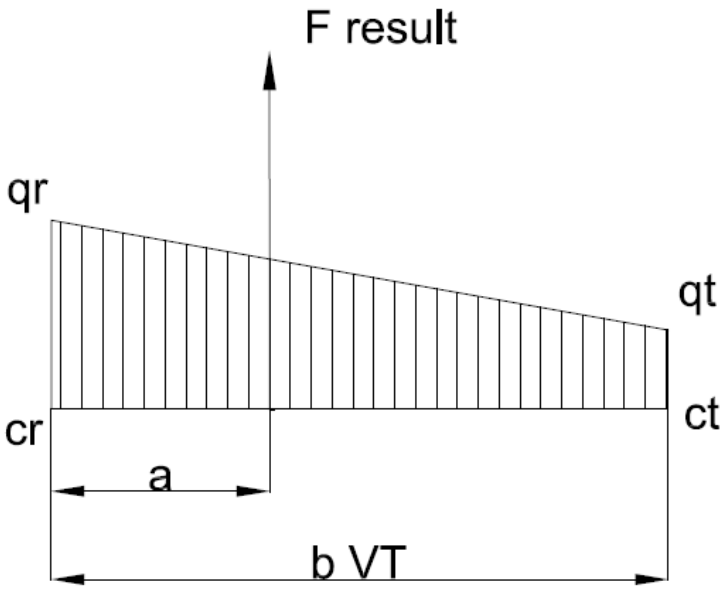

Fig. 15 Resultant force acting place

Forces acting on the hinges were computed afterwards as reaction forces on beam.

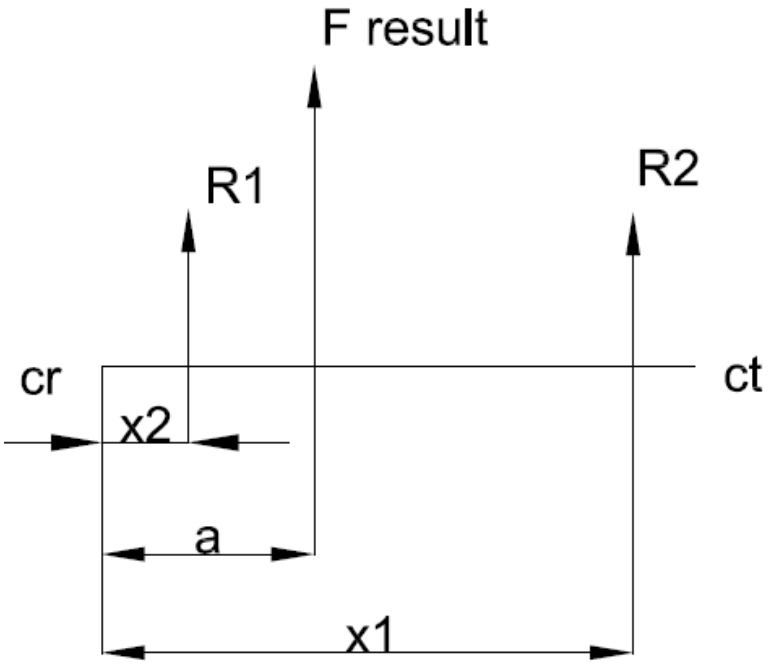

Fig. 16 Reaction forces acting along rudder span

$$\sum F = 0 : R_1 + R_2 + F_{result} = 0$$

Moment equivalence was computed to the point where reaction R_1 acts to get reaction force R_2 easier.

$$\sum M_o = 0 : R_2 \,.\, (x_1 - x_2) + F_{result} \,.\, (a - x_2) = 0$$

There was also necessary to set distance of the hinges from horizontal tail root:

$x_1 = 1.54\ m$

$x_2 = 0.11\ m$

From moment equivalence:

$$R_2 = \frac{\left(-F_{result} \,.\, (a - x_2)\right)}{x_1 - x_2} = -77.08\ N$$

From force equivalence:

$$R_1 = -F_{result} - R_2 = -108.69\ N$$

These forces act in hinges of the rudder, for applying them on fin they has to have opposite direction.

After applying forces to the graph of the load distribution of the rudder and fin:

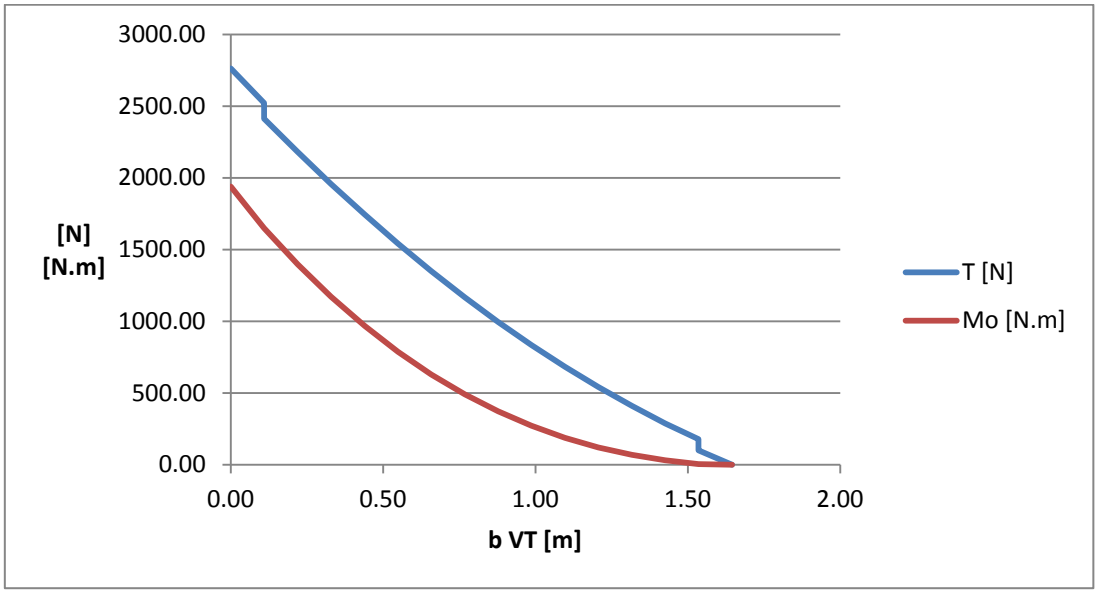

Fig. 17 Gust load distribution on fin with reaction forces included

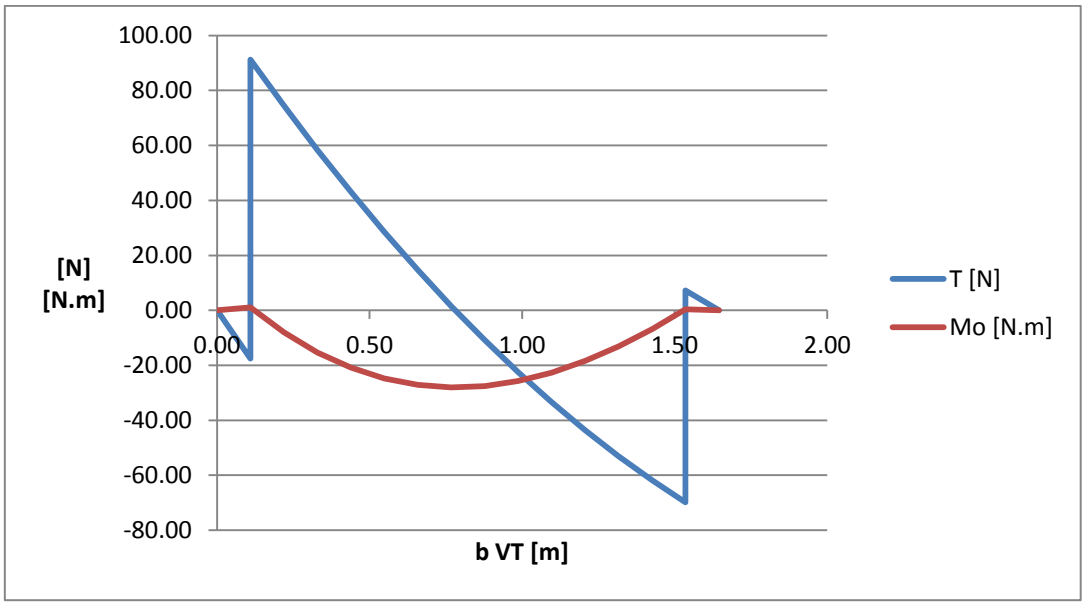

Fig. 18 Gust load distribution on rudder with reaction forces included

Negative force distribution will not be computed because it has exactly the same value as positive, so it is assumed that everything will be the same, just the direction is opposite.

6.2 Manoeuvre load distribution

The same process was used also to compute load distribution along vertical tail during manoeuvring. Tail surface was again divided to 15 sections where was applied surface loading dependent on chord length. This process led to achieve linear loading which was further numerically integrated to achieve force and moment acting on fin and rudder.

From rudder force and moment were afterwards computed reaction forces in rudder hinges and applied into graphs of fin load distribution.

The lowest force distribution will not be computed, because it has the same direction but smaller value than maximum force.

$F_{VT,man}$ $[N]$	$\overline{w}_{VT,man}$ $[N/m2]$
3258.96	1905.82

Tab. 19 Vertical tail surface loading for manoeuvre

section no.	b_{VT} $[m]$	c_{VT} $[m]$	$q_{man}[N/m]$
15.00	1.65	0.58	1105.38
14.00	1.54	0.64	1222.27
13.00	1.43	0.70	1339.16
12.00	1.32	0.76	1456.05
11.00	1.21	0.83	1572.94
10.00	1.10	0.89	1689.83
9.00	0.99	0.95	1806.72
8.00	0.88	1.01	1923.61
7.00	0.77	1.07	2040.50
6.00	0.66	1.13	2157.39
5.00	0.55	1.19	2274.28
4.00	0.44	1.25	2391.17
3.00	0.33	1.32	2508.06
2.00	0.22	1.38	2624.95
1.00	0.11	1.44	2741.84
0.00	0.00	1.50	2858.74

Tab. 20 Vertical tail linear loading for manoeuvre

$\overline{w}_{VT,man}$ was also used to compute load distribution along chord

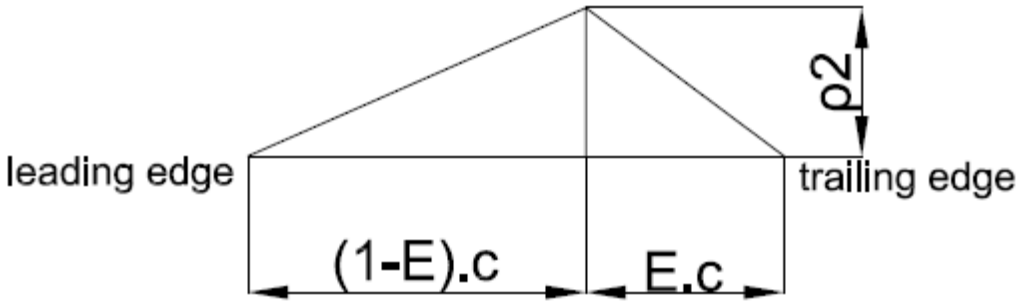

Fig. 19 Load distribution along chord for manoeuvres

It was estimated that $\rho 1 = 0$

From CS 23 Appendix A was excluded d' from formula for computing $\rho 1$

$$d' = \frac{2 - E}{3} = 0.53$$

Where $E = 0.41$

This value was afterwards used to compute $\rho 2$ and from $\rho 2$ was computed relative force proportions for fin and rudder.

The force acting point on fin was also computed for further substitution in FEM.

section no.	fin force acting point (from LE) $[m]$	q_{fin} $[N/m]$	T_{fin} $[N]$	$M_{o,fin}$ $[N.m]$	q_{rud} $[N/m]$	T_{rud} $[N]$	$M_{o,rud}$ $[N.m]$
15.00	0.23	649.03	0.00	0.00	456.35	0.00	0.00
14.00	0.25	717.66	74.94	4.11	504.61	52.69	2.89
13.00	0.28	786.29	157.41	16.85	552.86	110.68	11.85
12.00	0.30	854.93	247.40	39.05	601.12	173.95	27.45
11.00	0.32	923.56	344.92	71.53	649.38	242.52	50.29
10.00	0.35	992.19	449.97	115.11	697.64	316.38	80.94
9.00	0.37	1060.83	562.54	170.63	745.89	395.54	119.98
8.00	0.40	1129.46	682.64	238.91	794.15	479.98	167.98
7.00	0.42	1198.09	810.27	320.77	842.41	569.72	225.54
6.00	0.44	1266.73	945.42	417.04	890.67	664.75	293.23
5.00	0.47	1335.36	1088.11	528.55	938.92	765.07	371.63
4.00	0.49	1403.99	1238.31	656.11	987.18	870.69	461.33
3.00	0.52	1472.62	1396.05	800.56	1035.44	981.60	562.90
2.00	0.54	1541.26	1561.31	962.72	1083.70	1097.80	676.92
1.00	0.56	1609.89	1734.10	1143.42	1131.95	1219.29	803.97
0.00	0.59	1678.52	1914.41	1343.48	1180.21	1346.07	944.64

Tab. 21 Vertical tail manoeuvre loading distribution

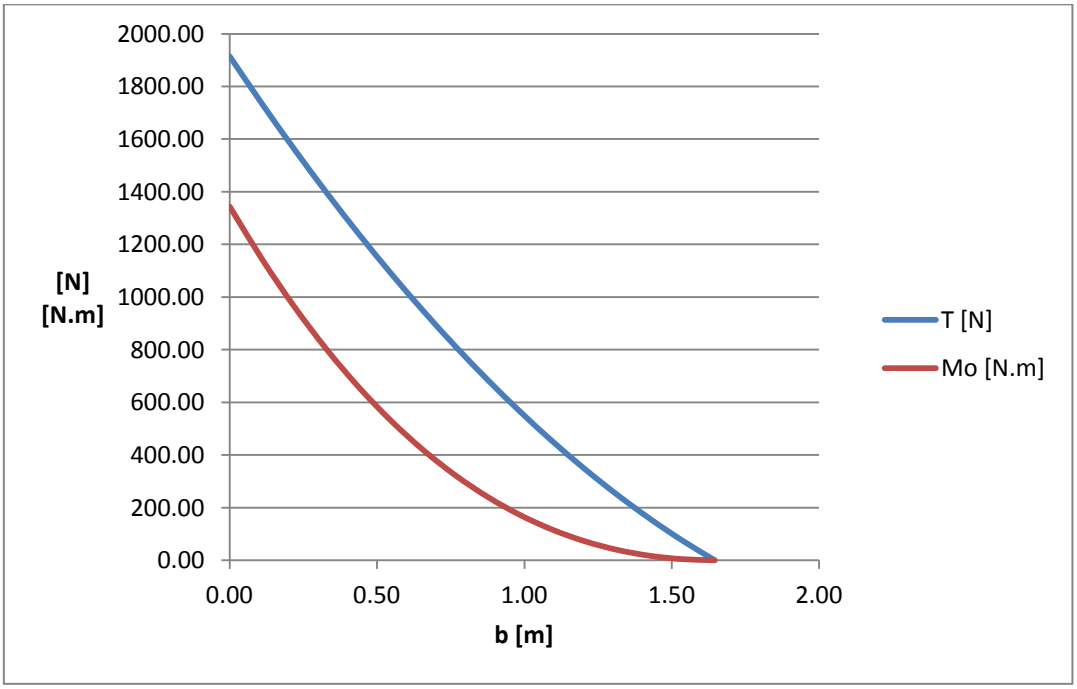

Fig. 20 Fin load distribution from manoeuvres without reaction forces

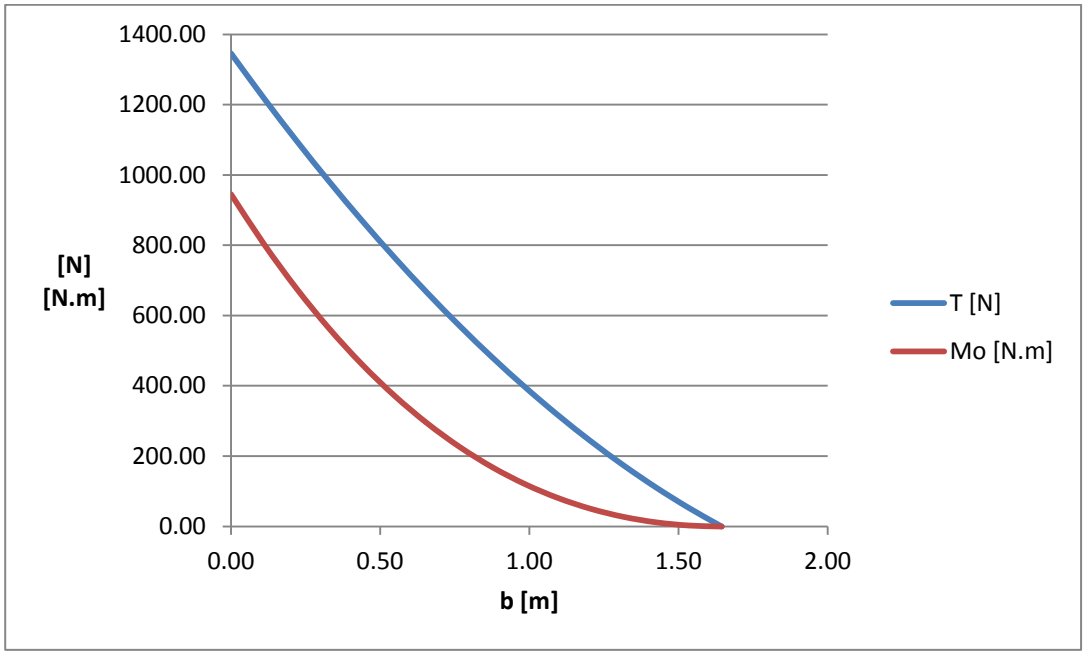

Fig. 21 Rudder load distribution for manoeuvre loading without reaction forces

Then the resultant force from line loading over the rudder was necessary to compute:

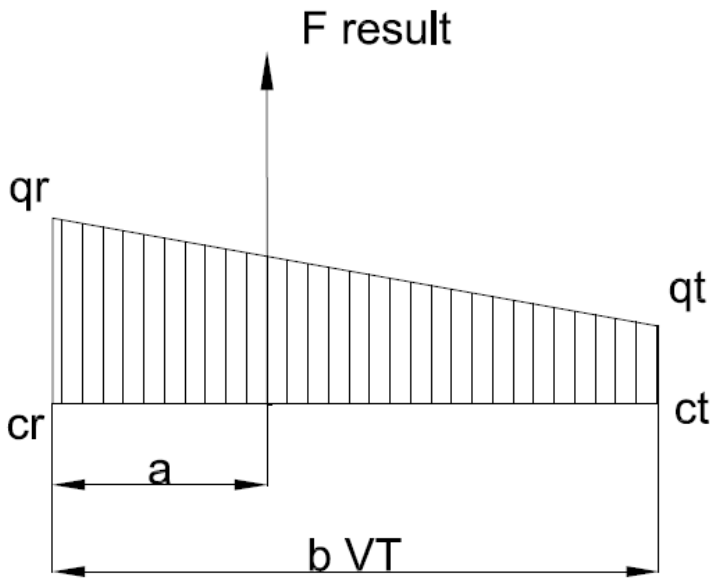

Fig. 22 Resultant force from line loading

$$a = \frac{\left(q_k \,.\, \frac{b_{VT}^2}{2} \,.+ (q_r - q_t) \,.\, \frac{b_{VT}^2}{6}\right)}{q_t \,.\, b_{VT} + (q_r - q_t) \,.\, \frac{b_{VT}}{2}} = 0.7\ m$$

Then the reaction forces was needed to compute, process was the same as for computing the reaction forces in rudder hinges for gust loading. At first there was used force and moment equivalence which led to achieve R_1 and R_2 forces.

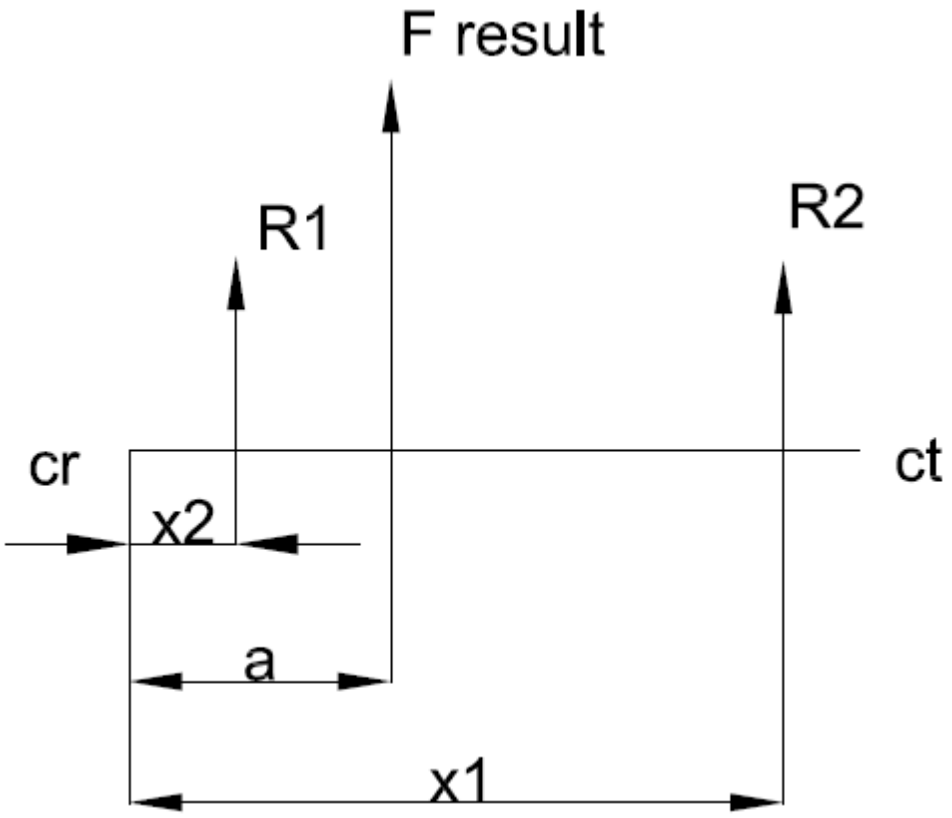

Fig. 23 Reaction forces on rudder

$$R_2 = \frac{\left(-F_{result} \,.\, (a - x_2)\right)}{x_1 - x_2} = -558.54\ N$$

$$R_1 = -F_{result} - R_2 = -787.53\ N$$

After applying the forces on the rudder and fin distribution graphs of load distribution along span were received.

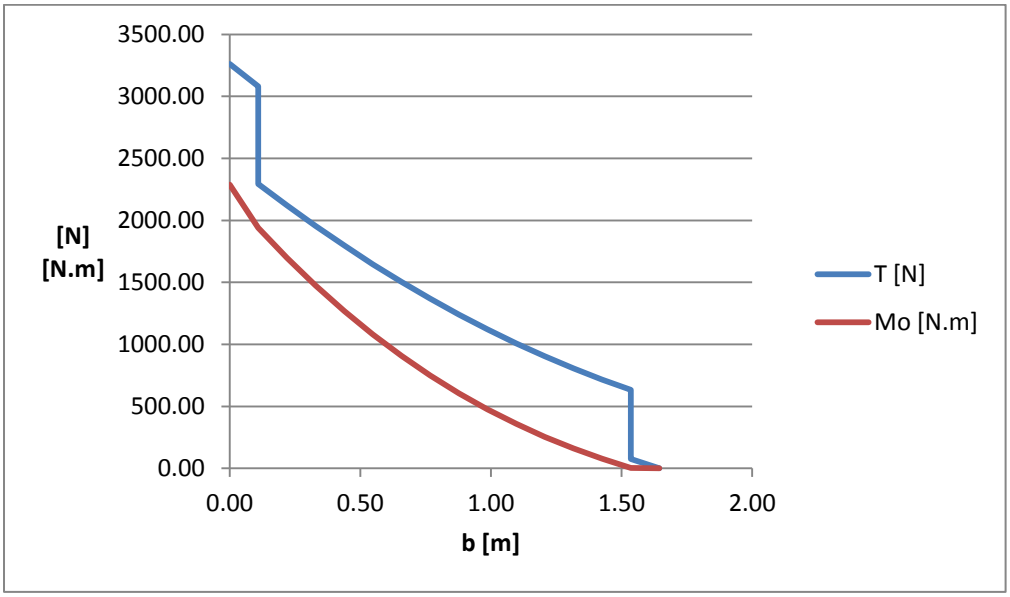

Fig. 24 Load distribution along fin, reaction forces included

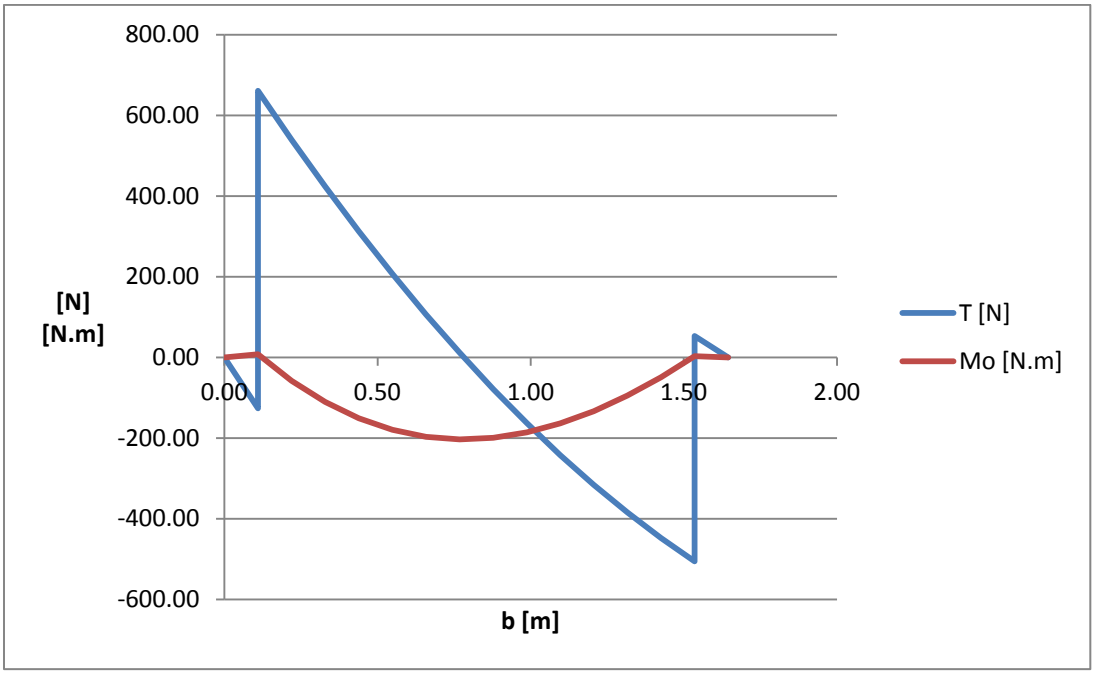

Fig. 25 Load distribution along rudder, reaction forces included

7. Load combination

With respect to the CS 23 there were assumed five cases that can occur during flight. All the forces will be evaluated for root chord and in FEM model will be applied to the fuselage even for forces acting on fin, because control surfaces has no effect on each other along span due to fuselage attachment of the horizontal tail.

The safety factor for all these forces is $sf = 2.25$ according to CS-VLA with consideration to the size of the aircraft, the forces will be evaluated in chapter, where also compensation forces will be specified.

7.1 Gust for vertical tail and trim for horizontal tail

For this load case would be sufficient trim load for load factor $n = 1$ but there was preferred more conservative assumption and chosen was maximum trim load that can occur.

$F_{VT,gust} = 2761.98\ N$

$F_{HT,trim} = -4735.97\ N$

7.2 Vertical tail manoeuvre and horizontal tail trim

In this load case was again used maximal forces that acts on tail surfaces.

$F_{VT,man} = 3258.96\ N$

$F_{HT,trim} = -4735.97\ N$

7.3 Tail manoeuvre forces

In this load case there was again used CS-VLA 447 regulation which says that "75% of the loads according to CS-VLA 423 for the horizontal tail and CS-VLA 441 for the vertical tail must be assumed to be acting simultaneously."[5]

$F_{VT,man} = 3258.96\ N\ .\ 0.75 = 2445.36\ N$

$F_{HT,man} = -4884.77\ N\ .\ 0.75 = -3664.19\ N$

In further computation manoeuvring forces do not have to be considered, because there are bigger forces acting in the same direction, for example in previous chapter $F_{VT,man}$ with combination of $F_{HT,trim}$.

7.4 Maximum horizontal tail loading

In this case it is required to achieve maximum bending moment in vertical direction acting on the rear part of the aircraft.

The maximum forces acting on horizontal tail are in case of manoeuvre – upwards and gust – downwards.

$F_{HT,man} = 3036.14\ N$

$F_{HTgust} = -5796.13\ N$

7.5 Unsymmetrical horizontal tail loading

For this sub chapter was used CS 23.427 regulation paragraph (b)

In the absence of more rational data for aeroplanes that are conventional in regard to location of engines, wings, horizontal surfaces other than main wing, and fuselage shape –

1) 100% of the maximum loading from the symmetrical flight conditions may be assumed on the surface on one side of the plane of symmetry; and
2) The following percentage of that loading must be applied to the opposite side:

   $\% = 100 - 10\ (n - 1)$, where n is the specified positive manoeuvring load factor, but this value may not be more than 80%. [2]

The loading which will be worked with is maximum loading applied on horizontal tail. This loading acts on tail during negative gusts.

$F_{HT,gust} = -5796.13\ N$

$M_{o,HT,gust} = -5186.95\ N\,.m$

The force and moment above act on both halves of horizontal tail simultaneously so it needs to be divided into left and right half.

$F_{HT,gust,R,L} = -2898.55\ N$

$M_{o,HT,gust,R,L} = -2593.47\ N\,.m$

At this point the formula from regulation can be applied, where $n = n_1$, what is the maximum design load factor.

$\% = 100 - 10\,(n-1) = 72\ \%$

$F_{HT,gust\ 72} = -2086.96\ N$

$M_{o,HT,gust,72} = -1867.30\ N.m$

This sub chapter in FEM analysis will be performed by inserting of arm in the place of horizontal tail on which will be applied difference of forces computed above. From moment and force difference there will be computed arm length.

$F_{HT,gust,diff} = -811.59\ N$

$M_{o,HT,gust,diff} = -726.17\ N\,.m$

$r = \frac{M_{o,HT,gust,diff}}{F_{HT,gust,diff}} = 0.89\ m$

8. Structure layout

The aircraft is made of composite, so in that case the outer shape will be made in two halves made in moulds which will be glued together after all inner structure will be set onto its place.

Inner structure consists of inner wing spars, frame which reinforces the cut outs for windows, passenger doors and baggage door, bulkheads, wing rib and tail ribs and spars.

8.1 Fuselage

The fuselage layout was created with inner wing, with wings attached to the fuselage spars by pivots, what was preferred due to transportation of the aircraft, where whole aircraft has to fit into ship container.

The fuselage structure will be made as sandwich, with first ply made of glass fabric, after which follows carbon fabric, Herex and the last ply is carbon fabric. Critical places will be reinforced by unidirectional carbon fibres.

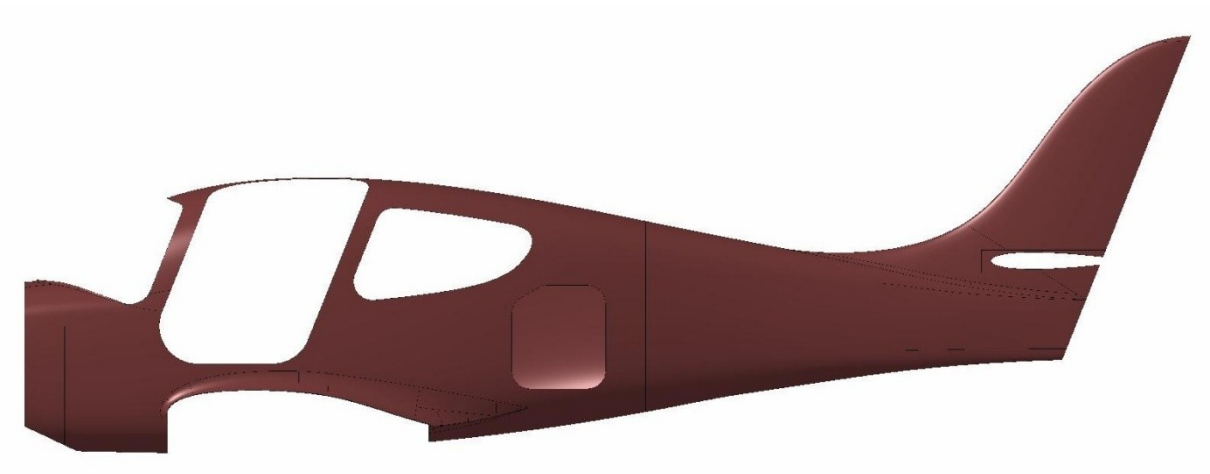

Fig. 26 Fuselage

8.2 Window and luggage door frame

The primary purpose of these frames is to reinforce frame which structural stiffness is low due to cut outs for windows and doors.

The frames will be made just from layers of carbon fabric.

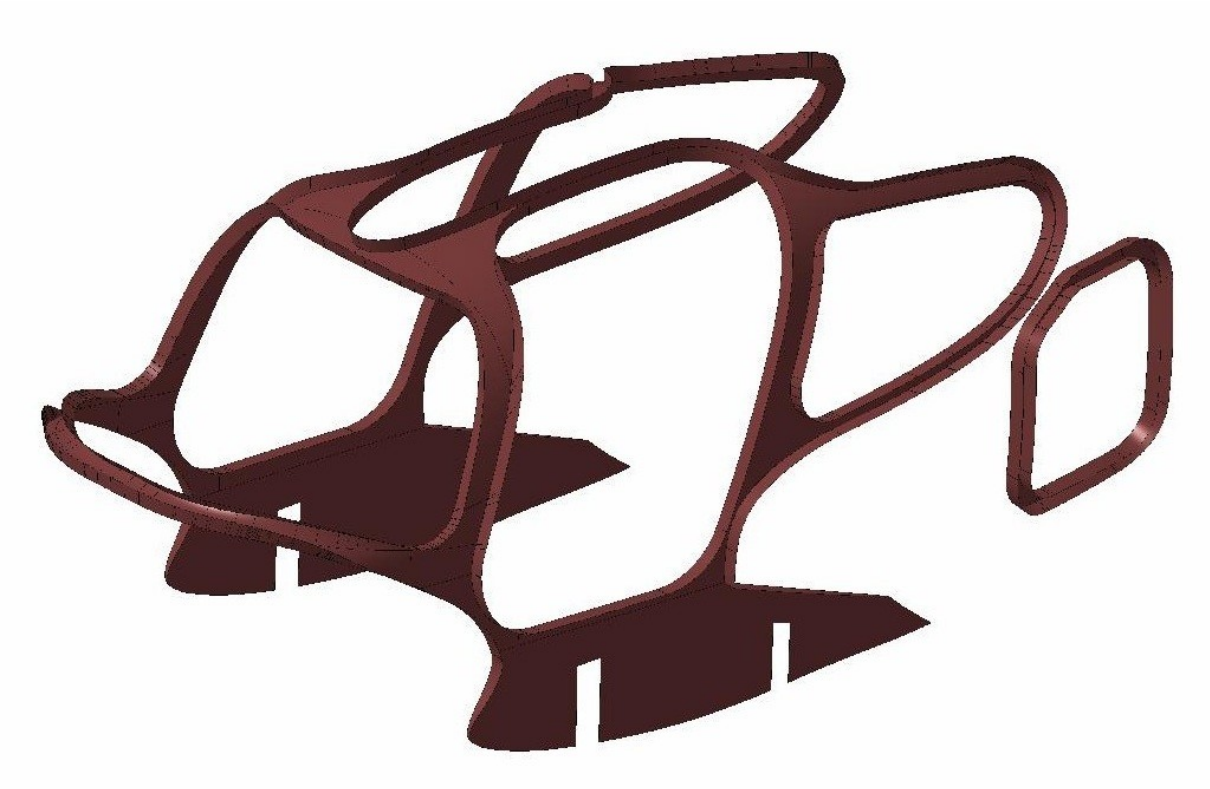

Fig. 27 Fuselage frame

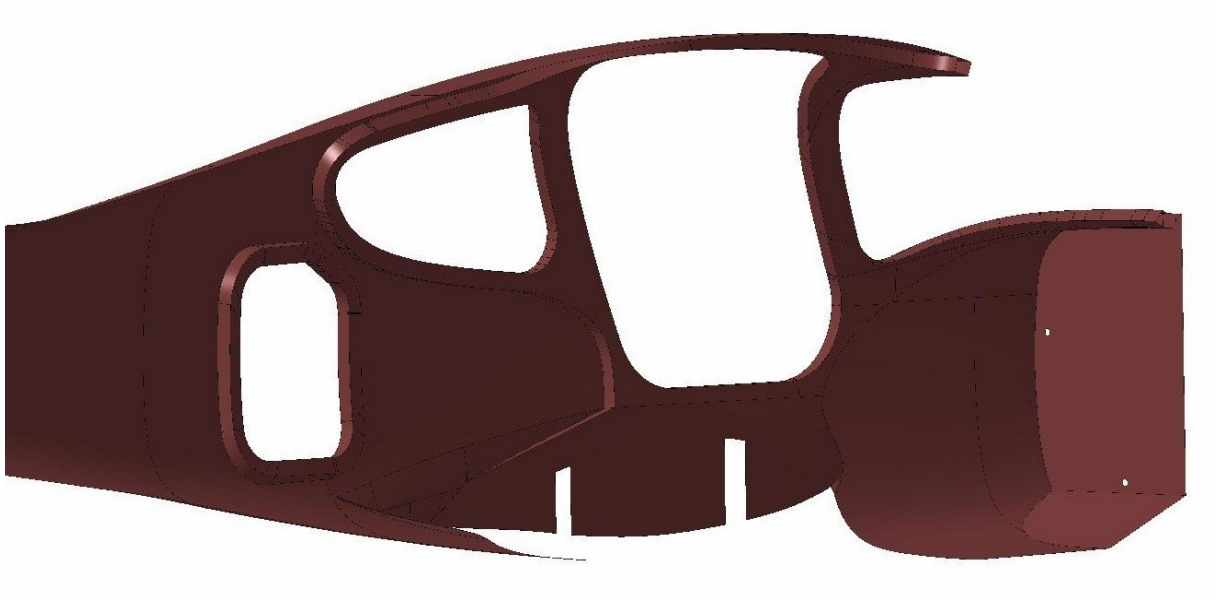

Fig. 28 Frame inside fuselage

The frame design from technological and structural point of view cannot be used, its purpose in this thesis is just to show that somehow this way it could be designed, but considering fact that at first the moulding of the frame is provided and afterwards it has to be fitted into fuselage, which is already glued together it could be impossible to fit. Second thing is that on this frame, especially in the rib-part, where should landing gear be mounted what is also nearly impossible.

8.3 Inner wing spars

The wing inner structure carries loading via two spars. Those two spars are attached to the inner wing spars by steel pivots, two for each spar.

The inner wing spars will be made of unidirectional carbon fibers and carbon fabric with brass bushes on the places, where pivots from wing spars will be attached to the inner wing, what prevents buckling of laminate structure. After the inner wing spars will be manufactured, it will be glued to the inner wing cover all these parts will be glued to the fuselage. The inner wing cover will have the same layers as fuselage.

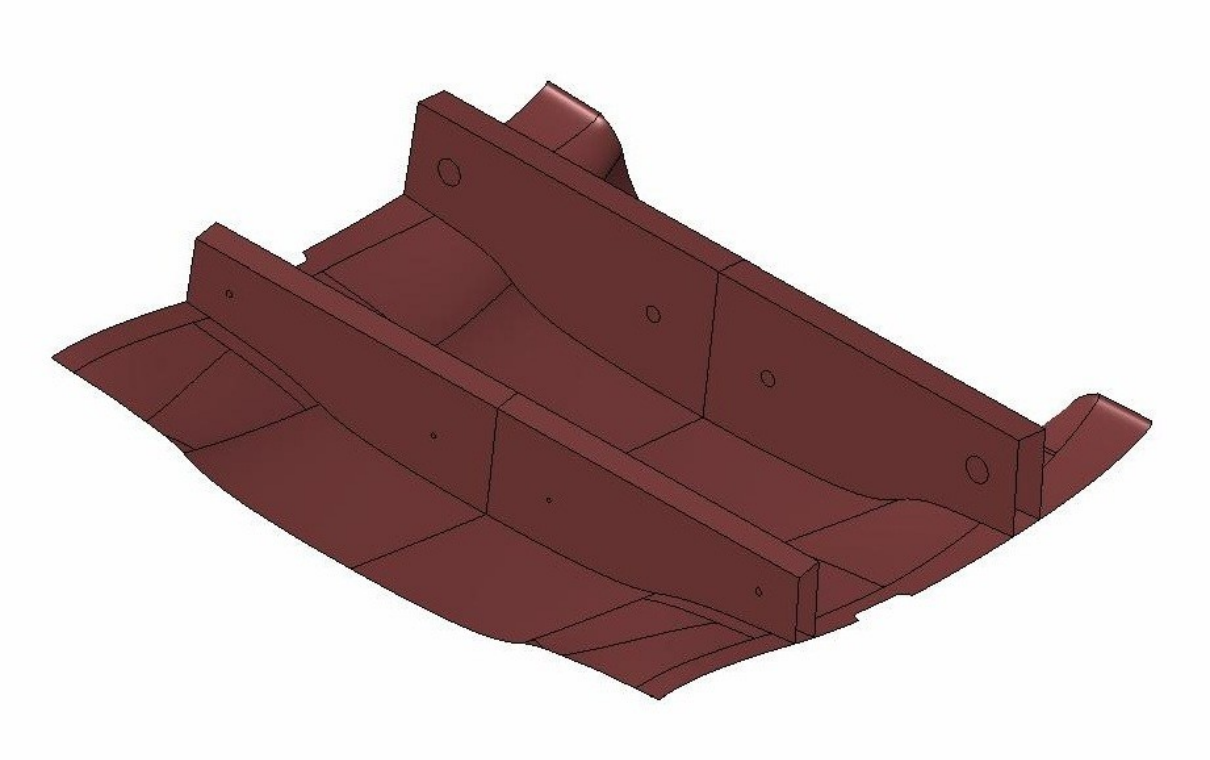

Fig. 29 Inner wing spars, inner wing cover

The pivot diameters were computed from maximum wing loading.

Front spar:

$M_{o,front} = 115\,910\ N\,.m$

$T_{front} = 54\,000\ N$

These forces include safety factor $sf = 2.25$

Then the distance between pivots was selected, the inner wing spars has the same length, so distance between pivots is the same for both spars:

$r = 0.541\ m$

From these values reaction forces on each pivot were computed:

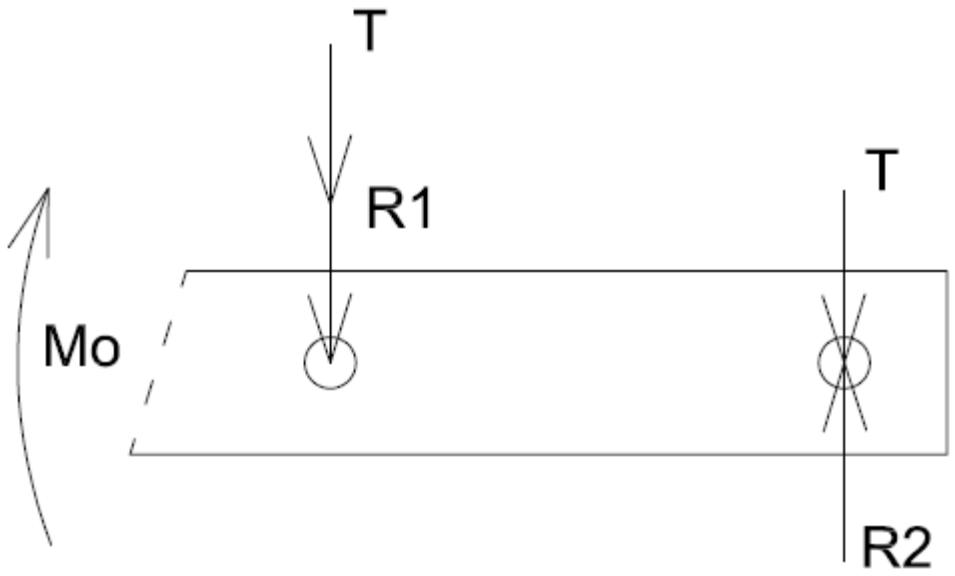

Fig. 30 Inner wing reaction forces

$R1 = 268251.39\ N$

$R2 = 160251.39\ N$

Front wing spar thickness was set to $70\ mm$ and wall thickness of the inner wing spar was set to $10\ mm$. The reaction forces were divided by wall thickness of wing and inner wing to evaluate linear loading acting on the pivot.

$q1_{R1} = 3832162\ N/m$

$q2_{R1} = 13412569\ N/m$

$q1_{R2} = 2289305\ N/m$

$q2_{R2} = 8012569\ N/m$

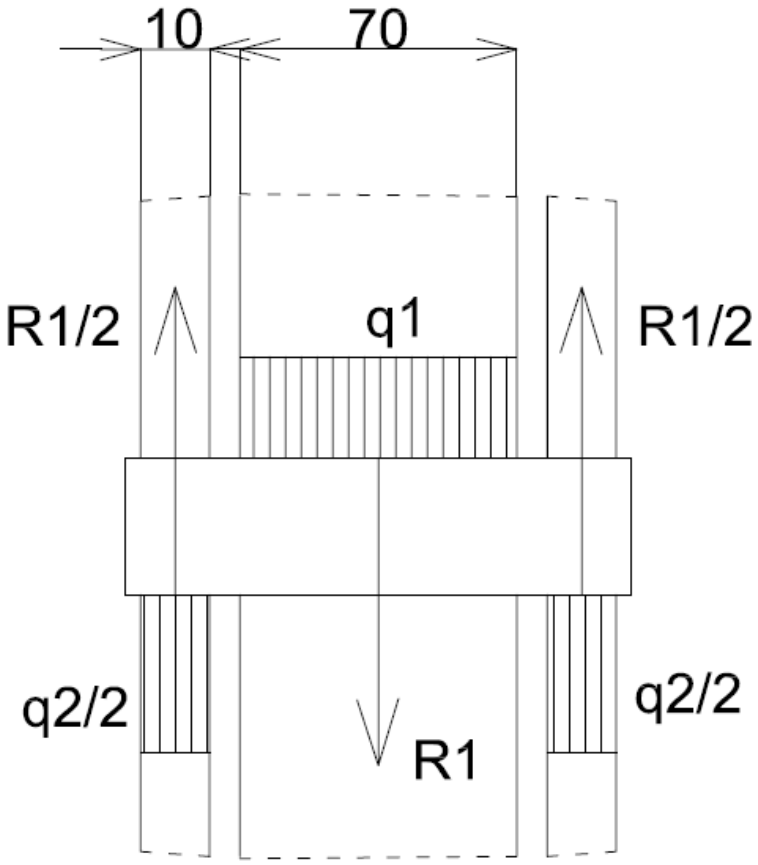

Fig. 31 Linear loading acting on pivot

Linear loading was afterwards used to compute maximum force and moment acting on the pivots:

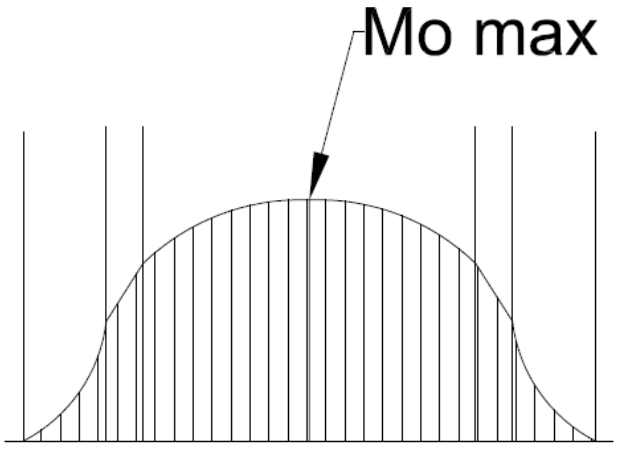

Fig. 32 Maximum moment acting on pivot

Outer pivot:

$F_{max} = 134125\ N$

$M_{o,max} = 3353\ N.m$

Inner pivot:

$F_{max} = 80125\ N$

$M_{o,max} = 2003\ N.m$

The steel for pivot was chosen L-W6H.6 with ultimate tensile strength $Rm = 640\ MPa$ and maximum stress for loading combination bending and shear was computed with HMH condition.

Pivot outer diameter:

$D = 56\ mm$

Pivot inner diameter:

$d = 34\ mm$

Bending stress:

$$\sigma = \frac{M_o}{W_o} = 3.21\ MPa$$

Shear stress:

$\tau = 352.84\ MPa$

$\sigma_{HMH} = \sqrt{\sigma^2 + 3.\tau^2} = 611\ MPa$

Pivot safety factor:

$$sf_{stress} = \frac{Rm}{\sigma_{HMH}} = 1.05$$

Then safety factor for inner wing spar wall (this value has to be lower than 1 to prevent delamination):

$$sf_{delam} = \frac{R1}{1.6\ .150\ .10\ .2\ .\ D} = 0.998$$

The same process was used for inner pivot:

Pivot outer diameter:

$D = 34\ mm$

Pivot inner diameter:

$d = 17\ mm$

Bending stress:

$$\sigma = \frac{M_o}{W_o} = 4.15\ MPa$$

Shear stress:

$\tau = 353\ MPa$

$\sigma_{HMH} = \sqrt{\sigma^2 + 3.\tau^2} = 611\ MPa$

Pivot safety factor:

$$sf_{stress} = \frac{Rm}{\sigma_{HMH}} = 1.05$$

Then failure indices for inner wing spar wall (this value has to be lower than 1 to prevent delamination):

$$FI_{delam} = \frac{R1}{1.6\,.150\,.10\,.2\,.D} = 0.98$$

The same process was used for rear spar of inner wing:

$$M_{o,front} = 15201\ N\,.m$$

$$T_{front} = 7090\ N$$

$$R1 = 28098\ N$$

$$R2 = 21008\ N$$

Front wing spar thickness was set to 50 mm and wall thickness of the inner wing spar was set to 4 mm. The reaction forces were divided by wall thickness of wing and inner wing to evaluate linear loading acting on the pivot.

$$q1_{R1} = 561959\ N/m$$

$$q2_{R1} = 3512245\ N/m$$

$$q1_{R2} = 420159\ N/m$$

$$q2_{R2} = 2625996\ N/m$$

Outer pivot:

$$F_{max} = 14048\ N$$

$$M_{o,max} = 238\ N.m$$

Inner pivot:

$$F_{max} = 10503\ N$$

$$M_{o,max} = 178\ N.m$$

Pivot diameter

$$D = 15\ mm$$

Bending stress:

$$\sigma = \frac{M_o}{W_o} = 0.72\ MPa$$

Shear stress:

$$\tau = 79.5\ MPa$$

$$\sigma_{HMH} = \sqrt{\sigma^2 + 3.\tau^2} = 138\ MPa$$

$$sf_{stress} = \frac{Rm}{\sigma_{HMH}} = 4.6$$

This safety factor for stress is high because it would be difficult to make hole in such thin pivot.

$$sf_{delam} = \frac{R1}{1.6\ .150\ .10\ .2\ .D} = 0.98$$

The same process was used for inner pivot:

Pivot diameter:

$$D = 11\ mm$$

Bending stress:

$$\sigma = \frac{M_o}{W_o} = 1.37\ MPa$$

Shear stress:

$$\tau = 110.5\ MPa$$

$$\sigma_{HMH} = \sqrt{\sigma^2 + 3.\tau^2} = 191\ MPa$$

Stress safety factor is high again due to small pivot diameter.

$$sf_{stress} = \frac{Rm}{\sigma_{HMH}} = 3.34$$

$$sf = \frac{R1}{1.6\ .150\ .10\ .2\ .D} = 0.99$$

Different pivot diameter is not ideal considering manufacturing factor, but considering pivot weight is better to design pivots as light as possible.

Pilot and passenger seats were also taken into account. Designing distance between wing spars, the seat for the passenger is suggested in such position that person sitting on the rear seat will have legs between spars.

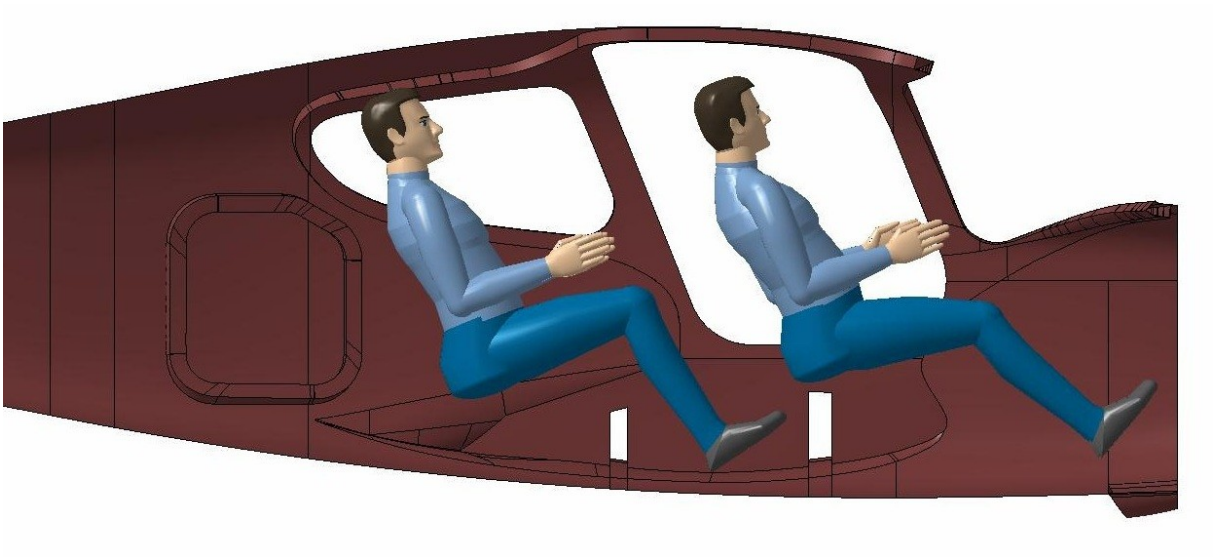

Fig. 33 Pilot and passenger position

8.4 Bulkheads

In the first bulkhead layout is four bulkheads along fuselage. This is too much for composite fuselage, but this is because of further FEM computation, where will be picked one or two of these bulkheads, depending on place where loading is high.

The first bulkhead behind cabin has thicker wall than the others because of separating the luggage and tail part of the aircraft. This bulkhead will have Velcro around the edge, which will be used for attaching thin laminate wall that close the hole in bulkhead and prevents luggage from moving to the tail part of the aircraft.

The first bulkhead will be used for attaching engine mounts. Due to that it has to be really stiff to withstand thrust, mass force and torque moment created by engine. The engine mounts will be attached to this bulkhead by four bolts.

The bulkhead layers will consist of carbon fabric with Herex core and the area around point where bolts are attached will be reinforced by plywood and additional fabric layers.

On the bottom side of the bulkheads is created gap, where is suggestion of placing push – pull rods for controlling elevator and rudder.

Layers of the tail bulkheads will be made just from carbon fibres and Herex core.

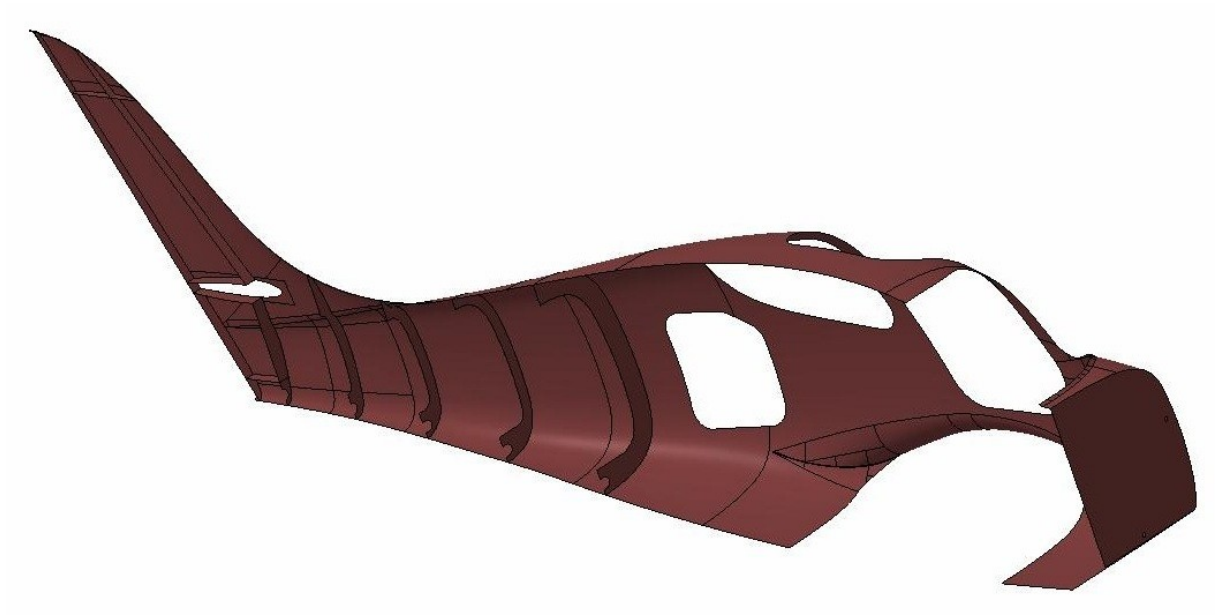

Fig. 34 Bulkheads, horizontal tail attachment and tail ribs inside the fuselage

8.5 Fuselage rib

Purpose of fuselage rib is to keep airfoil shape still during all flight conditions, transfer shear flow and prevent wing from moving forward or rear by holes (see figure below). The wing spars are $5\ mm$ thinner than actual distance between inner wing walls to prevent abrasion during wing mounting or dismantling what could have negative effect on structural strength. Due to that factor there are two pins laminated into wing root rib which will be set into fuselage rib during mounting of the wing. The housing of those pins will be made from brass and laminated into rib.

Inside wing box rib is made hole where will be landing gear placed. This part of the rib also supports landing gear and transfer landing gear loads into fuselage skin and cabin reinforcement.

The fuselage rib plies consists of carbon fabric and Herex.

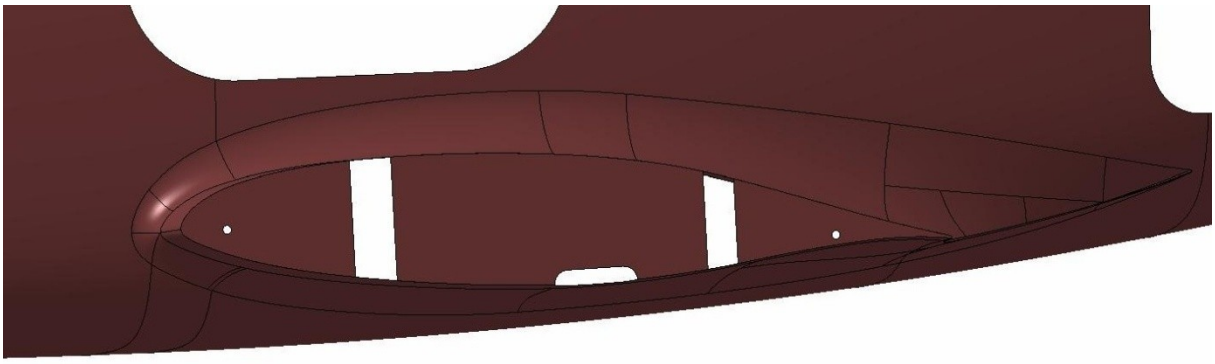

Fig. 35 Fairing rib

8.6 Horizontal tail attachment

This part is important to transfer force and moment from horizontal tail to fuselage. The horizontal tail will be glued on the top and bottom to the flange which is inside the fuselage. The flange is attached to the fuselage skin on the sides and fin spars on the top and bottom.

Flange consists of carbon fabric plies and Herex.

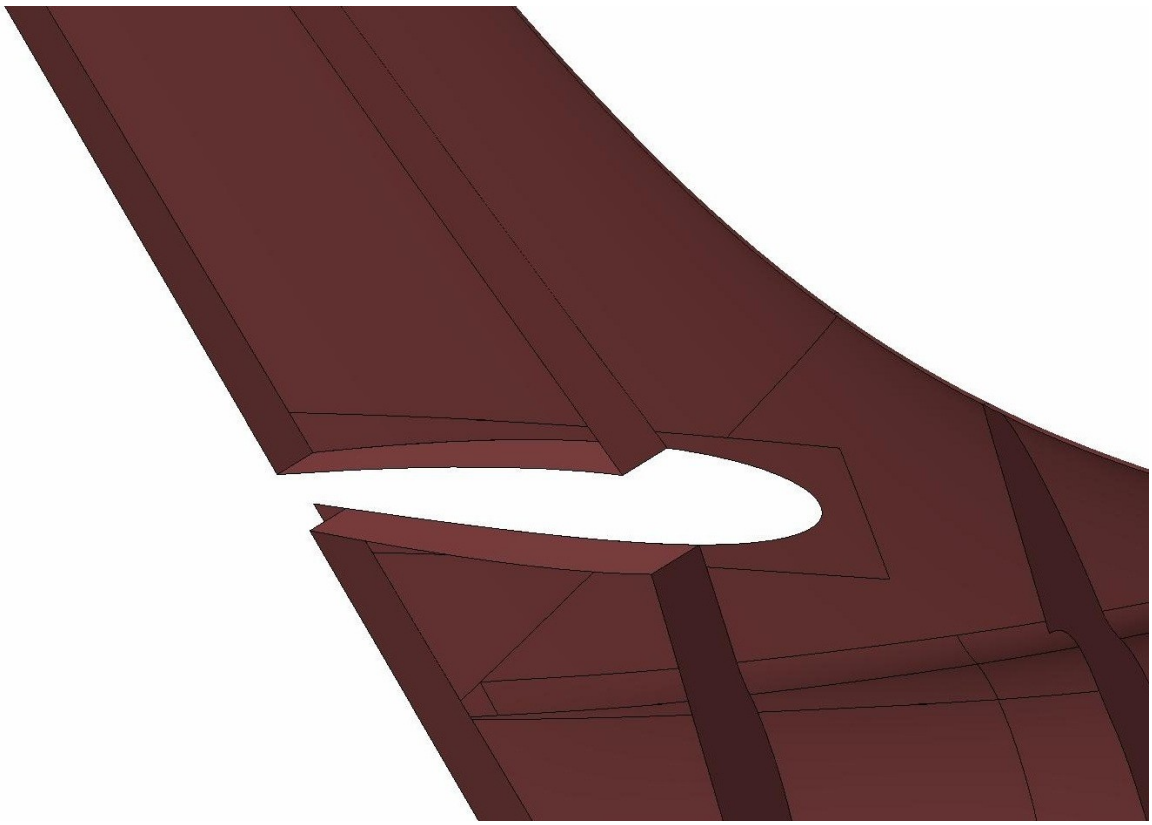

Fig. 36 Horizontal tail mounting flange

Mounting of the horizontal tail will be provided from rear side of the aircraft. The glue will be applied to the flange surface and then stabilizer will be inserted through space in fin rear spar. This space will be afterwards closed by lamination with few plies of carbon fabric.

8.7 Fin ribs

In the fin structure there will be just two fins – on the top and on the bottom. On those ribs the rudder hinges will be attached, so it will help to transfer force acting on the rudder into fin.

Fin ribs consist of carbon fabric plies with Herex core.

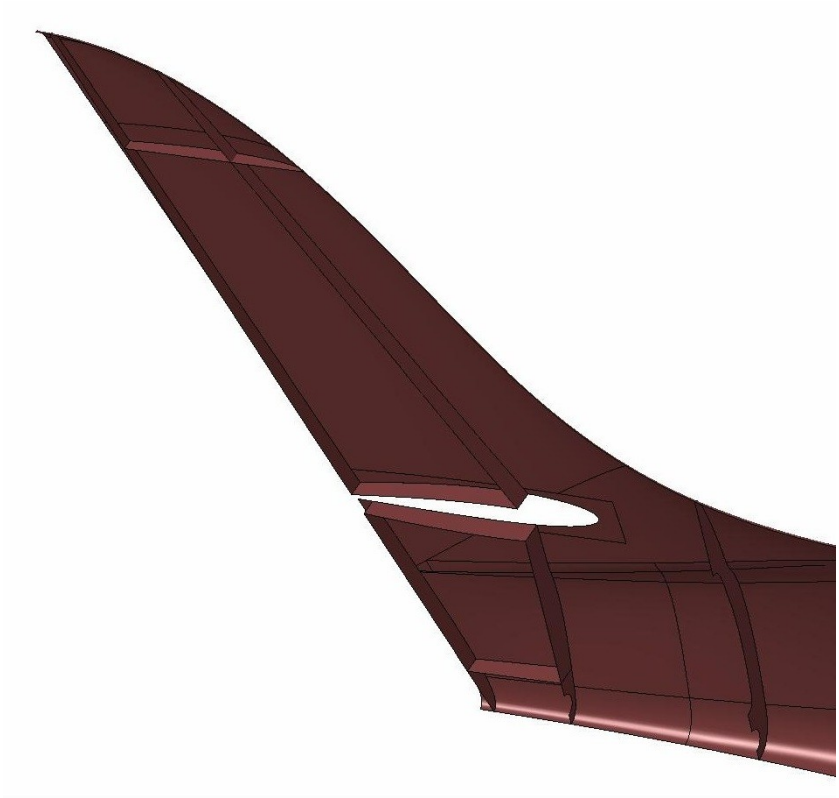

Fig. 37 Fin ribs

8.8 Inner wing reinforcements

The inner wing reinforcements have purpose in stiffening and better transferring loads from inner wing to fuselage skin and frame. They are created from carbon fabric plies and glued to the frame wall, inner wing and fuselage in the place where fairing is.

This solution probably will not be used on real aircraft. It is just for illustration of possible way how to solve stiffness of this part.

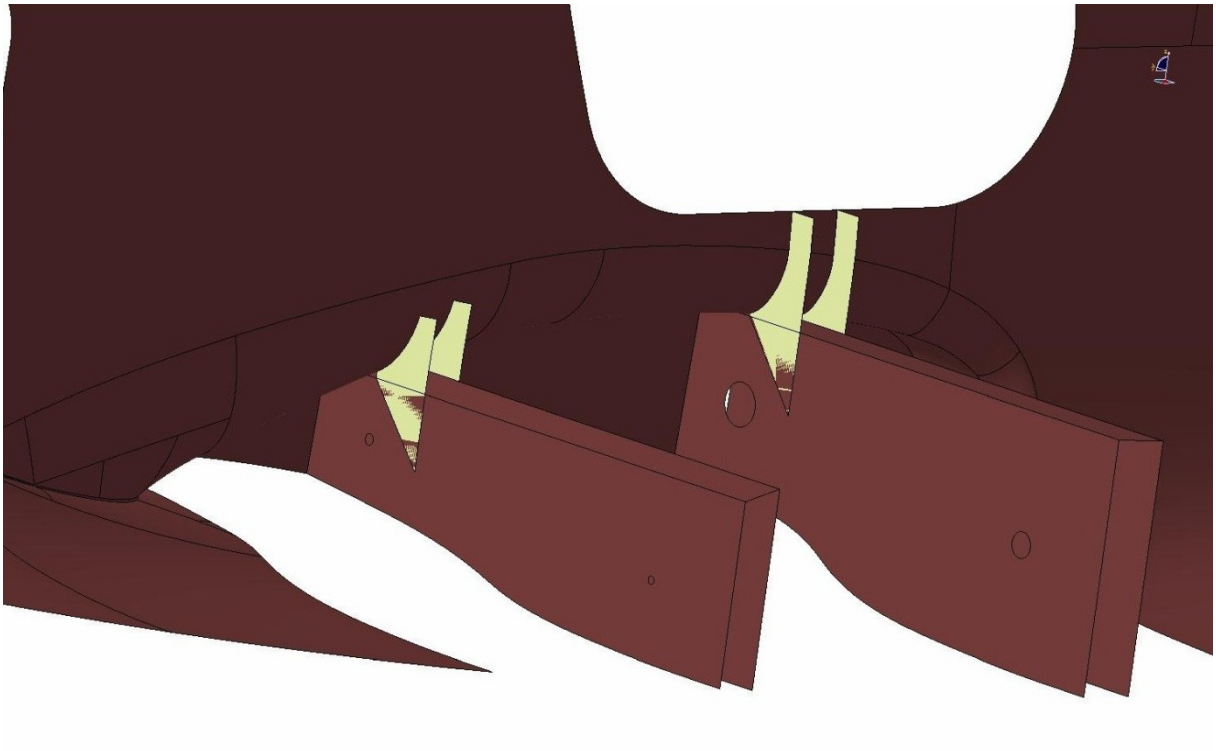

Fig. 38 Inner wing reinforcements

9. FEM model

The FEM model was created using CATIA V5 software with corrections and force applying in MSC Patran software after which follows linear analysis in MSC Nastran.

9.1 Mesh

The mesh model was created in CATIA V5 using TRIA3 and QUAD4 elements with size 30 mm. On tighter surfaces as leading and trailing edge of the wing, leading edge at the root of horizontal tail, bolt holes for engine mounts and local places of cabin frame was used mesh size 10 mm.

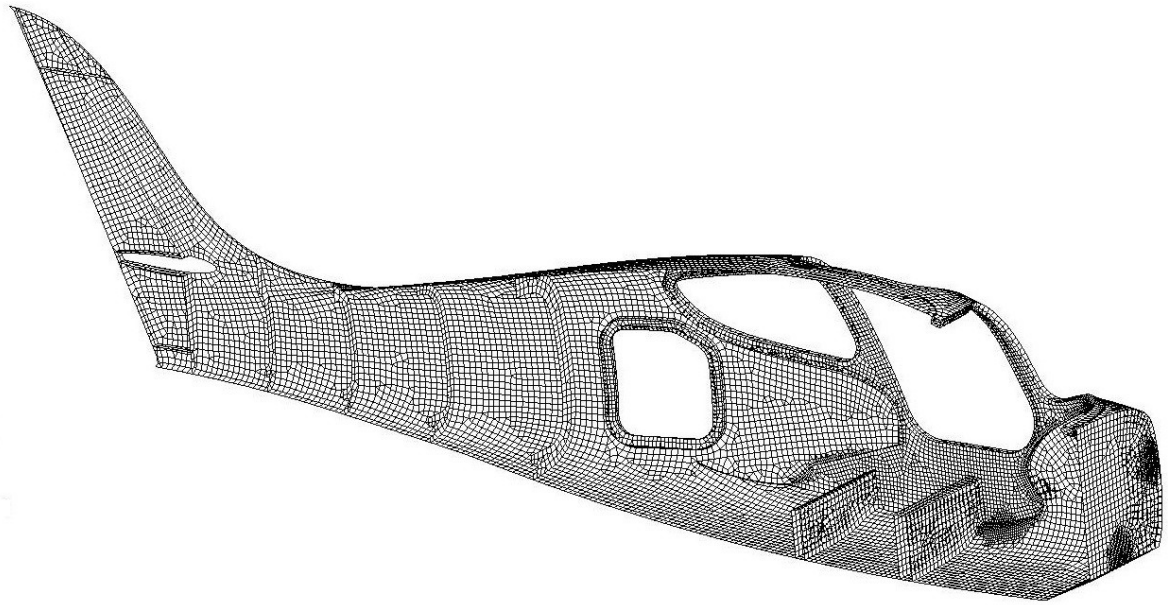

Fig. 39 Fuselage mesh

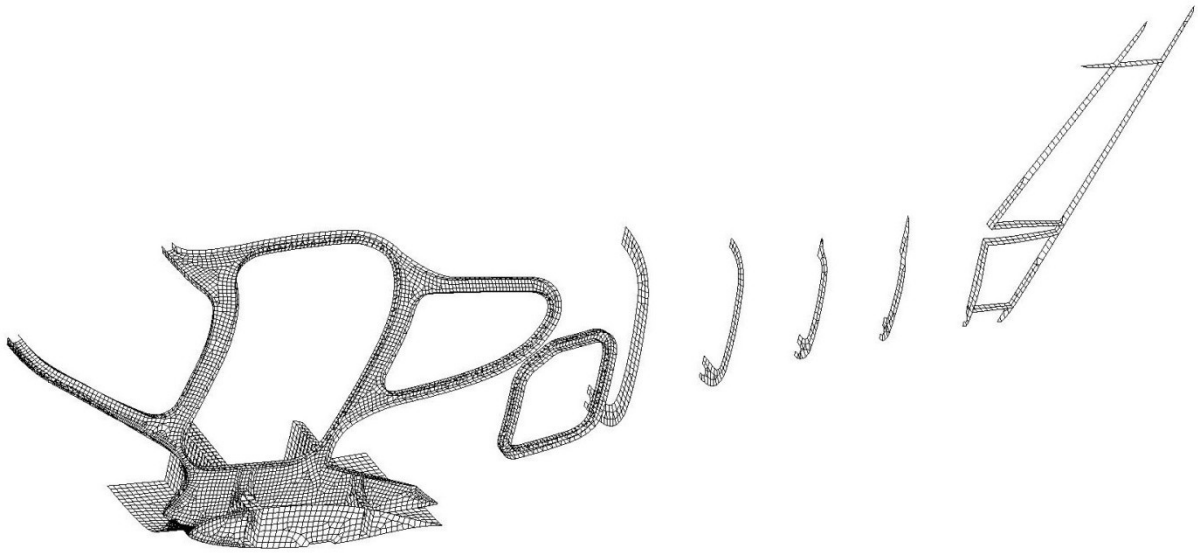

Fig. 40 Internal structure mesh

9.2 Boundary conditions

The engine mounts were replaced in Patran with structure made of four beams connected in engine centre of gravity. Into this point will be applied mass force and thrust as well as engine torque moment.

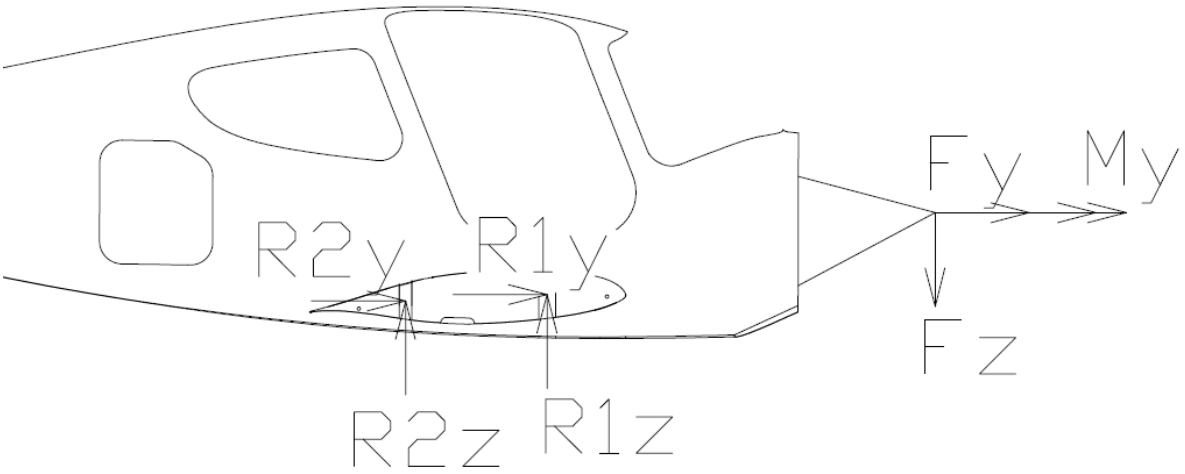

Fig. 41 Engine forces and fuselage displacement

9.3 Forces applied on the model

The forces acting on fin were compensated by five forces applied along fin span, in centre of force acting in each section of fin, and forces acting on the rudder hinges. The hinge forces were computed before and they do not need any compensation.

Forces acting on horizontal tail were reduced into one point, which was in 25% of horizontal tail root chord. For the case of unsymmetrical loading, there were two additional beams in the FEM model with arm computed in chapter 7. On those beams were applied forces acting on horizontal tail during unsymmetrical loading.

For these forces was applied safety factor $sf = 2.25$

9.3.1 Vertical tail load compensation

Manoeuvre loading

section no.	Force position along span [m]	$T\ [N]$	$T_{additional}\ [N]$	$M_{o,result}[N.m]$	force acting point from fin LE [m]
6.00	1.65	100.00	100.00	0.00	0.23
5.00	1.37	300.00	200.00	27.42	0.29
4.00	1.10	600.00	300.00	109.67	0.35
3.00	0.82	900.00	300.00	274.17	0.41
2.00	0.55	1300.00	400.00	520.92	0.47
1.00	0.27	1914.41	614.41	877.33	0.53
0.00	0.00	0.00	0.00	1402.20	0.59

Tab. 22 Manoeuvre loading compensation forces

The last line in table is just to check the resultant moment acting on the fin.

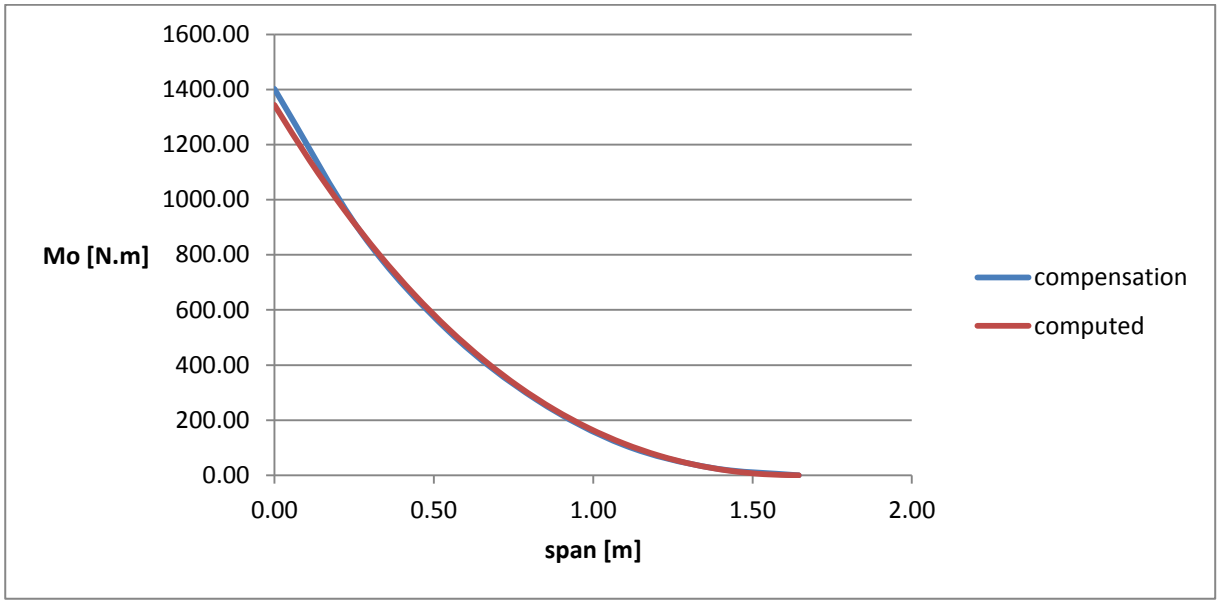

Fig. 42 Manoeuvre loading moment along fin span

Safety factor included:

section no.	force position along span [m]	force acting point from LE [m]	$T_{2.25}$ $[N]$	hinge forces [N]	
6.00	1.65	0.23	225.00		
5.00	1.37	0.29	450.00	1256.71	top
4.00	1.10	0.35	675.00		
3.00	0.82	0.41	675.00		
2.00	0.55	0.47	900.00		
1.00	0.27	0.53	1382.43	1771.95	bottom

Tab. 23 Manoeuvre loading – forces applied on model

Gust loading

section no.	position along span	T $[N]$	$T_{additional}$ $[N]$	$M_{o,result}$ $[N.m]$	force acting point from fin LE [m]
6.00	1.65	150.00	150.00	0.00	0.13
5.00	1.37	400.00	250.00	41.13	0.16
4.00	1.10	800.00	400.00	150.79	0.19
3.00	0.82	1200.00	400.00	370.13	0.22
2.00	0.55	1700.00	500.00	699.13	0.26
1.00	0.27	2577.50	877.50	1165.21	0.29
0.00	0.00	0.00	0.00	1871.87	0.32

Tab. 24 Gust loading compensation forces

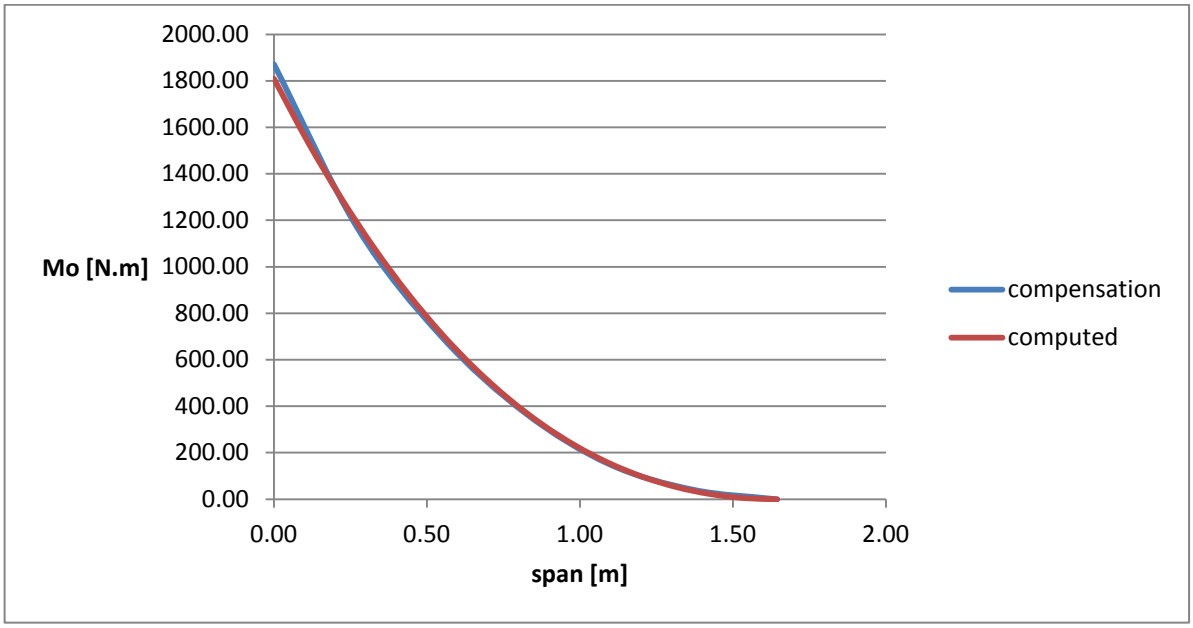

Fig. 43 Gust moment along fin span

Forces including safety factor:

section no.	position along span	force acting point from fin LE [m]	$T_{2.25}$ $[N]$	hinge forces [N]	
6.00	1.65	0.13	337.50		
5.00	1.37	0.16	562.50	173.44	top
4.00	1.10	0.19	900.00		
3.00	0.82	0.22	900.00		
2.00	0.55	0.26	1125.00		
1.00	0.27	0.29	1974.37	244.55	bottom

Fig. 44 Gust loading – forces applied on model

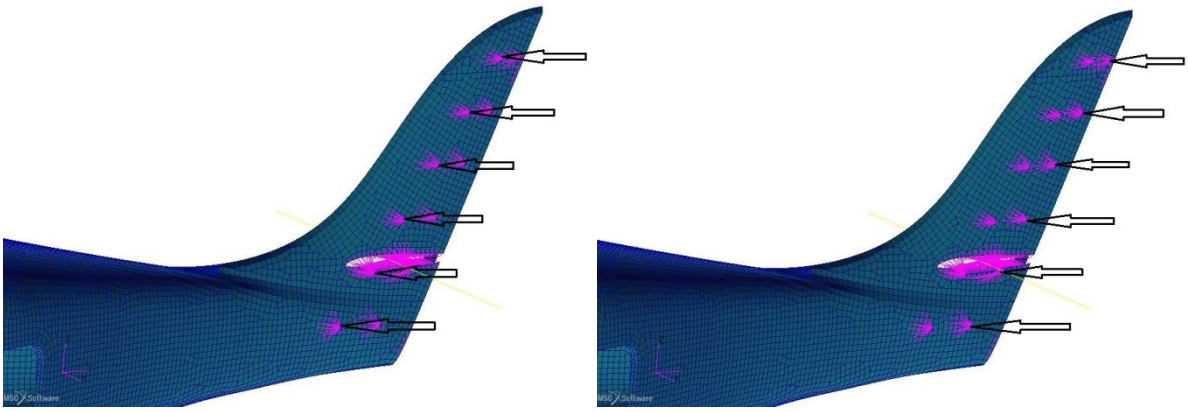

Fig. 45 Gust forces compensation (left), Manoeuvre forces compensation (right)

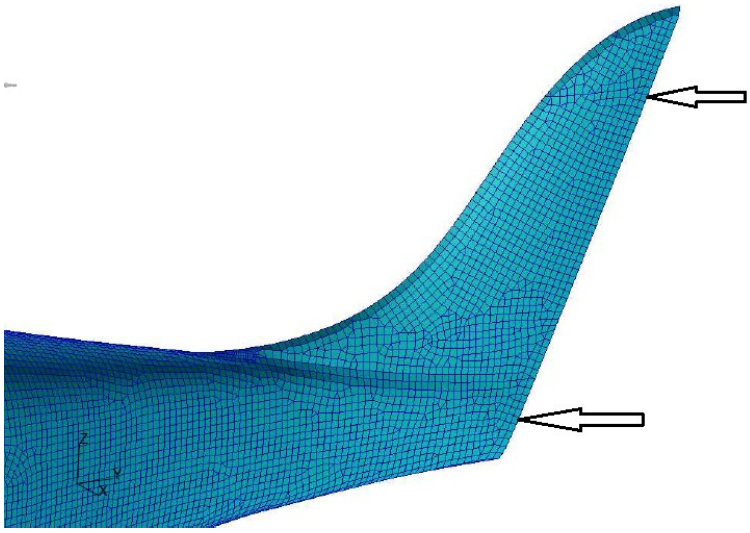

Fig. 46 Rudder hinge forces

9.3.2 Horizontal tail loads

F_{HT} $[N]$	$sf = 1.00$	$sf = 2.25$
Maximum up (manoeuvre)	3036.14	6831.31
Maximum down (gust)	-5796.13	-13041.29
Trim	-4735.97	-10655.93

Tab. 25 Horizontal tail loads

Horizontal tail unsymmetrical loading

$F_{HT,gust}$ $[N]$	$sf = 1$	$sf = 2.25$
100%	-2898.55	-6521.74
72%	-2086.96	-4695.65

Tab. 26 Horizontal tail unsymmetrical forces

Horizontal tail loads were applied in the aerodynamic centre of horizontal tail at root chord.

From all these forces will be considered tail loading combination:

- Vertical tail gust + Horizontal tail trim
- Vertical tail manoeuvre + Horizontal tail trim
- Maximum Horizontal tail force up
- Maximum Horizontal tail force down
- Horizontal tail unsymmetrical loading

9.3.3 Additional forces

Except the computed empennage loads the analysis will be provided with loads from engine, which acts at the point of engine centre of gravity and these loads are translated by engine mounts compensation.

gust			manoeuvre		
thrust Fy [N]	mass Fz [N]	torque My [N.mm]	thrust Fy [N]	mass Fz [N]	torque My [N.mm]
-3564.00	-23813.00	-1629900.00	-3564.00	-16800.00	-1629900.00

Tab. 27 Engine loads

9.4 Materials

The material properties were taken from IDAFLIEG [7] which purpose is to consider defects and imperfections caused by handmade manufacturing of the small aircrafts and gliders.

The types of composite fabrics were given by TL aircraft.

Material characteristics:

- Hexcel 43161 carbon fabric, weight 160 $\mathrm{g/m^2}$
- Hexcel 43199 carbon fabric, weight 200 $\mathrm{g/m^2}$
- Hexcel 48330 carbon UD 50 mm (300 g/m^2)
- Hexcel 2116 glass fabric, weight 105 $\mathrm{g/m^2}$
- Hexcel 1039 glass fabric, weight 163 $\mathrm{g/m^2}$
- Hexcel 1102 glass fabric, weight 285 $\mathrm{g/m^2}$
- Divinycell H60 sandwich foam core, density 60 $\mathrm{kg/m^3}$

	43161	43199	48330	2116	1039	1102
$E_1\ [MPa]$	39470	39470	39470	16600	16600	16600
$E_2\ [MPa]$	39470	39470	39470	16600	16600	16600
$\mu_{12}\ [-]$	0.037	0.037	0.037	0.037	0.037	0.037
$G_{12}\ [MPa]$	1620	1620	1620	3800	3800	3800
$G_{23}\ [MPa]$	1620	1620	1620	3800	3800	3800
$G_{13}\ [MPa]$	1620	1620	1620	3800	3800	3800
$\sigma_{1t}\ [MPa]$	146	146	146	95	95	95
$\sigma_{1c}\ [MPa]$	146	146	146	95	95	95
$\sigma_{2t}\ [MPa]$	146	146	146	95	95	95
$\sigma_{2c}\ [MPa]$	146	146	146	95	95	95
$\tau_x\ [MPa]$	146	146	146	95	95	95
$\rho\ [kg/m^3]$	1637	1637	1637	1637	1637	1637
$t\ [mm]$	0.26	0.32	0.48	0.12	0.18	0.3

Tab. 28 Carbon and glass fibre properties

	Divinycell H60	Plywood
$E\ [MPa]$	70.00	1000.00
$\mu_{12}\ [-]$	0.20	0.30
$\sigma_t\ [MPa]$	1.80	70.00
$\sigma_c\ [MPa]$	0.90	70.00
$\tau_c\ [MPa]$	0.70	20.00
$\rho\ [kg/m^3]$	60.00	800.00
$t\ [mm]$	5; 8	5.00

Tab. 29 Plywood and Divinycell properties

9.5 Element properties

To create element properties was used Laminate Modeller, what is one of Patran modules. Each layout was defined with thickness, area and orientation of each layer, which was afterwards set ply by ply on every structural part as seen in Appendix A.

10. Results

The structural analysis was made using mode solution 101 in Patran and further proceeded in Nastran, where was computed all load combinations.

For evaluation of laminate structure were used maximum failure indices criteria as a plot from Nastran output2 in Patran and for evaluation of sandwich structure was used ComPost software. For qualification of laminate and sandwich failures was used failure indices.

$$FI = \frac{computed\ stress}{allowable\ stress}$$

For this condition should be $FI < 1$ in whole fuselage structure.

10.1 Conditions of calculation

The material characteristics are severely under limits, what is caused by used literature, which is old and used for handmade computation where is considered, that places with stress concentrations will not be found, especially at the places with structural attachments. Due to this fact the stress indices computed in Patran may slightly exceed 1.

The failure indices for main supporting layers with big areas have to be under 1 to stay on the safe side.

The fuselage structure was evaluated considering the manufacturing process part by part, where the stress plot was displayed and maximum failure indices were shown as first step, following step was using ComPost which computed sandwich failure of each element. After the element failures were detected, the areas had been found and elements evaluated in detail.

10.2 Results evaluation

10.2.1 Fuselage skin

The fuselage loading failure indices were computed for all load cases, from these load from which were specified areas with potential failure of the structure.

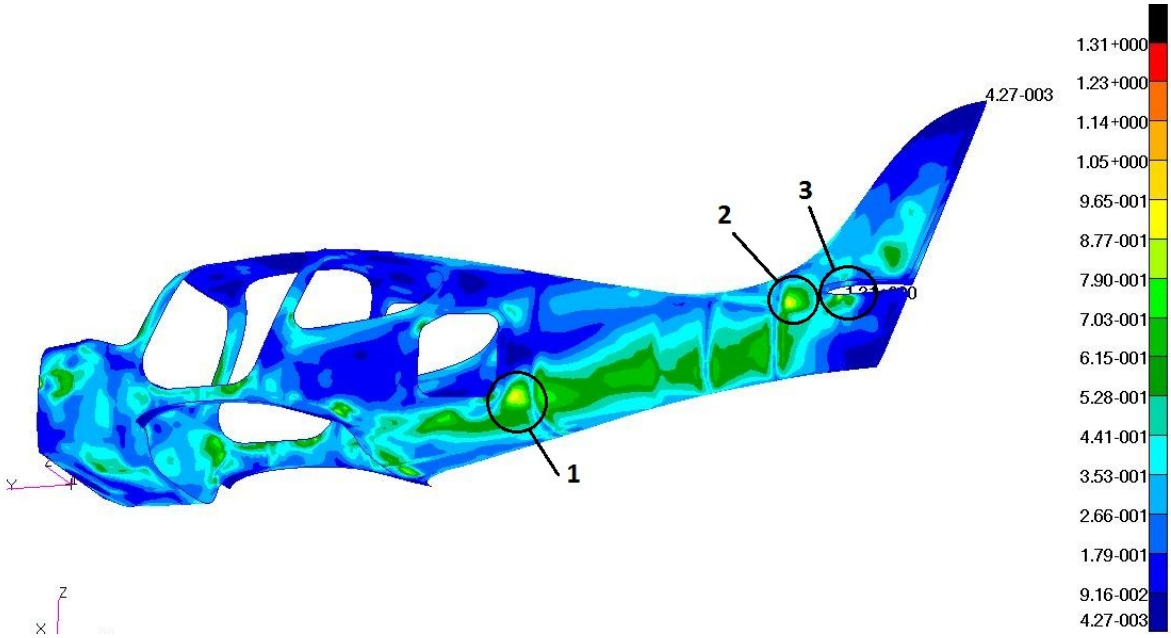

Fig. 47 Fuselage skin left side

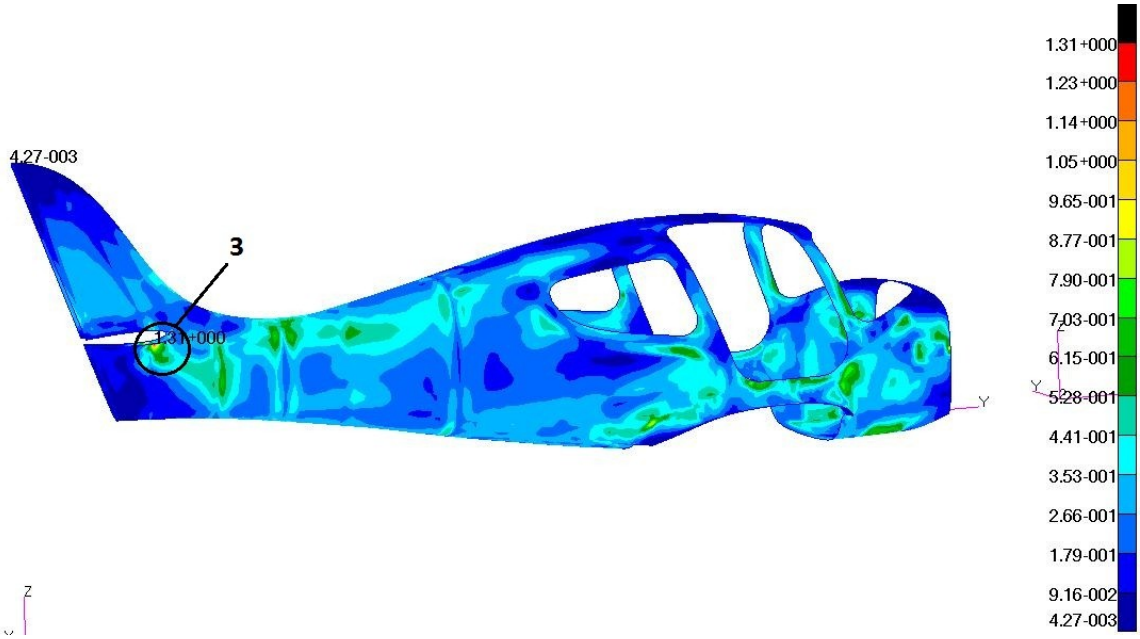

Fig. 48 Fuselage skin right side

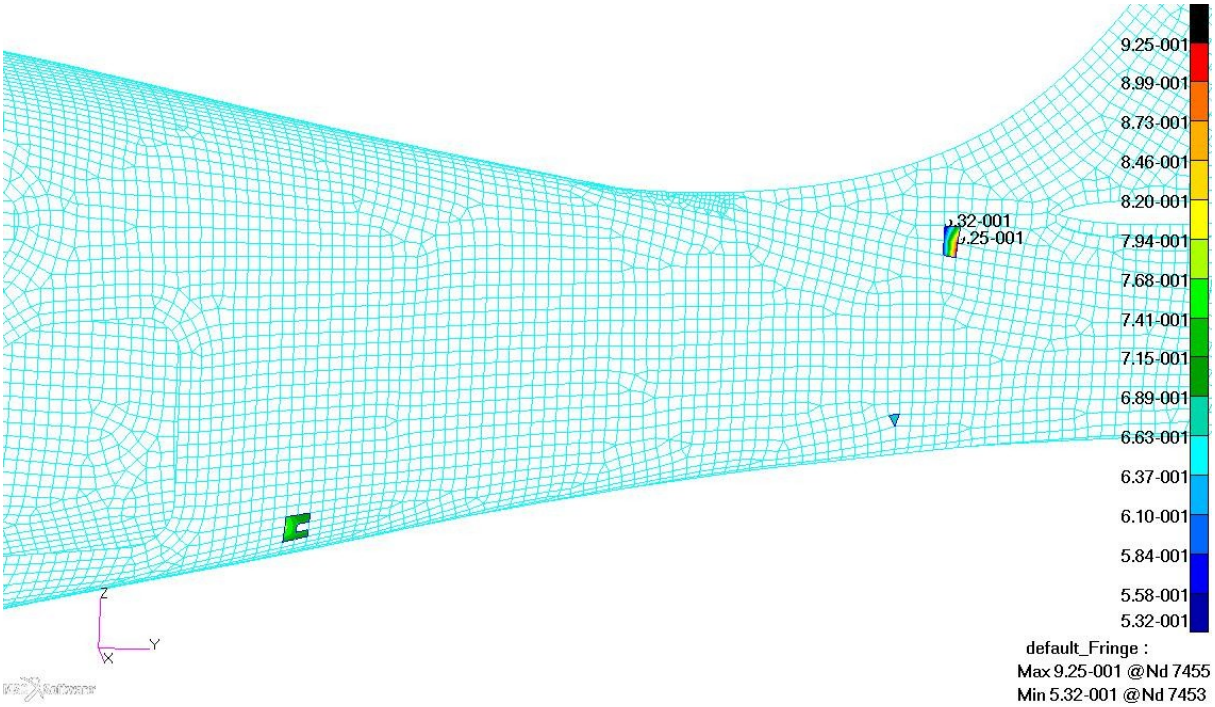

Fig. 49 Critical sandwich areas of the fuselage skin

Critical area 1

In this area acts compressive stress caused by empennage in the outer layers which is concentrated behind first bulkhead in the corner of foam core. The biggest stress in elements acts outer sandwich layer.

Considering high safety factor and small value of failure indices $FI = 1.069 \div 1.004$ the possible solution for this problem would be one extra laminate ply (for example 160g carbon fabric) applied to the bottom half of the fuselage skin at the edge of sandwich layer.

Critical area 2

In this area there are two elements which are supposed to have damaged last layer of the sandwich by tension stress. These elements are placed in the corner of the sandwich layer with $FI = 1.28$ and 1.09.

The solution for this could be reordering laminate layers, what means putting one layer from the outside to the inside, so there would be one more closing layer, because stress value on the outer layers is small. According to Appendix A it could be one of the layer number 11, which covers back part of the aircraft.

The small element at the bottom will not be taken into account as it is in the sandwich corner and its $FI = 1.03$.

Critical area 3

In this area there is highest computed laminate loading with $FI = 1.31$ but because of its position damage of the laminate in this area is improbable. The high failure indices were caused with

horizontal and vertical loading compensation forces which were applied to the corners of the hole for horizontal tail. Second thing is that in future there will be glued horizontal stabilizer, which will reinforce whole area around hole.

10.2.2 Internal structure

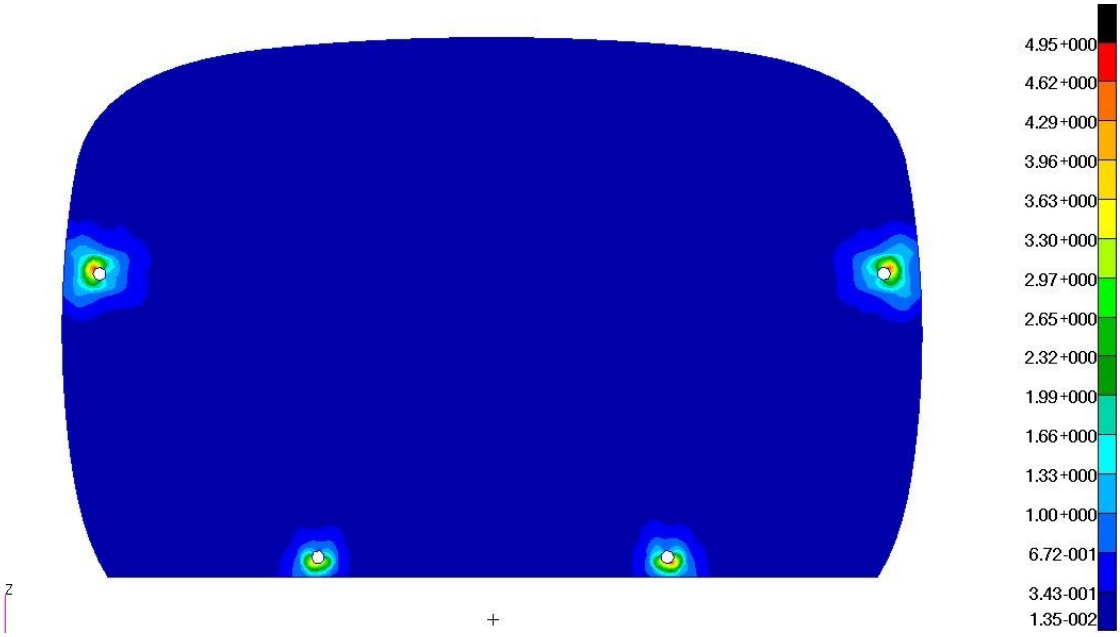

Fig. 50 Engine mounts attachment bulkhead

In this bulkhead there is concentrated stress at the areas, where bolts for engine mounts are attached. In reality this bulkhead will be reinforced by stainless steel metal sheet as fire protection, where also all the bolts will be attached. Here was not considered the metal sheet plate, what is the reason of high failure indices.

From bolt attachment the stress is translated also into fuselage skin, where acts on small skin areas closest to the bolt and creates failure indices $FI = 1.05$, which will not be further considered, because of reduces material properties.

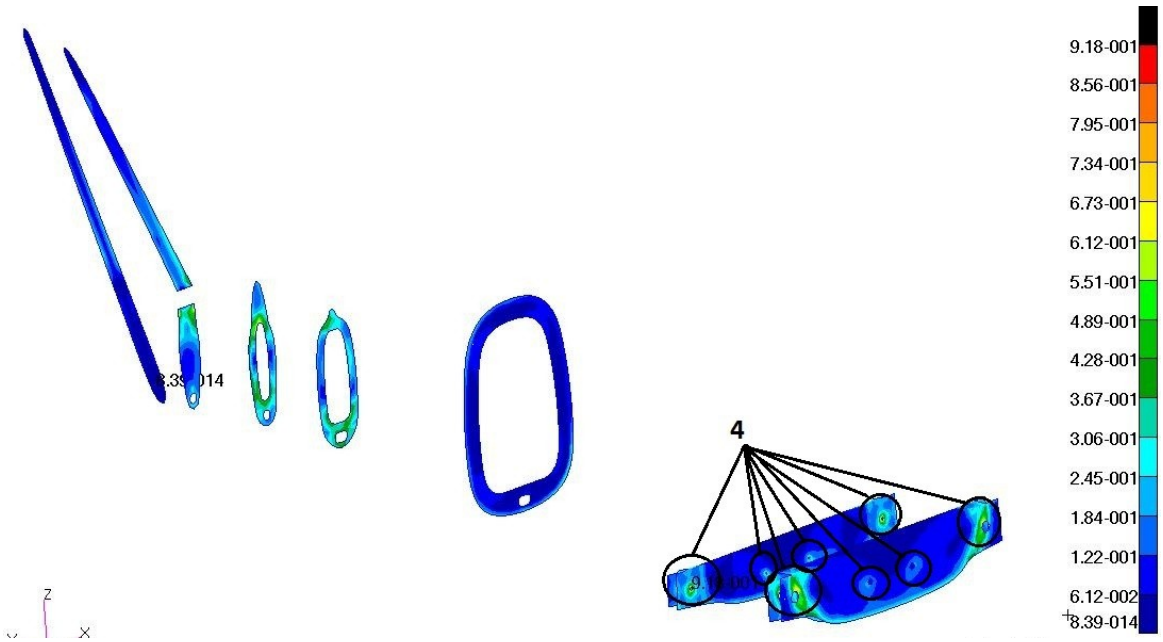

Fig. 51 Fuselage bulkheads and inner wing spars

On the Fig.51 there is missing second bulkhead from the front, which was removed during the analysis process due to big cross section area of the fuselage between first and third bulkhead and it appeared that second bulkhead has no particular effect considering fuselage skin stress.

Critical area 4

This area is critical because of wing pivots which will be attached in holes. Into these holes has to be laminated metal shells, which spreads the stress in laminate into bigger area and prevents delamination around wing pivots.

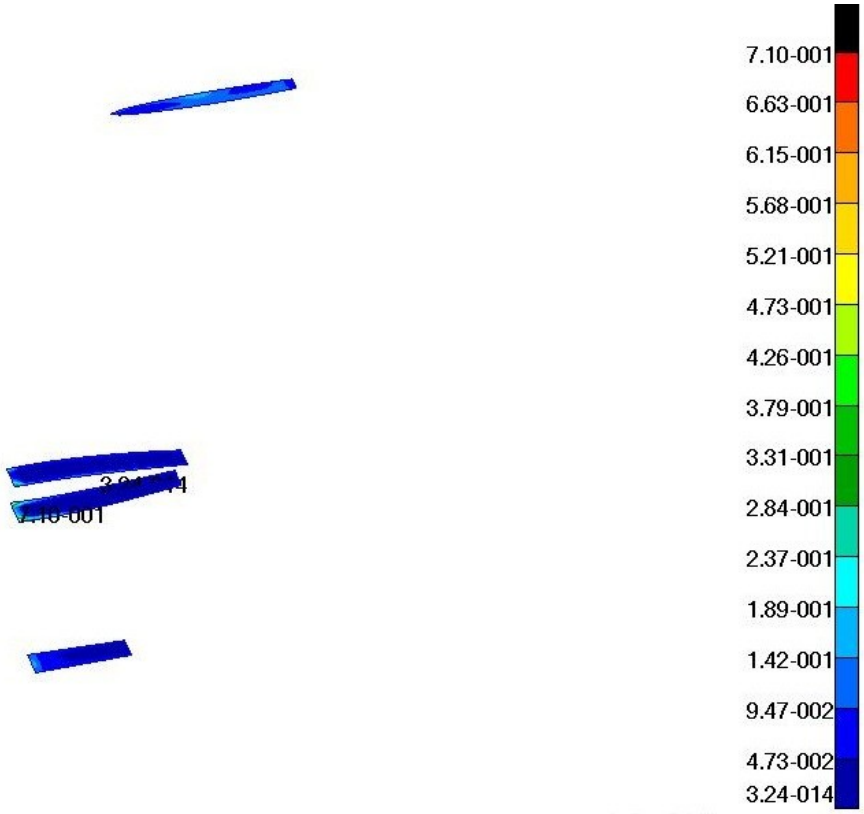

Fig. 52 Fin ribs and horizontal tail flange

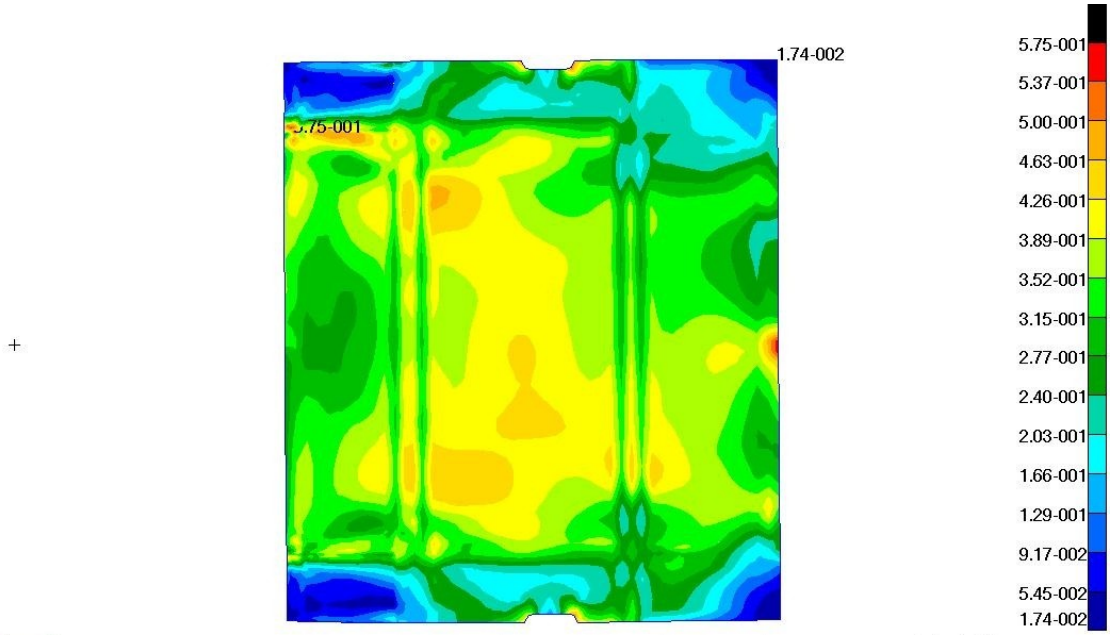

Fig. 53 Inner wing cover

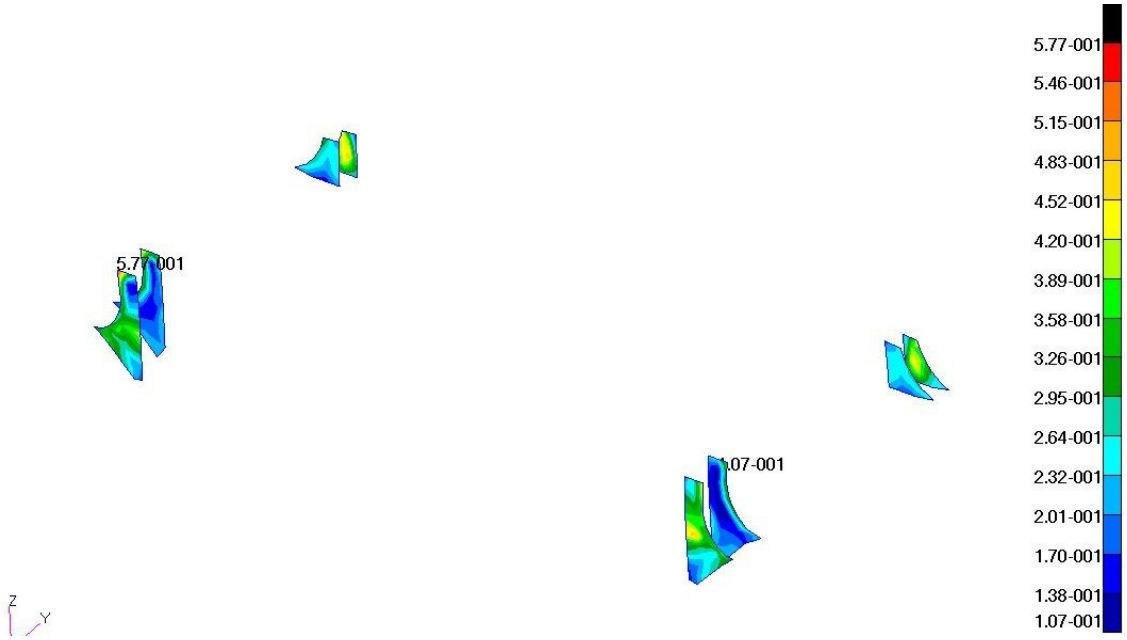

Fig. 54 Inner wing spars reinforcements

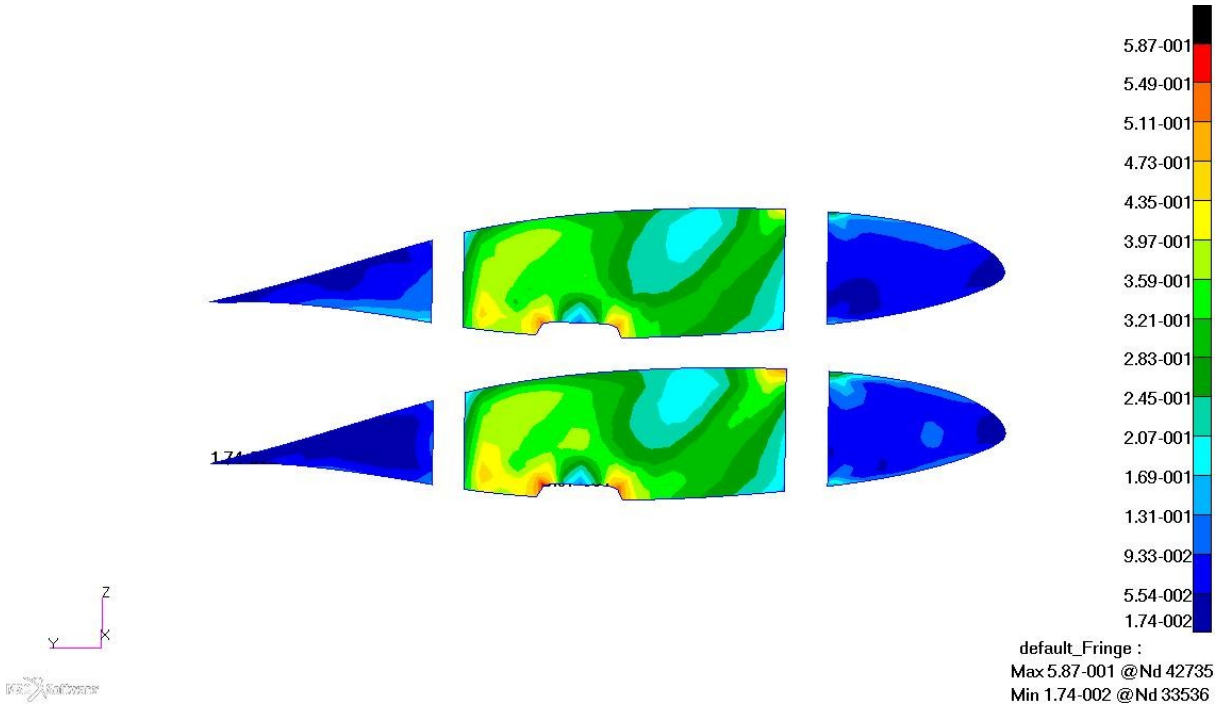

Fig. 55 Fuselage ribs

Fuselage ribs

After appendix A the fuselage ribs has small amount of layers and made are just from sandwich with foam core. This is the reason of not including the landing gear forces to the computation, otherwise these ribs would be much stiffer, because it is mentioned that landing gear leg, which would be attached to the fuselage frame is supported by these ribs.

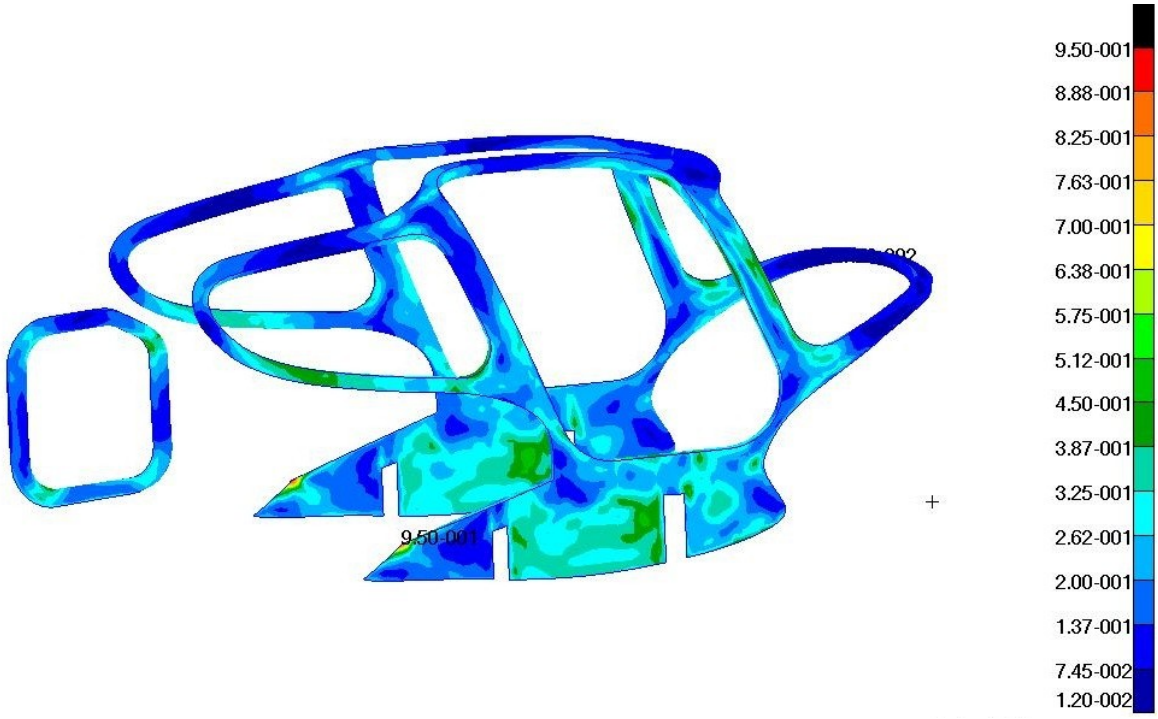

Fig. 56 Cabin and luggage door reinforcement

Cabin reinforcement

The laminate layup for this structural part is much stiffer than is actually needed in computation. The reason of this choice was to make structural part which will take bigger part of the skin loading around doors and windows cut-outs.

Cabin reinforcement leads into rib, which is placed where fairing between fuselage and wings starts. At the trailing edge is sharp corner which acts as stress raiser ($FI = 0.95$) which translated its loads also into the fuselage skin. In this area there was necessary to put multiple plies and locally also sandwich core as seen in Appendix A.

10.3 Design recommendation

The cabin cut-outs design is not the best made especially considering the passenger doors. These doors has to be strongly reinforced especially in the lower rear corner, where is stress concentrated. In this thesis the landing gear loading was not taken into account. It is assumed, that forces from landing gear would load cabin frame even more because of its presumed attachment to the frame rib. Possible solution would be redesign frame rib, which would be curved tangentially to the fuselage skin at whole area of the wing fairing. This would transfer stresses from fuselage skin into frame more easily, without stress concentrations caused by empennage forces, which appears on the frame rib at the trailing edge section.

The door cutout has concentration of stress at the lower rear corner. To prevent this there would be door lower edge raised up, and lower edge radius would be preferred bigger what would cause problems with access to the rear seats for passengers on the other hand.

11. Conclusion

This thesis was focused on design and analysis of structural parts with focus on the composite layout of the rear part for TL-4000 aircraft.

In the first part of this thesis were the air loads computed and there was also set five most possible combination of these loads with respect to the CS regulations.

Second part was focused on design of the internal fuselage structure such as cabin frame, bulkheads and spars with description of the role of each part and following mesh creation.

Third part contains the FEM analysis of created laminate layup in MSC. Patran/Nastran software where failure indices of the laminate structure were computed and following analysis in ComPost software with failure indices of the sandwich structure. These analyses were computed for all five load cases with respect to the wing and engine mounting.

12. Bibliography

[1] Ing. Tomáš Koutník, Koncepční aerodynamický návrh letounu TL-4000, Brno University of Technology, 2013

[2] CS-23 regulation, European Aviation Safety Agency, Amendment 3, 20th July 2012

[3] Ing. Tomáš Koutník, AEROSTATICKÉ PODKLADY LETOUNU TL 4000, Brno University of Technology, 2014

[4] doc. Ing. Vladimír Daněk, CSc., Projektování letadel, Brno University of Technology, 1992

[5] CS-VLA regulation, European Aviation Safety Agency, Amendment 3, 14th November 2003

[6] Prof. Ing. Jaromír Špunda, Stavebná mechanika letadel I, Brno University of Technology, 1950

[7] IDAFLIEG, Dimensionierungsrichtwerte fur den Segel- und Motorsegelflugzeugbau, 1988

[8] Mališ, M., Špaček, P., Schoř, P.: Composite Postprocesor v 1.45 User manual, Brno University of Technology 2012

13. List of used symbols

ρ	[kg/m^3]	density
μg	[-]	aeroplane mass ratio
ε	[rad]	angular velocity
s	[ft]	distance penetrated into the gust
m	[kg]	empty weight
kg	[-]	gust alleviation factor
g	[m/s^2]	gravitational acceleration
b	[m]	wing span
S	[m^2]	wing area
FI	[-]	failure indices
ΔP	[N]	horizontal tail load increment from manoeuvre
$\Delta x_{A,fuselage}$	[m]	increment to the aerodynamic centre from fuselage
$\delta_{equivalent}$	[deg]	equivalent rudder deflection
$\alpha_{equivalent}$	[deg]	equivalent angle of attack of vertical tail
x_{cg}	[m]	centre of gravity position from wing leading edge
x_A	[m]	aerodynamic centre for wing and fuselage from leading edge
$x_{A,wing}$	[m]	aerodynamic centre of the wing from wing leading edge
$\overline{w}$	[N/m^2]	average surface loading
v_{sG}	[m/s]	stall speed for flight on back
v_{sF}	[m/s]	stall speed with flaps
v_s	[m/s]	stall speed
v_c	[m/s]	cruise speed
v_{Hmax}	[m/s]	maximum estimated horizontal flight speed
v_G	[m/s]	manoeuvring speed for flight on back
v_F	[m/s]	maximum speed with flaps
v_{AF}	[m/s]	manoeuvring speed with flaps
v_A	[m/s]	manoeuvring speed
n_2	[-]	maximum load factor for flight on back
m_p	[kg]	maximum payload
m_f	[kg]	maximum fuel weight

m_{TOW}	[kg]	maximum take off weight
m_{HT}	[kg]	horizontal tail estimated weight
$l_{fuselage}$	[m]	fuselage length
l_{HT}	[m]	horizontal tail arm
l_{HT}	[m]	horizontal tail arm
c_{m0}	[-]	moment coefficient at zero lift
$c_{l\alpha}$	[1/rad]	wing lift curve slope
c_{VT}	[m]	vertical tail chord
c_{MAC}	[m]	mean aerodynamical chord
c_{Lmin}	[-]	minimum lift coefficient
c_{Lmax}	[-]	maximum lift coefficient
c_{Lmax}	[-]	maximum lift coefficient
c_{Lflaps}	[-]	maximum lift coefficient with flaps
$c_{L,VT}$	[-]	vertical tail lift coefficient
$b_{fuselage}$	[m]	fuselage thickness
b_{VT}	[m]	vertical tail span
b_{HT}	[m]	horizontal tail span
a_{VT}	[1/rad]	vertical lift slope
U_{de}	[m/s]	derived gust velocity linearly between v_C and v_D. [m/s]
S_{HT}	[m^2]	horizontal tail surface
P_{max}	[kW]	maximum permanent engine power
J_z	[kg .m^2]	inertia moment around Z-axis
I_z	[m]	radius of gyration
F_{VT}	[N]	vertical tail force
F_{HT}	[N]	horizontal tail force
$F_{HT,trim}$	[N]	horizontal tail trim force
$\bar{C}$	[-]	relative mean geometric chord of the wing
$\Delta F_{HT,gust}$	[N]	horizontal tail force increment from gust
$\bar{x}_{cg}$	[-]	relative centre of gravity position from leading edge
$\bar{x}_A$	[-]	relative aerodynamic centre position from leading edge

14. List of figures

15. List of tables

Appendix

Appendix A – Laminate layers

The layers, which are not on the pictures covers whole area of the structural part.

fuselage (half)						
ply no.	material	number of layers	orientation [deg]	ply area [m^2]	weight [kg]	weight with epoxy [kg]
1.00	glass fabric 105g	1.00	0.00	6.81	0.72	1.28
2.00	carbon fabric 200g	1.00	45.00	6.81	1.36	2.68
3.00	carbon fabric 160g	1.00	0.00	6.81	1.09	2.34
4.00	carbon UD 50 mm (300 g/m^2)	5.00	0.00	1.64	2.46	4.33
5.00	carbon fabric 200g	3.00	45.00	1.00	0.60	1.18
6.00	carbon fabric 200g	2.00	0.00	1.22	0.49	0.96
7.00	carbon fabric 200g	1.00	45.00	1.14	0.23	0.45
8.00	carbon fabric 200g	1.00	45.00	5.50	1.10	2.16
9.00	carbon UD 50 mm (300 g/m^2)	2.00	0.00	0.10	0.06	0.11
10.00	carbon fabric 200g	2.00	45.00	1.00	0.40	0.79
11.00	carbon fabric 200g	3.00	45.00	1.20	0.72	1.41
12.00	carbon fabric 200g	1.00	0.00	0.82	0.16	0.32
13.00	carbon fabric 200g	2.00	45.00	1.20	0.48	0.94
14.00	carbon fabric 200g	7.00	0.00	0.60	0.84	1.65
15.00	carbon UD 50 mm (300 g/m^2)	10.00	0.00	0.40	1.20	2.11
16.00	divinycell 8mm	1.00	0.00	5.50	2.64	2.64
17.00	carbon fabric 200g	1.00	45.00	5.50	1.10	2.16
18.00	carbon fabric 160g	1.00	45.00	6.81	1.09	2.34
				sum	33.50	59.71

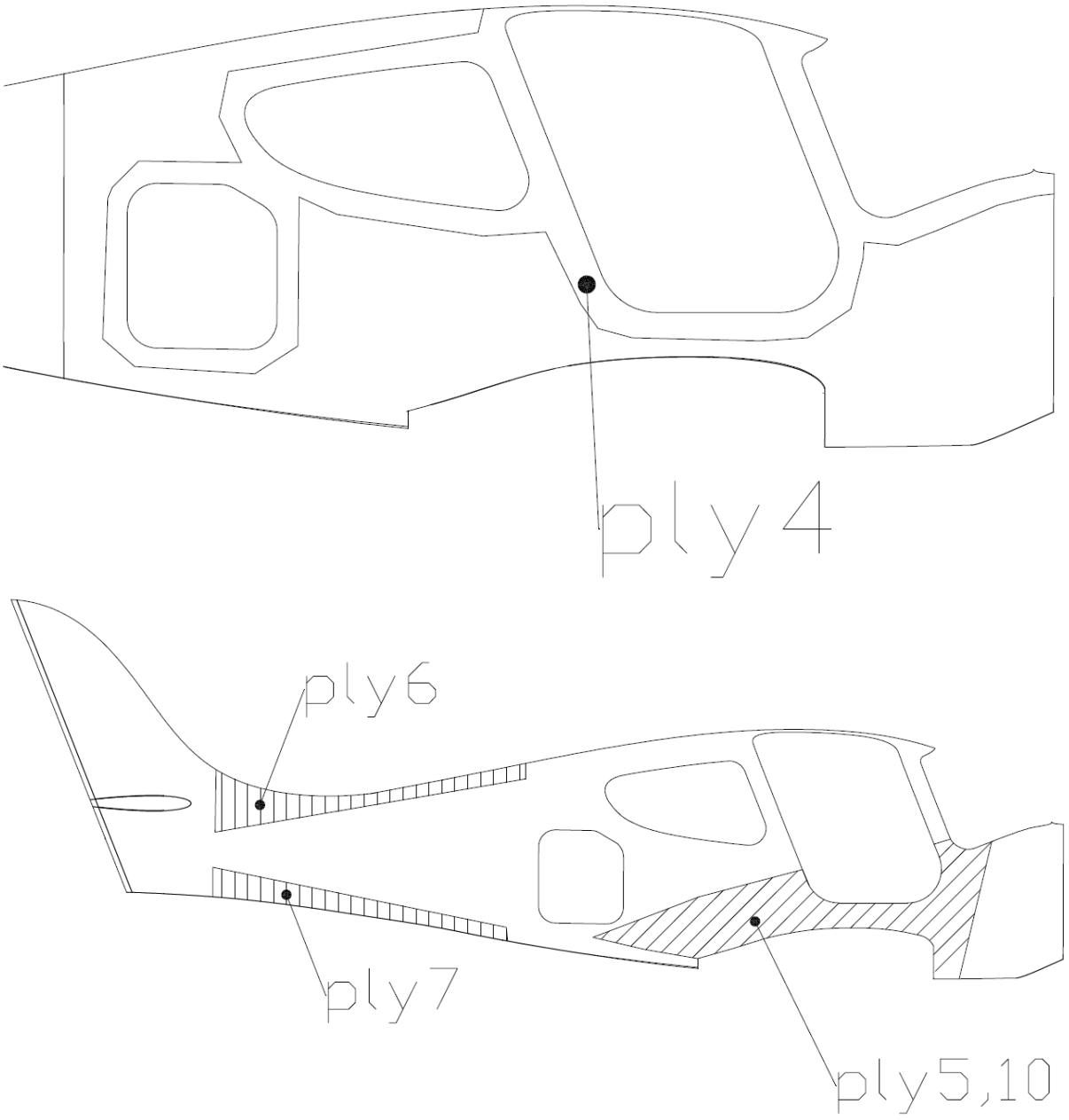
ply 4
ply6
ply7
ply5,10

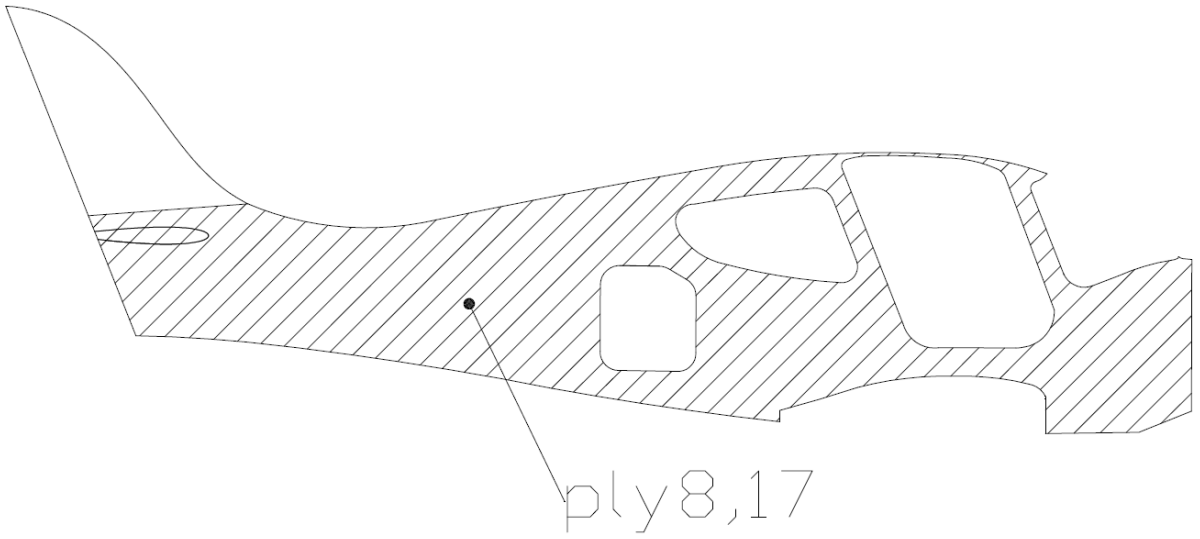
ply8,17

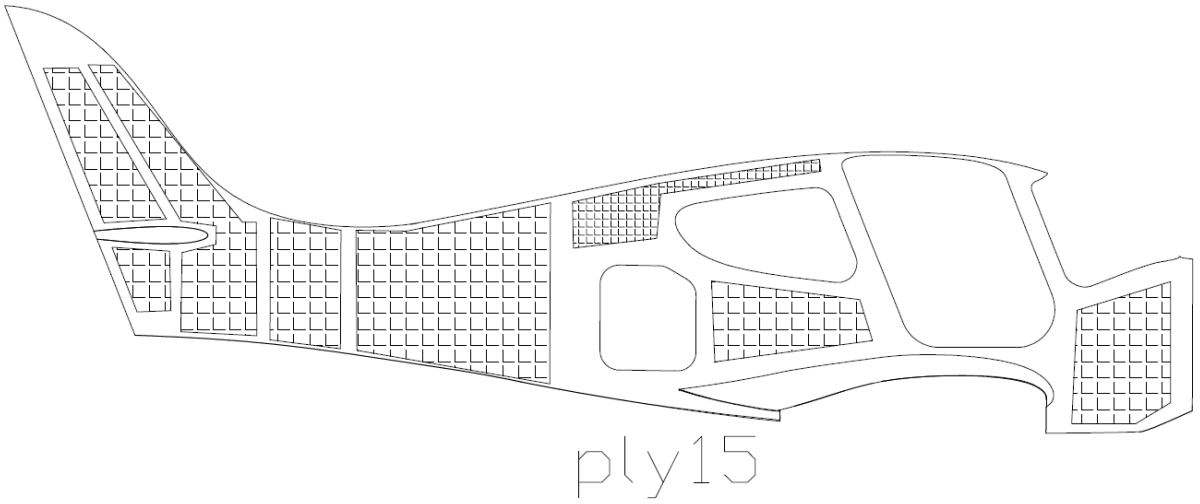
ply15

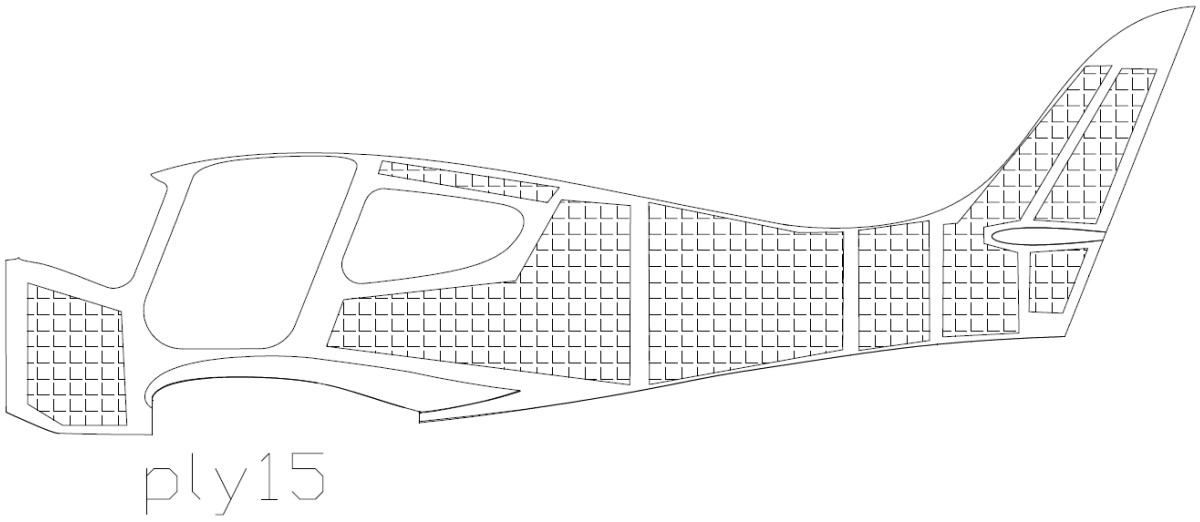
ply15

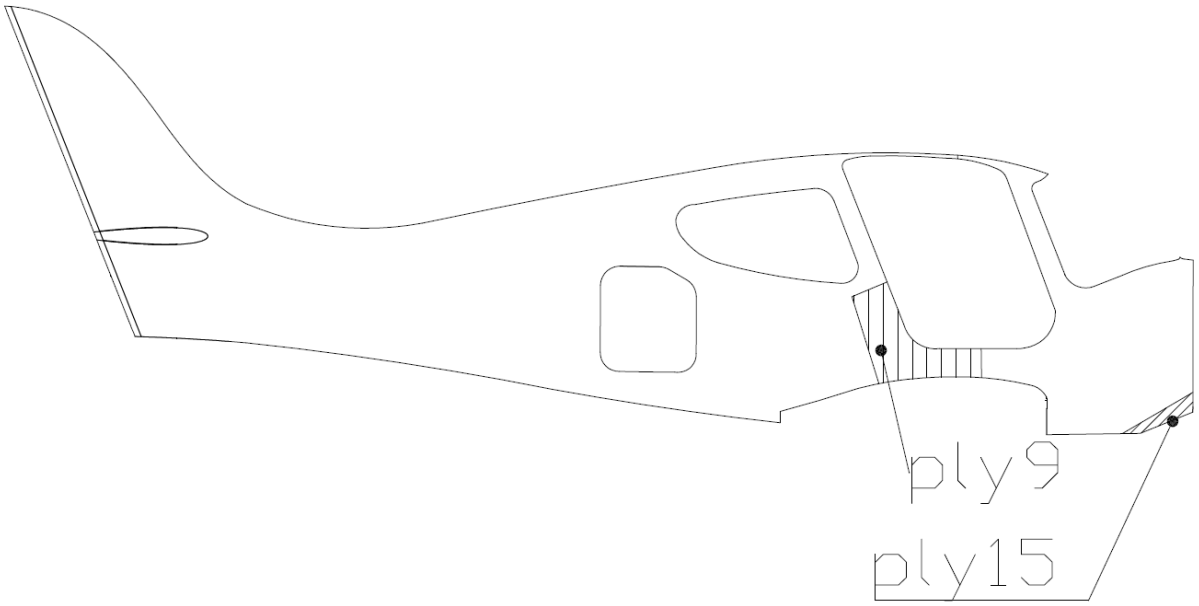

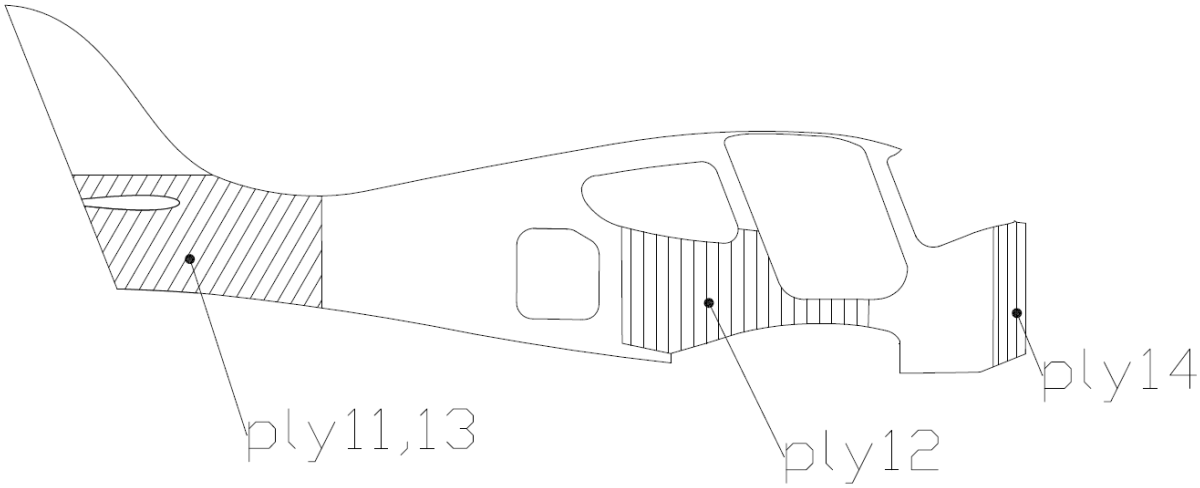

inner wing cover						
ply no.	material	number of layers	orientation [deg]	ply area $[m^2]$	weight [kg]	weight with epoxy [kg]
1.00	glass fabric 105g	1.00	0.00	2.25	0.238	0.42
2.00	carbon fabric 200g	1.00	45.00	2.25	0.450	0.88
3.00	carbon fabric 200g	1.00	0.00	2.25	0.45	0.88
4.00	carbon fabric 200g	1.00	45.00	2.25	0.45	0.88
5.00	carbon fabric 160g	1.00	0.00	2.25	0.360	0.77
6.00	carbon fabric 200g	1.00	45.00	2.25	0.45	0.88
7.00	divinycell 8mm	1.00	0.00	2.00	0.960	0.96
8.00	carbon fabric 200g	1.00	0.00	2.25	0.45	0.88
9.00	carbon fabric 200g	1.00	45.00	2.25	0.45	0.88
				sum	4.26	7.46

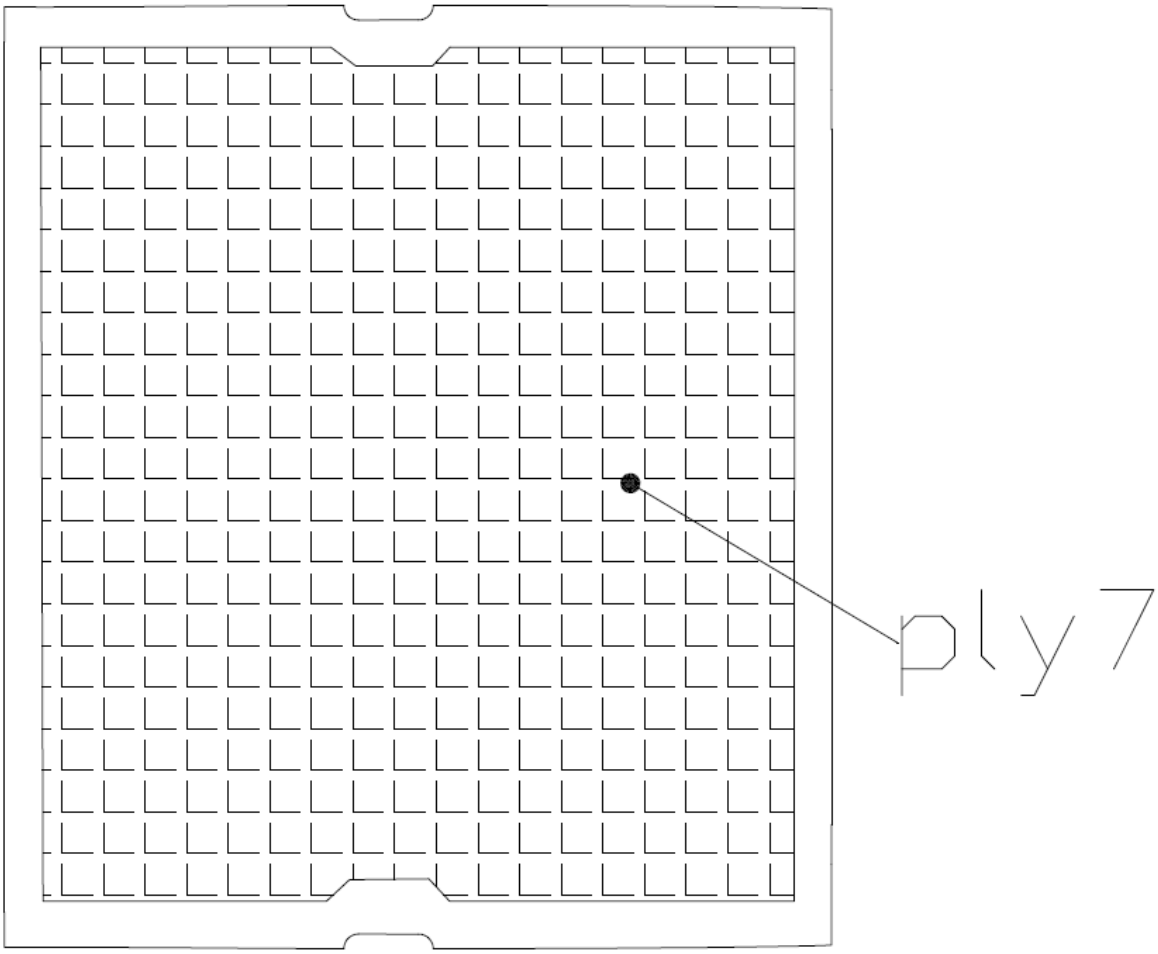

door frame

ply no.	material	number of layers	orientation [deg]	ply area $[m^2]$	weight [kg]	weight with epoxy [kg]
1.00	Carbon fabric 200g	5.00	45.00	1.46	1.46	2.88
2.00	Divinycell 8mm	1.00	0.00	0.18	0.09	0.09
3.00	Carbon fabric 200g	4.00	45.00	0.24	0.19	0.38
4.00	Carbon fabric 200g	5.00	45.00	0.35	0.35	0.69
				sum	2.09	4.03

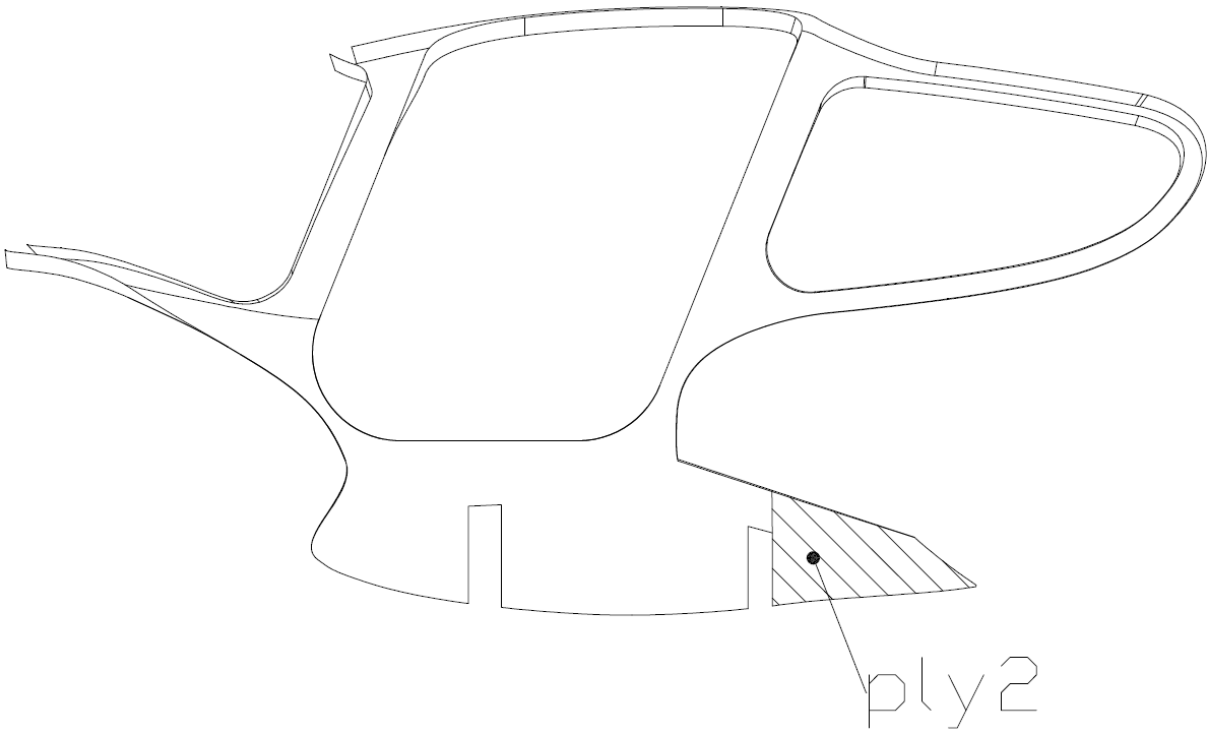
ply 2

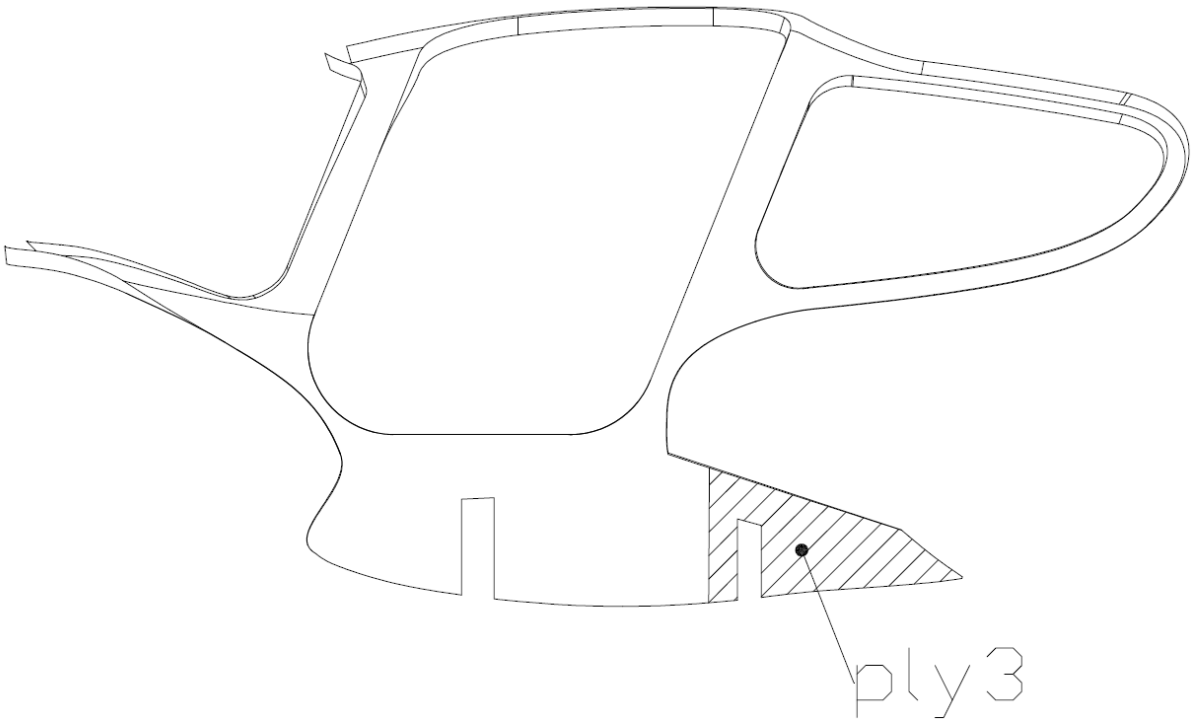
ply 3

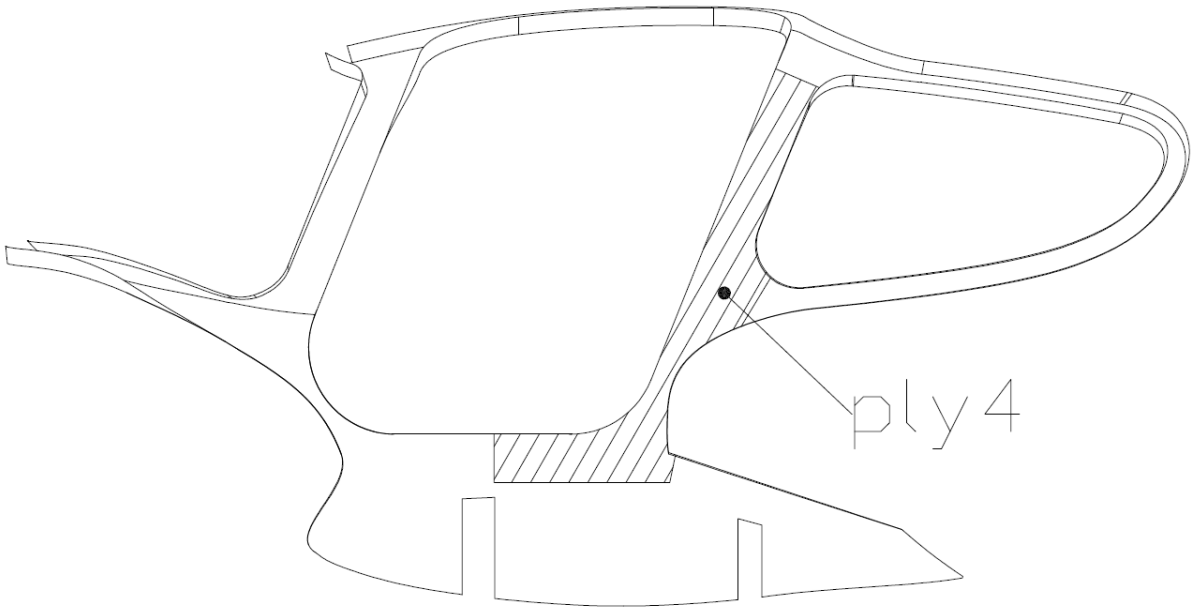

luggage door frame						
ply no.	material	number of layers	orientation [deg]	ply area $[m^2]$	weight [kg]	weight with epoxy [kg]
1.00	carbon fabric 200g	3.00	45.00	0.27	0.16	0.31

inner wing front spar						
ply no.	material	number of layers	orientation [deg]	ply area $[m^2]$	weight [kg]	weight with epoxy [kg]
1.00	carbon fabric 200g	6.00	45.00	0.49	0.59	1.16
2.00	carbon fabric 200g	10.00	45.00	0.22	0.44	0.86
				sum	1.03	2.03

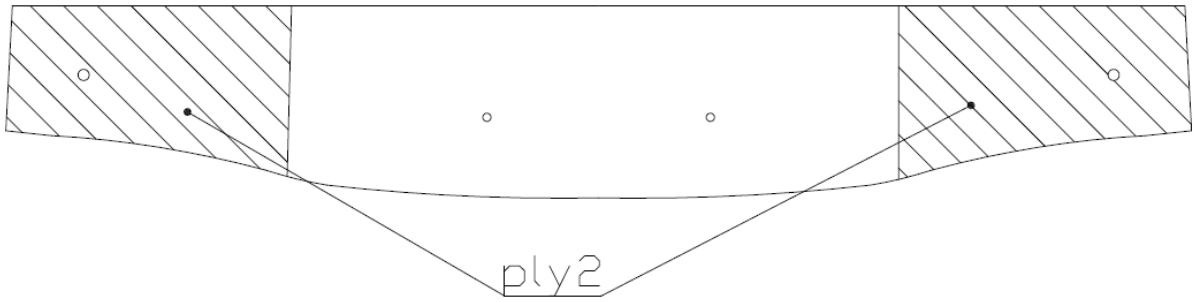

inner wing rear spar						
ply no.	material	number of layers	orientation [deg]	ply area $[m^2]$	weight [kg]	weight with epoxy [kg]
1.00	carbon fabric 200g	5.00	45.00	0.38	0.38	0.74
2.00	carbon fabric 200g	20.00	45.00	0.18	0.72	1.41
3.00	carbon fabric 200g	1.00	0.00	0.38	0.08	0.15
				sum	1.17	2.30

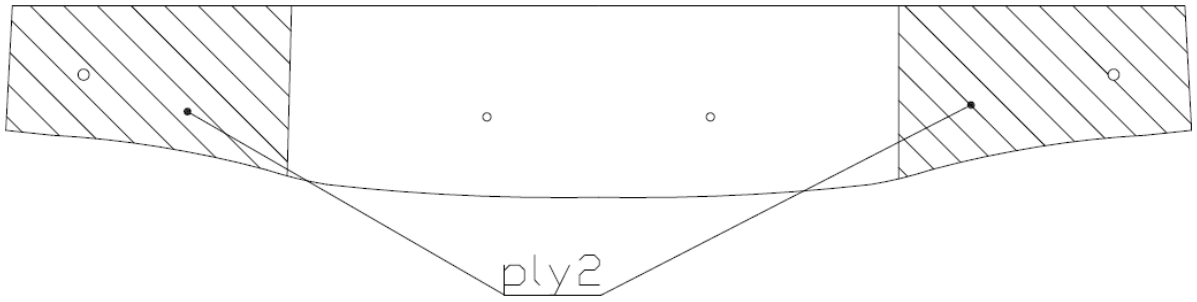

bulkhead 1						
ply no.	material	number of layers	orientation [deg]	ply area $[m^2]$	weight [kg]	weight with epoxy [kg]
1.00	carbon fabric 200g	1.00	45.00	0.27	0.05	0.11
2.00	divinicell 5mm	1.00	0.00	0.27	0.09	0.09
3.00	carbon fabric 200g	1.00	45.00	0.27	0.05	0.11
				sum	0.20	0.30

bulkhead 2						
ply no.	material	number of layers	orientation [deg]	ply area $[m^2]$	weight [kg]	weight with epoxy [kg]
1.00	carbon fabric 200g	1.00	45.00	0.074	0.015	0.03
2.00	divinicell 5mm	1.00	0.00	0.074	0.026	0.03
3.00	carbon fabric 200g	1.00	45.00	0.074	0.015	0.03
				sum	0.06	0.09

bulkhead 3						
ply no.	material	number of layers	orientation [deg]	ply area $[m^2]$	weight [kg]	weight with epoxy [kg]
1.00	carbon fabric 200g	2.00	45.00	0.066	0.026	0.05
2.00	divinicell 5mm	1.00	0.00	0.066	0.023	0.02
3.00	carbon fabric 200g	2.00	45.00	0.066	0.026	0.05
				sum	0.076	0.13

engine bulkhead						
ply no.	material	number of layers	orientation [deg]	ply area $[m^2]$	weight [kg]	weight with epoxy [kg]
1.00	glass fabric 163g	9.00	45.00	0.88	1.58	2.29
2.00	divinicell 5mm	1.00	0.00	0.84	0.29	0.29
3.00	plywood 5mm	1.00	0.00	0.04	0.16	0.16
4.00	glass fabric 163g	9.00	45.00	0.88	1.58	2.29
				sum	3.61	5.04

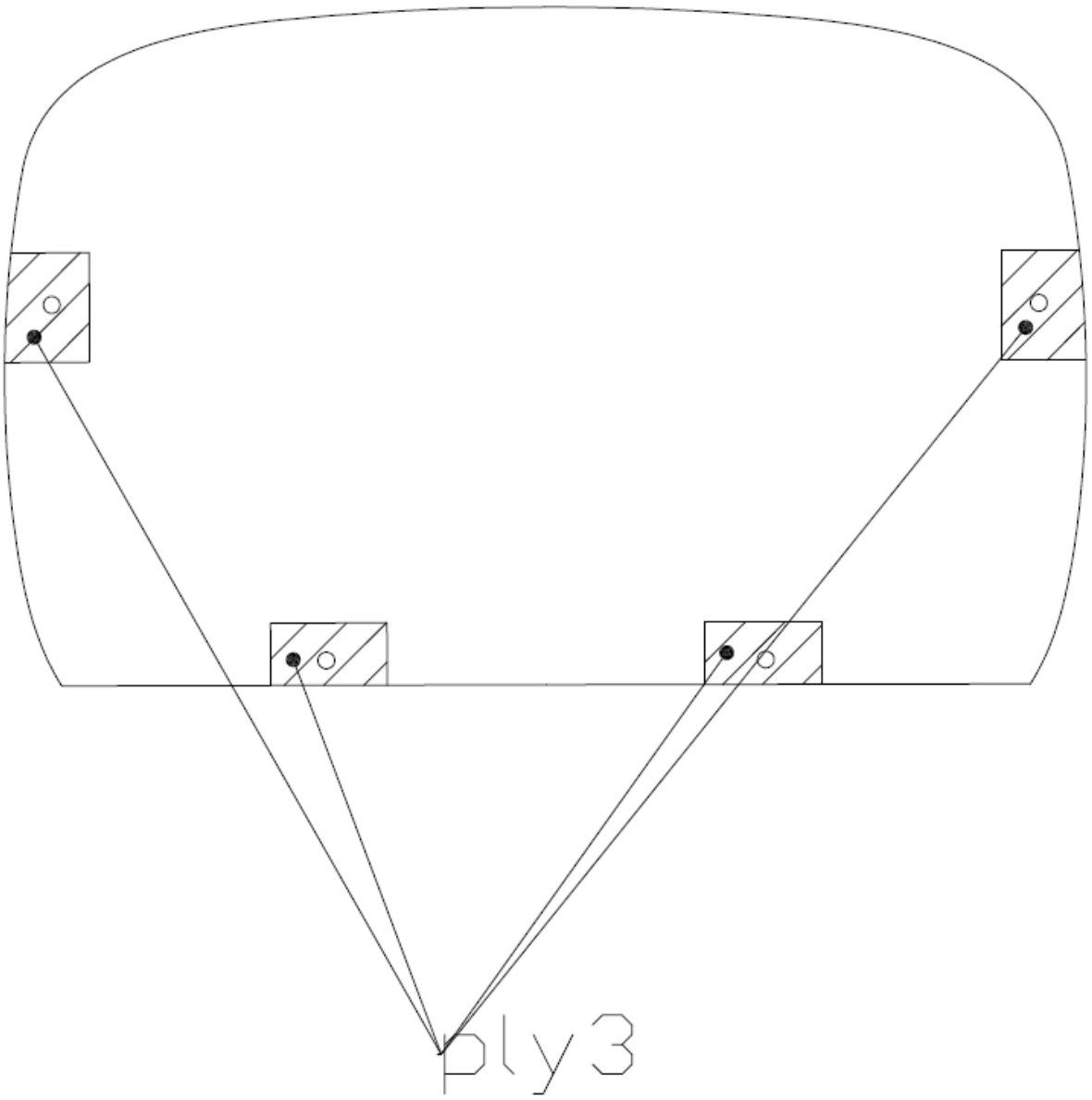

fuselage rib						
ply no.	material	number of layers	orientation [deg]	ply area $[m^2]$	weight [kg]	weight with epoxy [kg]
1.00	carbon fabric 200g	1.00	45.00	0.19	0.04	0.07
2.00	divinicell 5mm	1.00	0.00	0.19	0.07	0.07
3.00	carbon fabric 200g	1.00	45.00	0.19	0.04	0.07
				sum	0.15	0.21

HT flange						
ply no.	material	number of layers	orientation [deg]	ply area $[m^2]$	weight [kg]	weight with epoxy [kg]
1.00	carbon fabric 200g	1.00	45.00	0.04	0.01	0.02
2.00	divinicell 5mm	1.00	0.00	0.04	0.01	0.01
3.00	carbon fabric 200g	1.00	45.00	0.04	0.01	0.02
				sum	0.03	0.05

fin top rib						
ply no.	material	number of layers	orientation [deg]	ply area $[m^2]$	weight [kg]	weight with epoxy [kg]
1.00	carbon fabric 200g	1.00	45.00	0.02	0.00	0.01
2.00	divinicell 5mm	1.00	0.00	0.02	0.01	0.01
3.00	carbon fabric 200g	1.00	45.00	0.02	0.00	0.01
				sum	0.02	0.03

fin bottom rib						
ply no.	material	number of layers	orientation [deg]	ply area $[m^2]$	weight [kg]	weight with epoxy [kg]
1.00	carbon fabric 200g	1.00	45.00	0.02	0.00	0.01
2.00	divinicell 5mm	1.00	0.00	0.02	0.01	0.01
3.00	carbon fabric 200g	1.00	45.00	0.02	0.00	0.01
				sum	0.02	0.02

fin front spar						
ply no.	material	number of layers	orientation [deg]	ply area $[m^2]$	weight [kg]	weight with epoxy [kg]
1.00	carbon fabric 200g	1.00	45.00	0.15	0.03	0.06
2.00	divinicell 5mm	1.00	0.00	0.15	0.05	0.05
3.00	carbon fabric 200g	1.00	45.00	0.15	0.03	0.06
				sum	0.11	0.17

fin rear spar						
ply no.	material	number of layers	orientation [deg]	ply area $[m^2]$	weight [kg]	weight with epoxy [kg]
1.00	carbon fabric 200g	1.00	45.00	0.13	0.03	0.05
2.00	divinicell 5mm	1.00	0.00	0.13	0.05	0.05
3.00	carbon fabric 200g	1.00	45.00	0.13	0.03	0.05
				sum	0.10	0.15

inner wing front spar reinforcements						
ply no.	material	number of layers	orientation [deg]	ply area $[m^2]$	weight [kg]	weight with epoxy [kg]
1.00	carbon fabric 200g	5.00	0.00	0.05	0.05	0.09
2.00	carbon fabric 200g	5.00	45.00	0.05	0.05	0.09
				sum	0.10	0.19

inner wing rear spar reinforcements						
ply no.	material	number of layers	orientation [deg]	ply area $[m^2]$	weight [kg]	weight with epoxy [kg]
1.00	carbon fabric 200g	6.00	0.00	0.04	0.05	0.10
2.00	carbon fabric 200g	6.00	45.00	0.04	0.05	0.10
				sum	0.11	0.21

Total fuselage weight including internal structure

fuselage laminate plies weight without epoxy [kg]	fuselage weight epoxy included [kg]
80.63	142.76

Appendix B – Fuselage skin failure indices plot

B1 – Horizontal tail maximum force down (from gust)

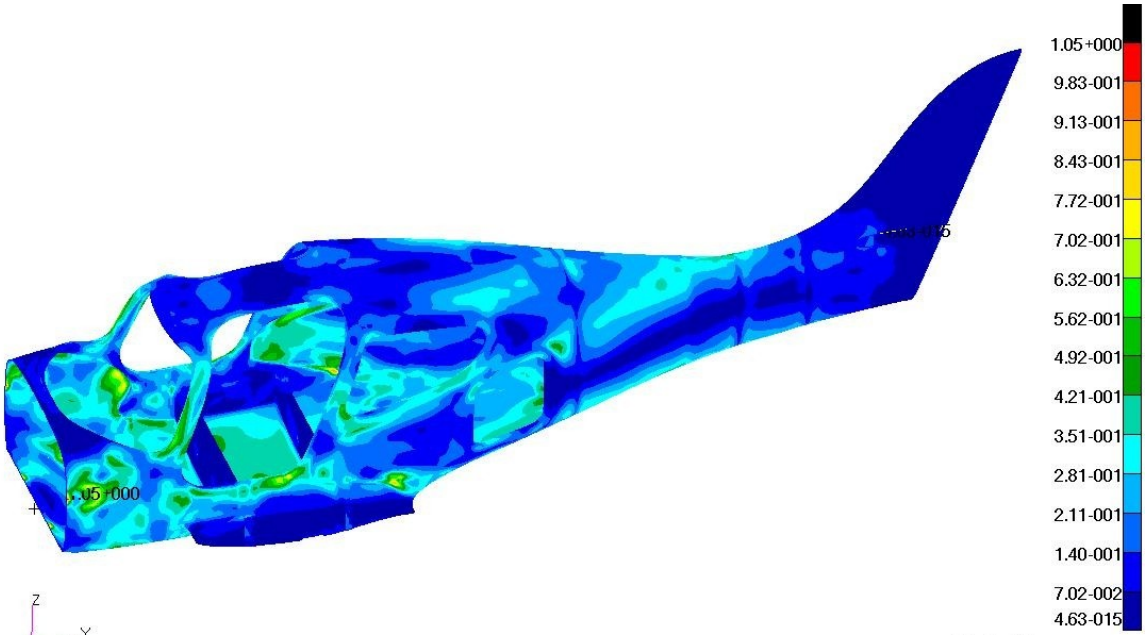

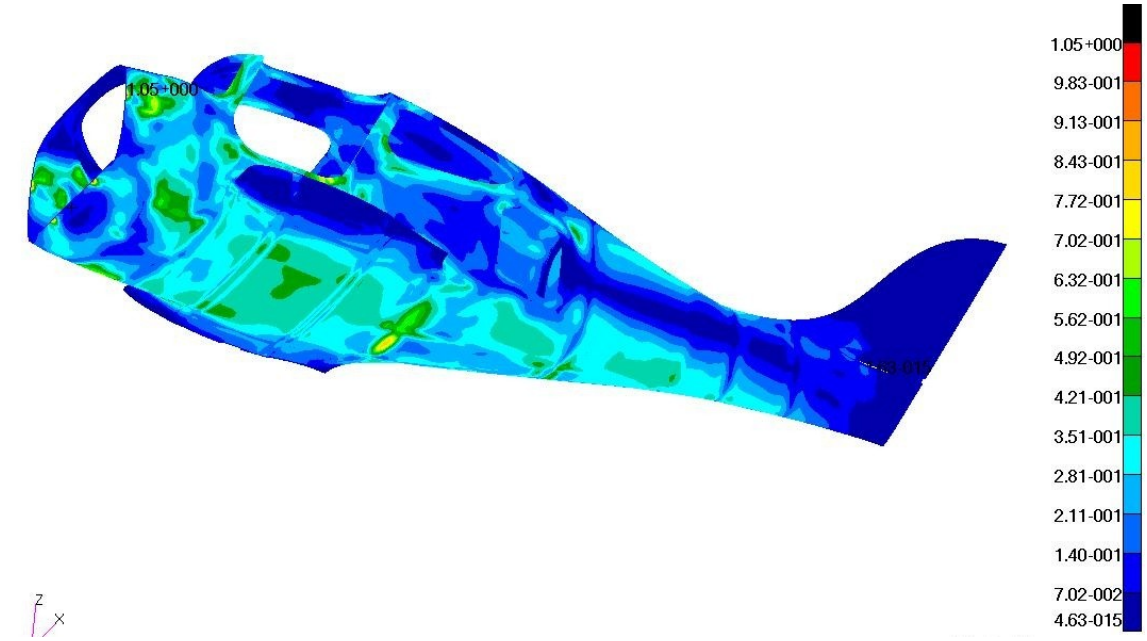

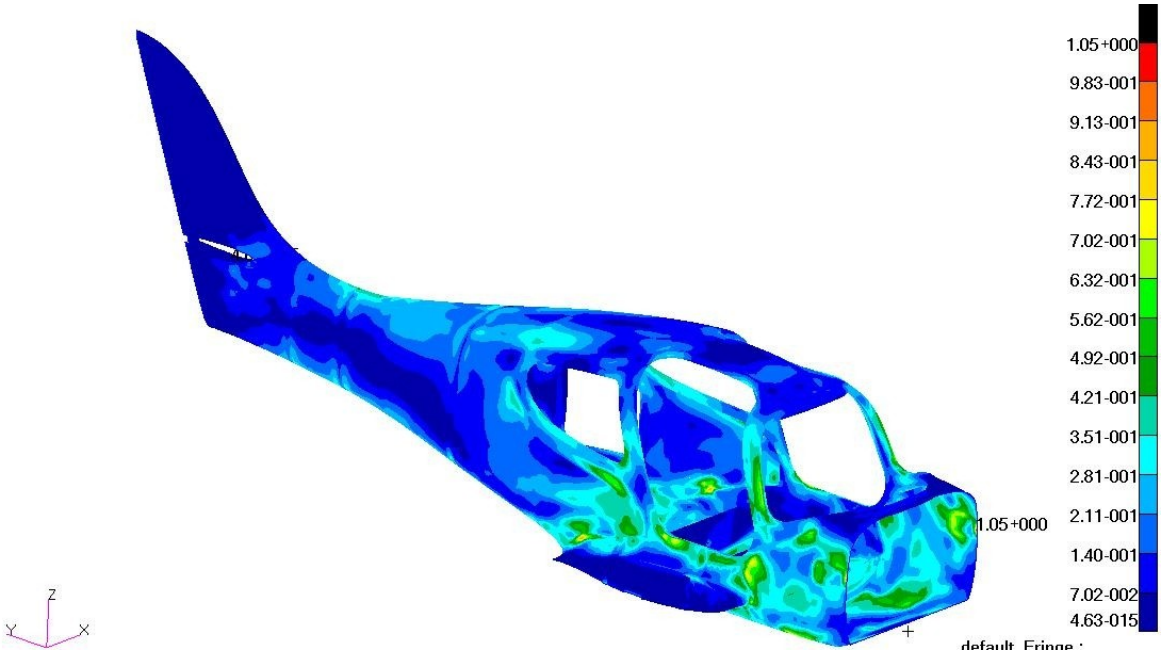

B2 – Horizontal tail maximum force up (from manoeuvre)

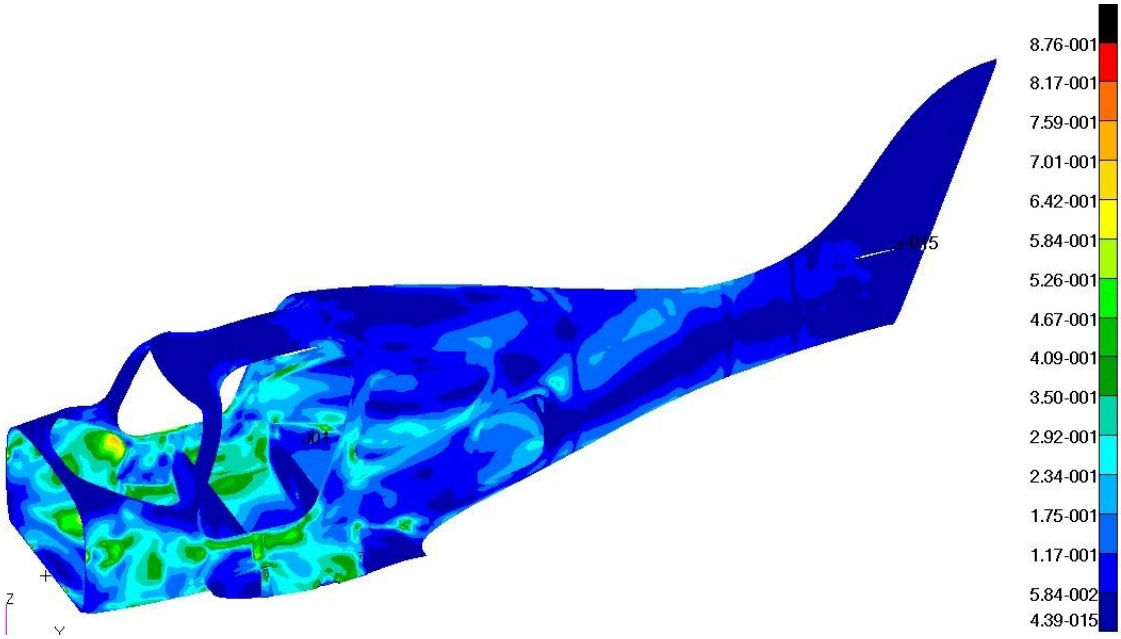

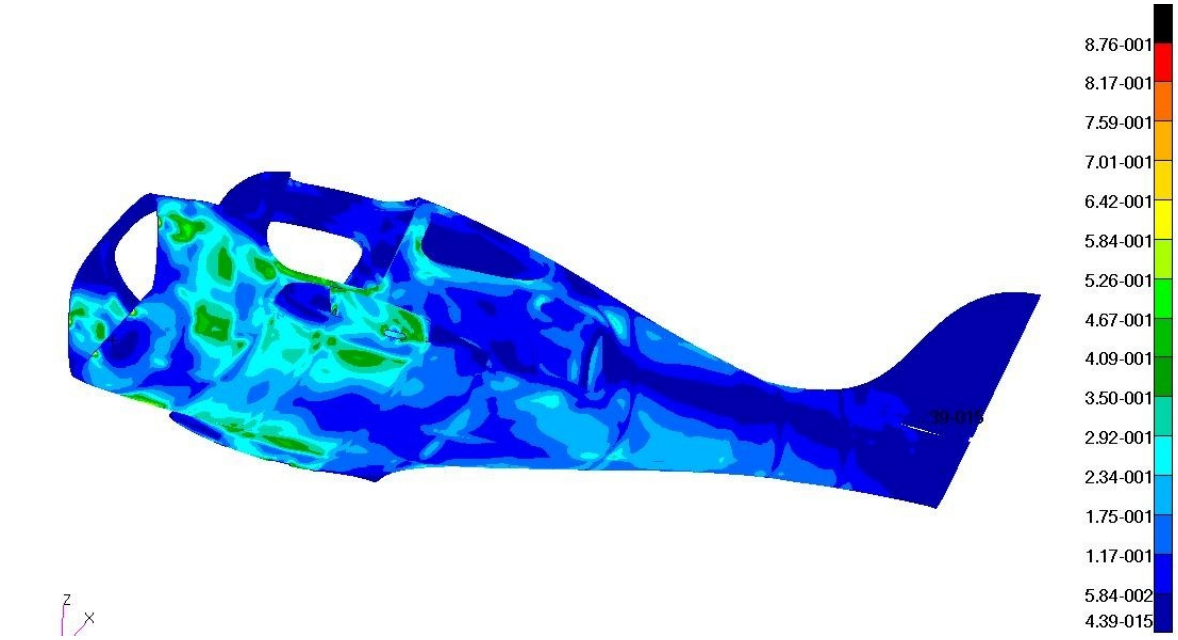
8.76-001
8.17-001
7.59-001
7.01-001
6.42-001
5.84-001
5.26-001
4.67-001
4.09-001
3.50-001
2.92-001
2.34-001
1.75-001
1.17-001
5.84-002
4.39-015
Z
X

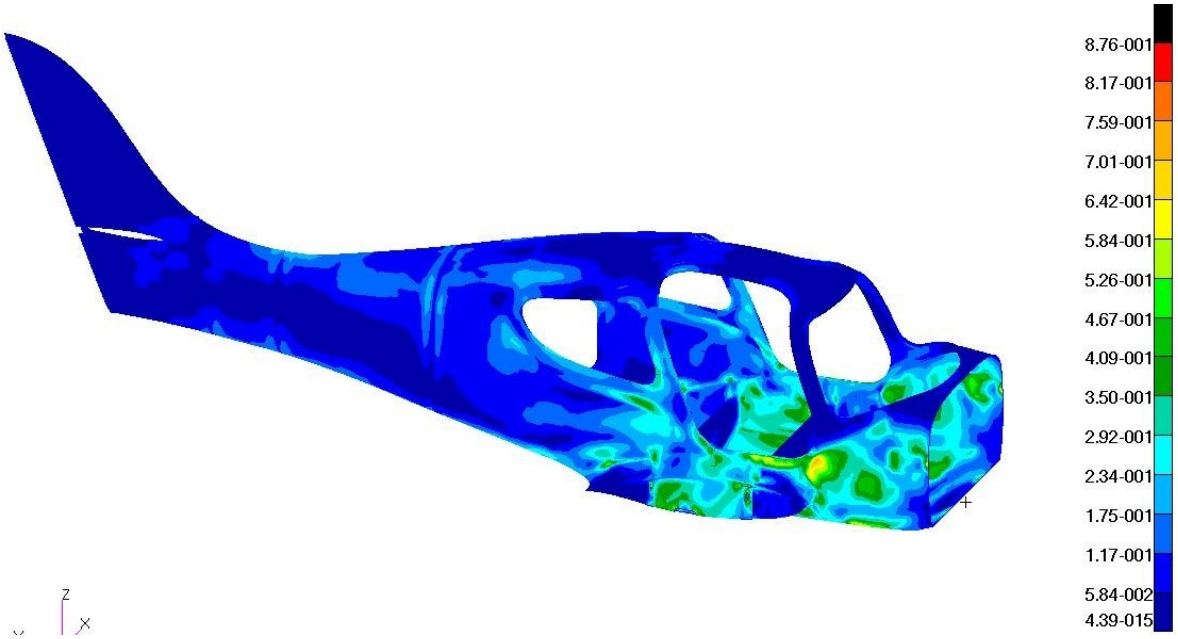
8.76-001
8.17-001
7.59-001
7.01-001
6.42-001
5.84-001
5.26-001
4.67-001
4.09-001
3.50-001
2.92-001
2.34-001
1.75-001
1.17-001
5.84-002
4.39-015
Z
X

B3 – Horizontal tail unsymmetrical loading

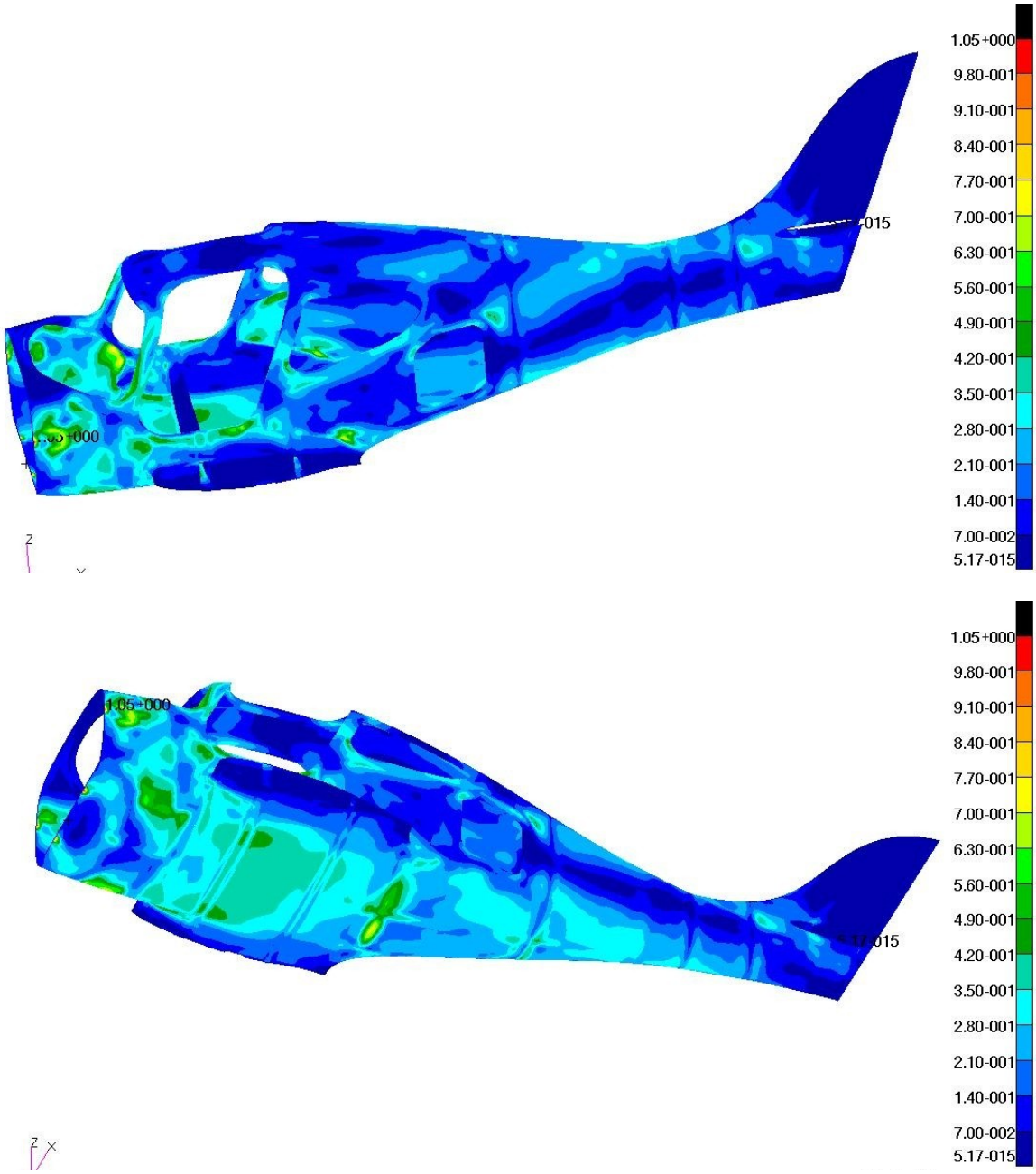

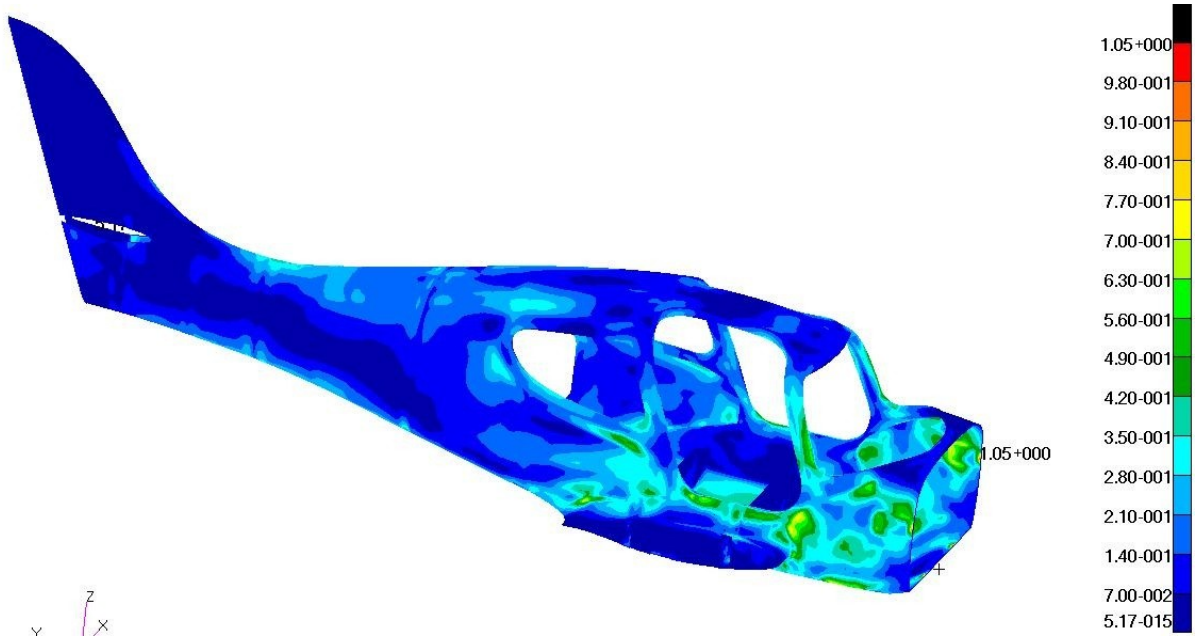

B4 – Vertical tail gust force and horizontal tail trim force

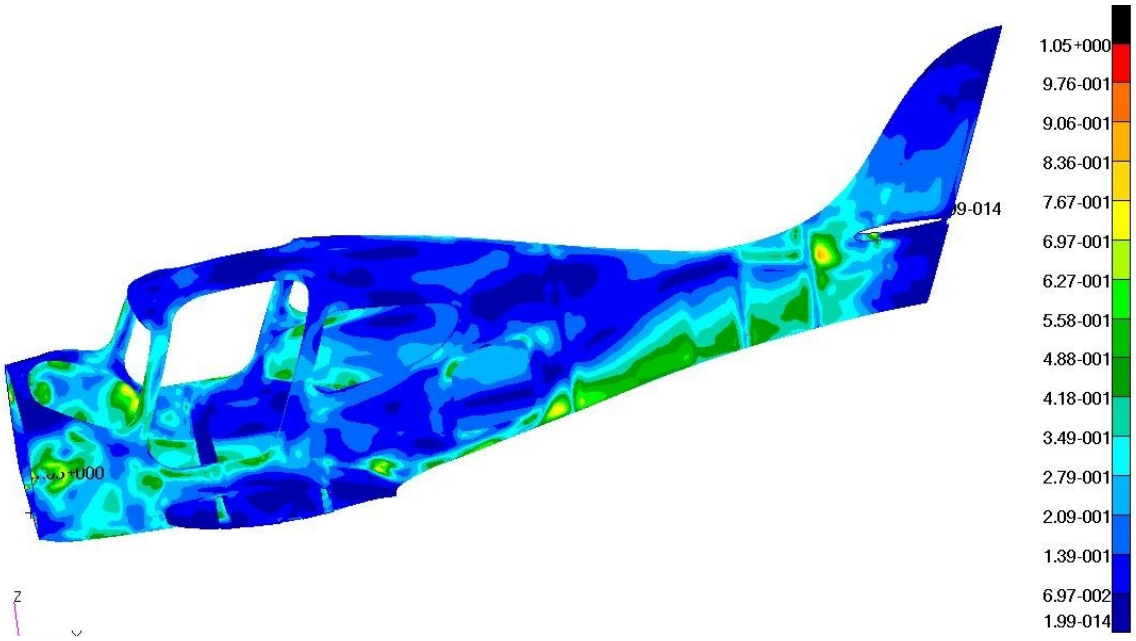

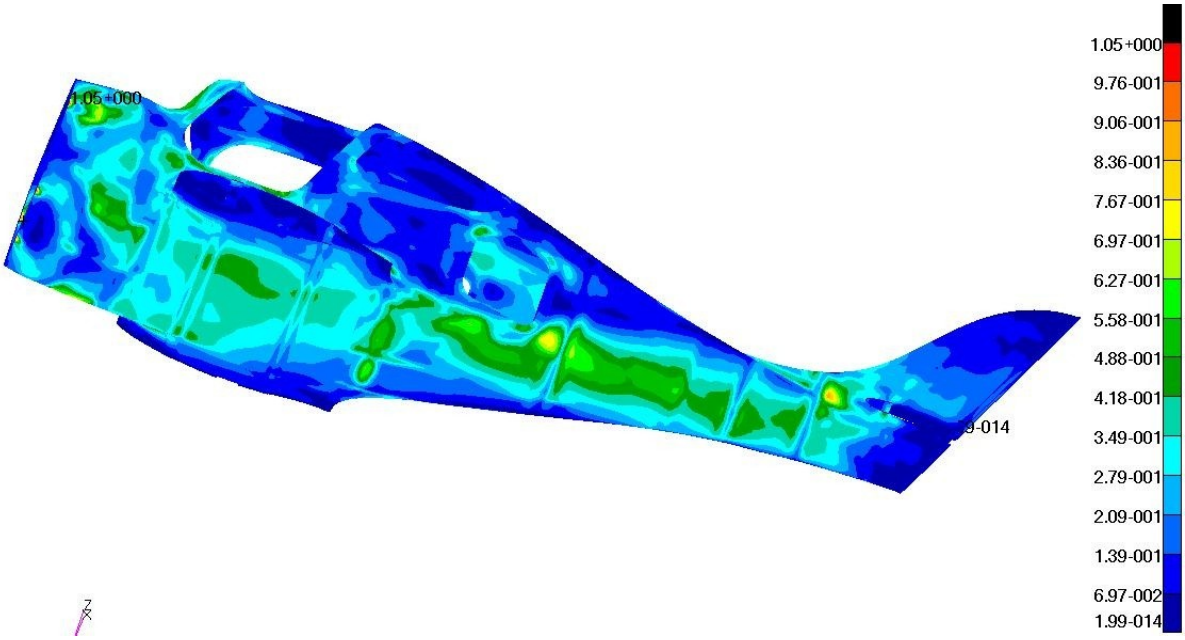
1.05+000
9.76-001
9.06-001
8.36-001
7.67-001
6.97-001
6.27-001
5.58-001
4.88-001
4.18-001
3.49-001
2.79-001
2.09-001
1.39-001
6.97-002
1.99-014

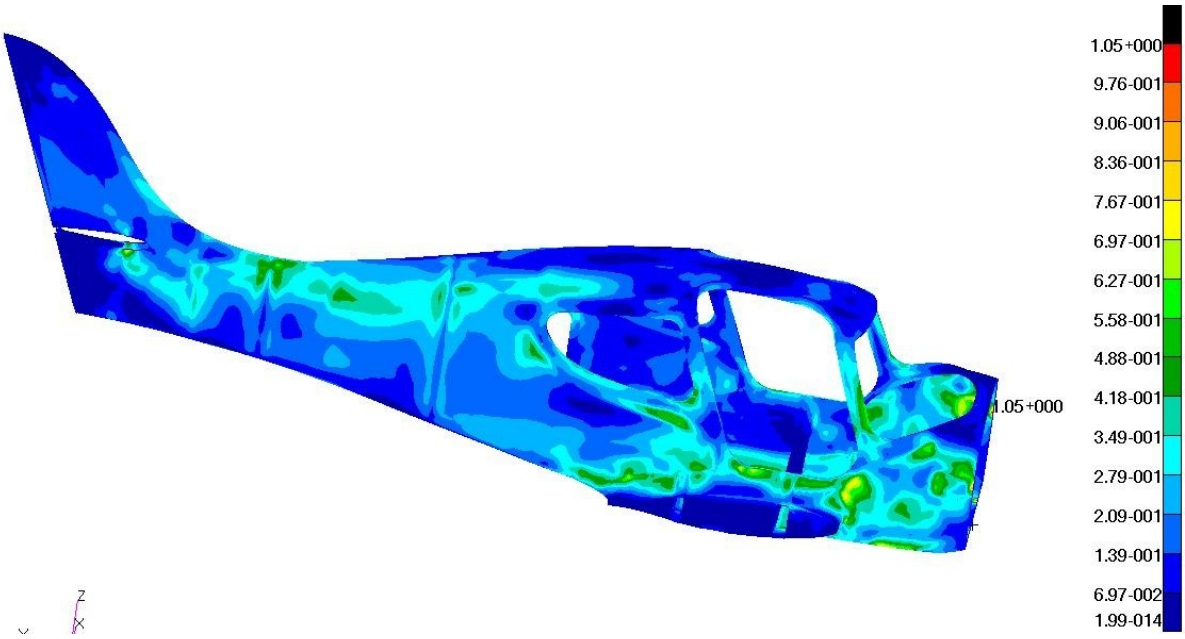
1.05+000
9.76-001
9.06-001
8.36-001
7.67-001
6.97-001
6.27-001
5.58-001
4.88-001
4.18-001
3.49-001
2.79-001
2.09-001
1.39-001
6.97-002
1.99-014

B5 – Vertical tail manoeuvre force and horizontal tail trim force

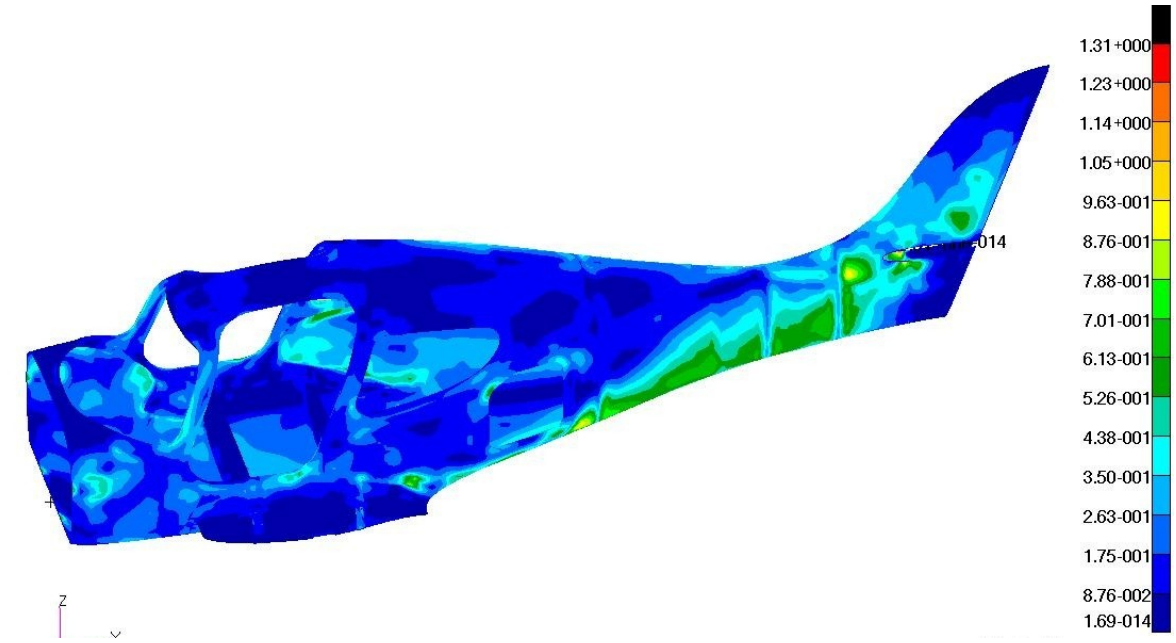

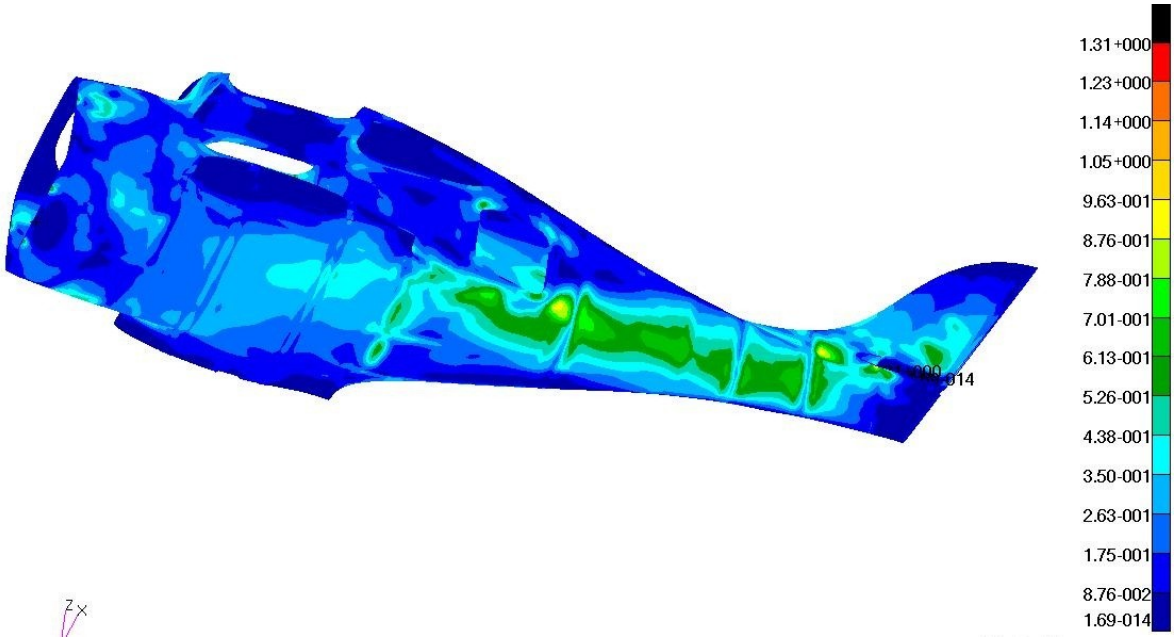

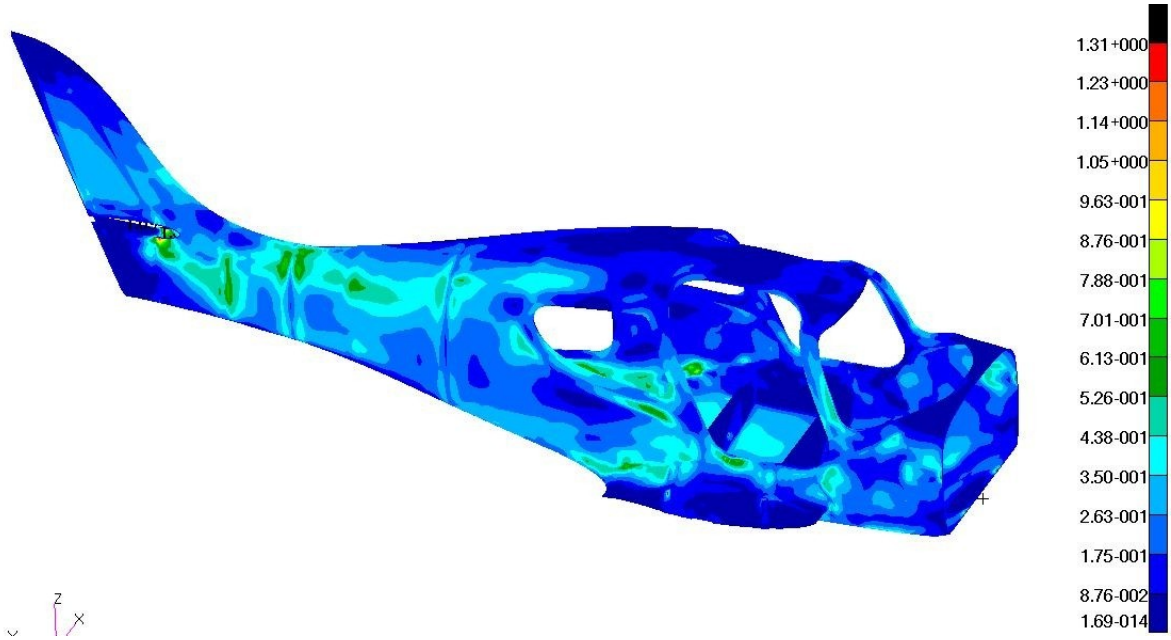
1.31+000
1.23+000
1.14+000
1.05+000
9.63-001
8.76-001
7.88-001
7.01-001
6.13-001
5.26-001
4.38-001
3.50-001
2.63-001
1.75-001
8.76-002
1.69-014
Z
X

Appendix C – Sandwich elements failure indices

Horizontal tail max down force

Subcase ID: 1

Processed elements count: 14660

Failed elements count: 0

Element ID	Layer	Failure type	Value
39866	1001	core-shear	0.957
29713	1070	MS-N1	0.946
31026	1002	TW	0.943
29714	1070	MS-N1	0.940
39885	1001	core-shear	0.937
12389	1095	MS-N1	0.932
29712	1070	MS-N1	0.931
12373	1001	core-shear	0.926
12371	1095	MS-N2	0.926
12368	1095	TW	0.921
29711	1070	MS-N1	0.920
39862	1001	core-shear	0.909
29710	1070	MS-N1	0.896
12372	1095	MS-N1	0.894
39884	1001	core-shear	0.892
39883	1001	core-shear	0.891
39864	1001	core-shear	0.891
29715	1070	MS-N1	0.891
31511	1003	TW	0.883

Horizontal tail max up force

Subcase ID: 2

Processed elements count: 14660

Failed elements count: 0

Element ID	Layer	Failure type	Value
31407	1003	TW	0.943
31512	1003	TW	0.842
31101	1003	TW	0.813
31511	1003	TH	0.783
31406	1003	TH	0.780
30820	1003	TW	0.768
31405	1003	TW	0.762
31513	1003	TW	0.750
31705	1003	TH	0.737
30819	1003	TW	0.722
31493	1003	TW	0.686
31482	1003	TW	0.676
12389	1095	MS-N1	0.667
12372	1095	MS-N1	0.665
12373	1001	core-shear	0.659
30827	1003	TW	0.652
31403	1003	TW	0.641
12371	1001	core-shear	0.638
12914	1095	MS-N2	0.624

Horizontal tail unsymmetrical

Subcase ID: 3

Processed elements count: 14660

Failed elements count: 0

Element ID	Layer	Failure type	Value
31026	1002	TH	0.932
12389	1095	MS-N1	0.930
39866	1001	core-shear	0.928
12373	1001	core-shear	0.926
12371	1095	MS-N2	0.921
12368	1095	TW	0.910
39885	1001	core-shear	0.904
31511	1003	TW	0.896
12372	1095	MS-N1	0.895
31493	1003	TW	0.886
39862	1001	core-shear	0.879
30819	1003	TH	0.870
31615	1003	TW	0.870
31101	1003	TW	0.868
31482	1003	TW	0.862
39864	1001	core-shear	0.860
39884	1001	core-shear	0.859
39883	1001	core-shear	0.858
12388	1095	MS-N2	0.851

Vertical tail gust and horizontal tail trim

Subcase ID: 4

Processed elements count: 14660

Failed elements count: 1

Element ID	Layer	Failure type	Value
6339	1095	TW	1.017
31026	1002	TH	0.943
39866	1001	core-shear	0.932
31511	1003	TW	0.924
12389	1095	MS-N1	0.924
31493	1003	TW	0.920
12373	1001	core-shear	0.919
12371	1095	MS-N2	0.915
39885	1001	core-shear	0.905
6429	1095	TW	0.901
12368	1095	TW	0.898
31101	1003	TW	0.896
6340	1095	MS-N1	0.896
30819	1003	TW	0.895
31482	1003	TW	0.894
31615	1003	TW	0.893
12372	1095	MS-N1	0.890
39862	1001	core-shear	0.880
31407	1003	TW	0.876

Vertical tail manoeuvre and horizontal tail trim

Subcase ID: 5

Processed elements count: 14660

Failed elements count: 8

Element ID	Layer	Failure type	Value
6339	1095	TW	1.280
6429	1095	TW	1.089
4844	1003	TW	1.069
5928	1003	TW	1.034
4842	1003	TW	1.031
4934	1003	TW	1.010
4932	1003	TW	1.008
4843	1003	TW	1.004
6340	1095	MS-N1	0.979
4933	1003	TW	0.979
12119	1003	TW	0.970
24524	1040	ILSS	0.967
5020	1003	TW	0.958
4845	1003	TW	0.946
6048	1003	TW	0.938
32606	1040	ILSS	0.932
4935	1003	TW	0.926
24766	1003	TW	0.925
10484	1003	TW	0.924

Appendix D – Failed elements detail analysis

Subcase: 5

Load step:

Element ID: 4842

Stress Table :

Layer	Material	Thickness	Orientation	σ_{11}	σ_{22}	τ_{12}	τ_{xz}	τ_{yz}
1001	glass	0.1200	52.438	-40.5	28.7	-2.34	0.08	0.14
1002	carbon	0.3200	6.784	-0.9	-29.1	-7.08	0.09	0.15
1003	carbon	0.2601	52.438	-101.4	68.7	-1.09	0.11	0.20
1055	carbon	0.3200	-84.136	-28.7	2.7	6.84	0.04	0.08
1090	herex	8.0013	52.508	-0.3	0.1	-0.03	0.13	0.22
1094	carbon	0.3200	-84.136	-26.4	3.4	6.70	-0.00	-0.00
1095	carbon	0.2600	6.784	-21.5	-87.4	-10.96	0.12	0.21

Sandwich Summary

Sandwich Type: isotropic

Minimal core Thickness : 3.0

Core Shear Strength correction factor : 1.0

Wrinkling correction factor K1 : 0.63

Sandwich Failures :

Sandwich Failure	FI
Core Crushing	0.000
Core Crimpling	0.255
Core Shear Strength	0.210
Wrinkling Top side	0.246
Wrinkling Bottom side	0.115

Subcase: 5

Load step:

Element ID: 4842

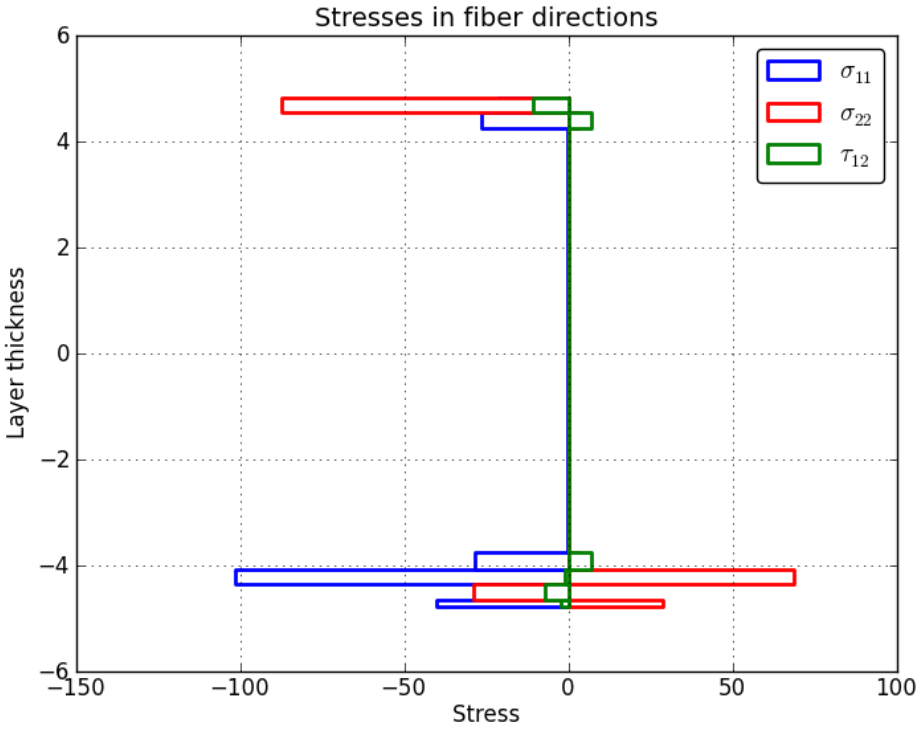
Stresses in fiber directions
Layer thickness
Stress
σ_{11}
σ_{22}
τ_{12}
6
4
2
0
−2
−4
−6
−150
−100
−50
0
50
100

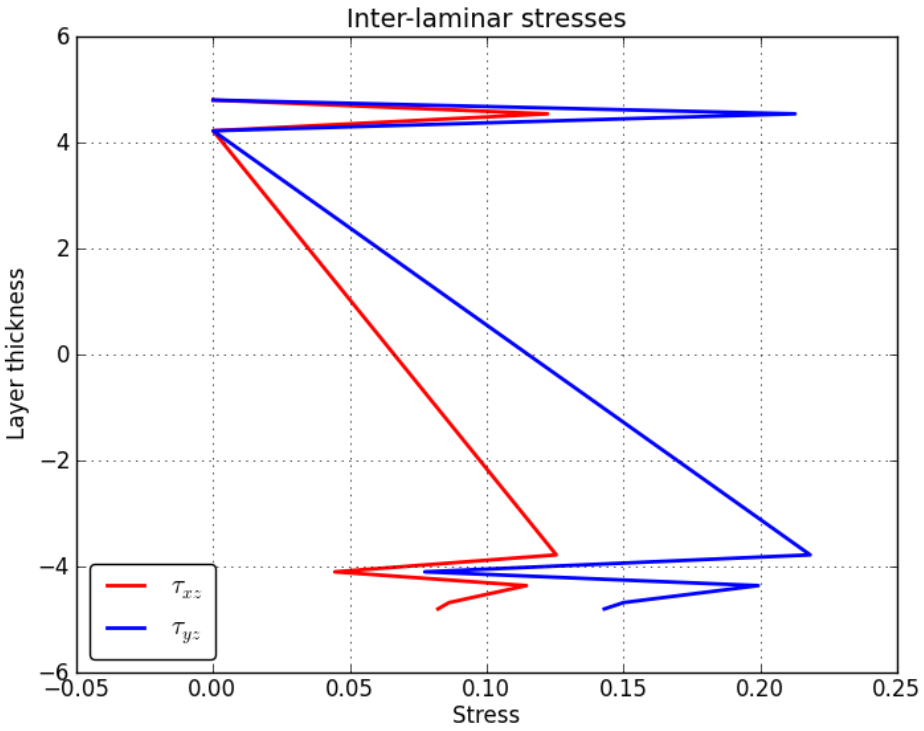
Inter-laminar stresses
Layer thickness
Stress
τ_{xz}
τ_{yz}
6
4
2
0
−2
−4
−6
−0.05
0.00
0.05
0.10
0.15
0.20
0.25

Subcase: 5

Load step:

Element ID: 4843

Stress Table :

Layer	Material	Thickness	Orientation	σ_{11}	σ_{22}	τ_{12}	τ_{xz}	τ_{yz}
1001	glass	0.1200	52.438	-41.3	27.0	-3.74	0.07	0.14
1002	carbon	0.3200	6.784	2.9	-39.0	-6.97	0.07	0.15
1003	carbon	0.2601	52.438	-103.1	64.2	-1.67	0.10	0.20
1055	carbon	0.3200	-84.136	-38.6	6.8	6.73	0.04	0.08
1090	herex	8.0013	52.508	-0.3	0.1	-0.04	0.11	0.22
1094	carbon	0.3200	-84.136	-36.5	7.7	6.61	-0.00	-0.00
1095	carbon	0.2600	6.784	-22.6	-95.9	-10.37	0.11	0.22

Sandwich Summary

Sandwich Type: isotropic

Minimal core Thickness : 3.0

Core Shear Strength correction factor : 1.0

Wrinkling correction factor K1 : 0.63

Sandwich Failures :

Sandwich Failure	FI
Core Crushing	0.000
Core Crimpling	0.309
Core Shear Strength	0.205
Wrinkling Top side	0.273
Wrinkling Bottom side	0.130

Subcase: 5

Load step:

Element ID: 4843

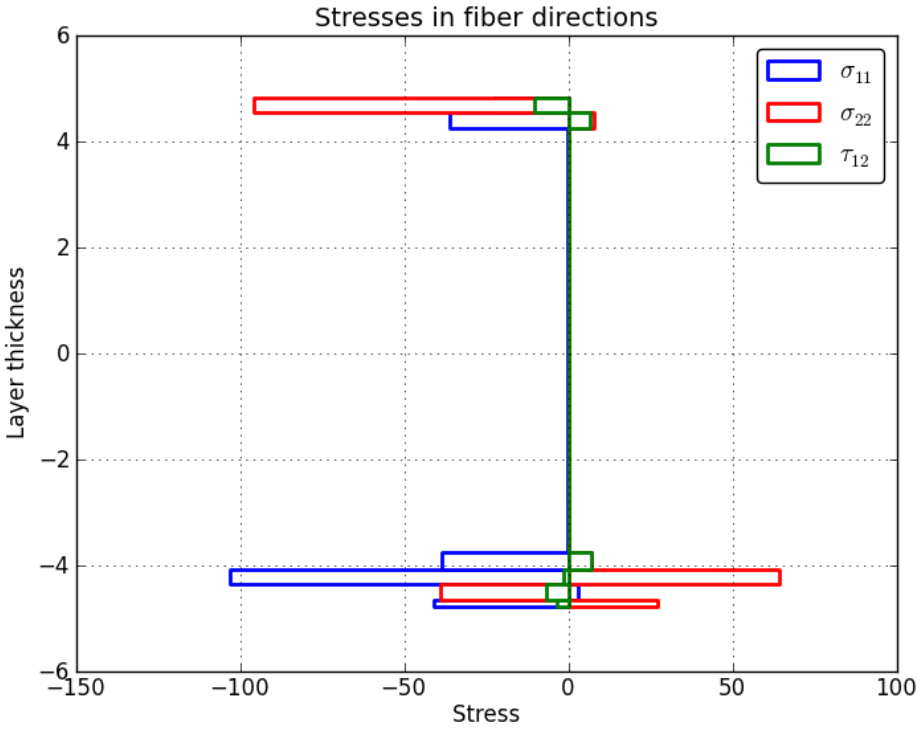
Stresses in fiber directions
Layer thickness
Stress
σ_{11}
σ_{22}
τ_{12}
6
4
2
0
−2
−4
−6
−150
−100
−50
0
50
100

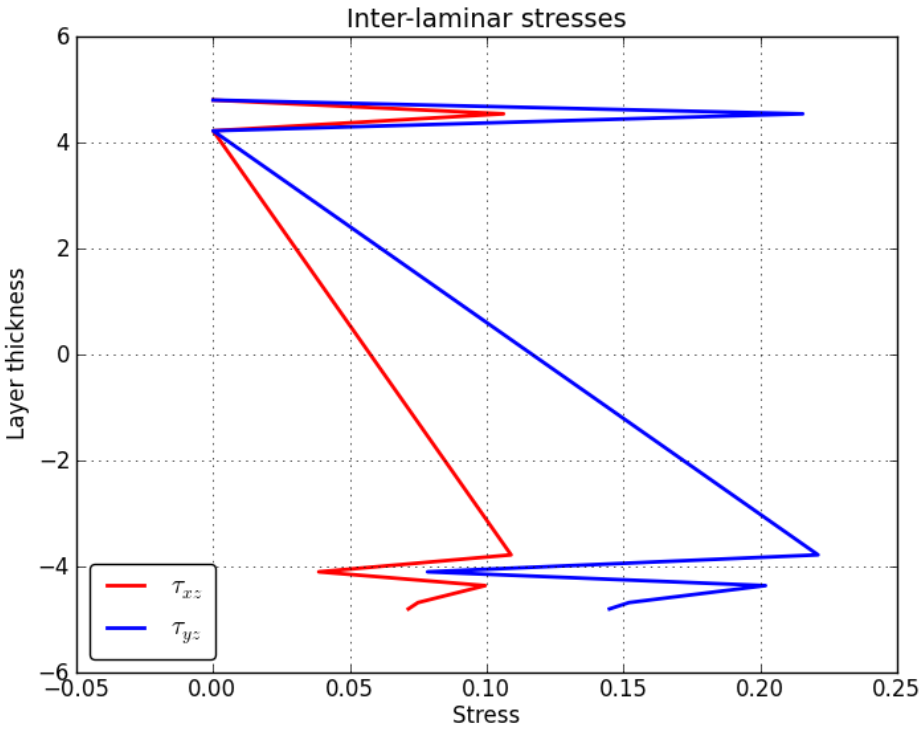
Inter-laminar stresses
Layer thickness
Stress
τ_{xz}
τ_{yz}
6
4
2
0
−2
−4
−6
−0.05
0.00
0.05
0.10
0.15
0.20
0.25

Subcase: 5

Load step:

Element ID: 4844

Stress Table :

Layer	Material	Thickness	Orientation	σ_{11}	σ_{22}	τ_{12}	τ_{xz}	τ_{yz}
1001	glass	0.1201	64.214	-41.1	29.7	-1.72	0.05	0.14
1002	carbon	0.3200	18.531	-3.4	-25.5	-7.24	0.05	0.15
1003	carbon	0.2603	64.214	-102.2	71.1	-0.82	0.06	0.19
1055	carbon	0.3201	-72.083	-24.6	-0.8	7.04	0.02	0.07
1090	herex	8.0040	64.129	-0.2	0.1	-0.03	0.07	0.22
1094	carbon	0.3201	-72.083	-22.7	-0.2	6.91	0.00	0.00
1095	carbon	0.2600	18.531	-19.5	-76.1	-10.69	0.07	0.21

Sandwich Summary

Sandwich Type: isotropic

Minimal core Thickness : 3.0

Core Shear Strength correction factor : 1.0

Wrinkling correction factor K1 : 0.63

Sandwich Failures :

Sandwich Failure	FI
Core Crushing	0.001
Core Crimpling	0.275
Core Shear Strength	0.192
Wrinkling Top side	0.143
Wrinkling Bottom side	0.122

Subcase: 5

Load step:

Element ID: 4844

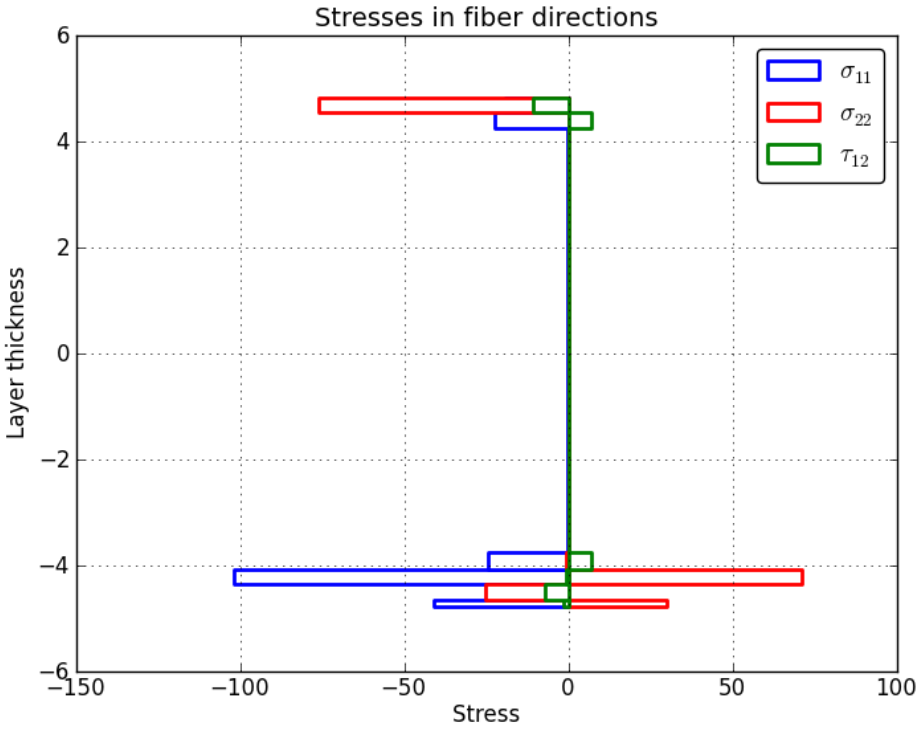
Stresses in fiber directions
Layer thickness
Stress
σ_{11}
σ_{22}
τ_{12}
6
4
2
0
−2
−4
−6
−150
−100
−50
0
50
100

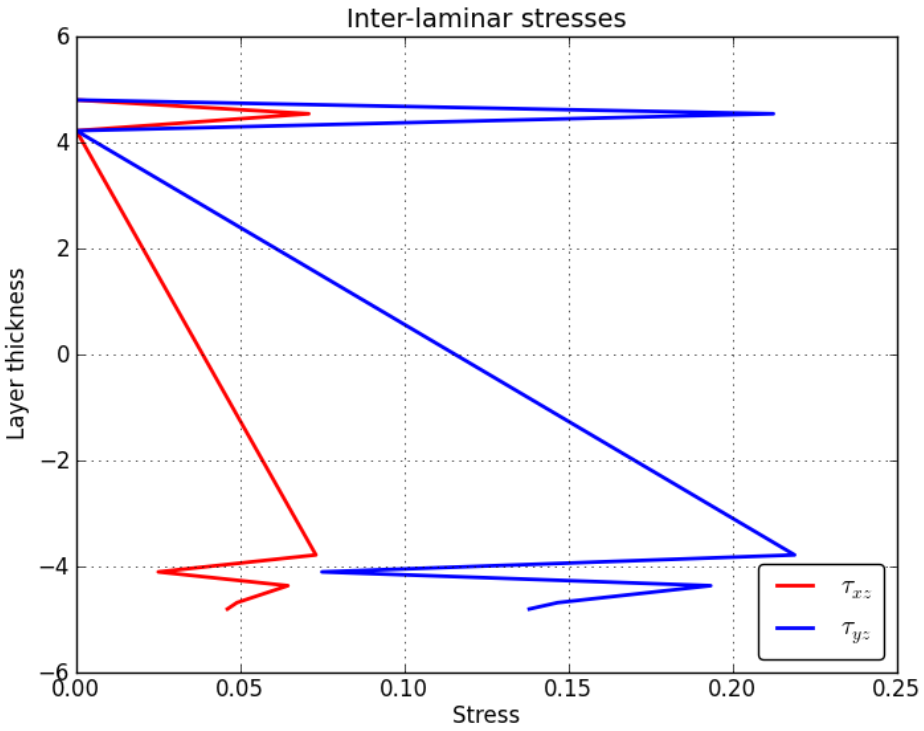
Inter-laminar stresses
Layer thickness
Stress
τ_{xz}
τ_{yz}
6
4
2
0
−2
−4
−6
0.00
0.05
0.10
0.15
0.20
0.25

Subcase: 5

Load step:

Element ID: 4932

Stress Table :

Layer	Material	Thickness	Orientation	σ_{11}	σ_{22}	τ_{12}	τ_{xz}	τ_{yz}
1001	glass	0.1200	52.438	-42.3	27.0	-2.49	0.05	0.08
1002	carbon	0.3200	6.784	-3.9	-33.3	-7.04	0.05	0.09
1003	carbon	0.2601	52.438	-103.0	64.8	-1.14	0.06	0.11
1055	carbon	0.3200	-84.136	-34.3	-1.2	6.89	0.02	0.04
1090	herex	8.0013	52.508	-0.2	0.1	-0.03	0.07	0.12
1094	carbon	0.3200	-84.136	-33.1	-1.3	6.82	-0.00	-0.00
1095	carbon	0.2600	6.784	-4.0	-64.5	-9.14	0.07	0.12

Sandwich Summary

Sandwich Type: isotropic

Minimal core Thickness : 3.0

Core Shear Strength correction factor : 1.0

Wrinkling correction factor K1 : 0.63

Sandwich Failures :

Sandwich Failure	FI
Core Crushing	0.000
Core Crimpling	0.258
Core Shear Strength	0.119
Wrinkling Top side	0.197
Wrinkling Bottom side	0.135

Subcase: 5

Load step:

Element ID: 4932

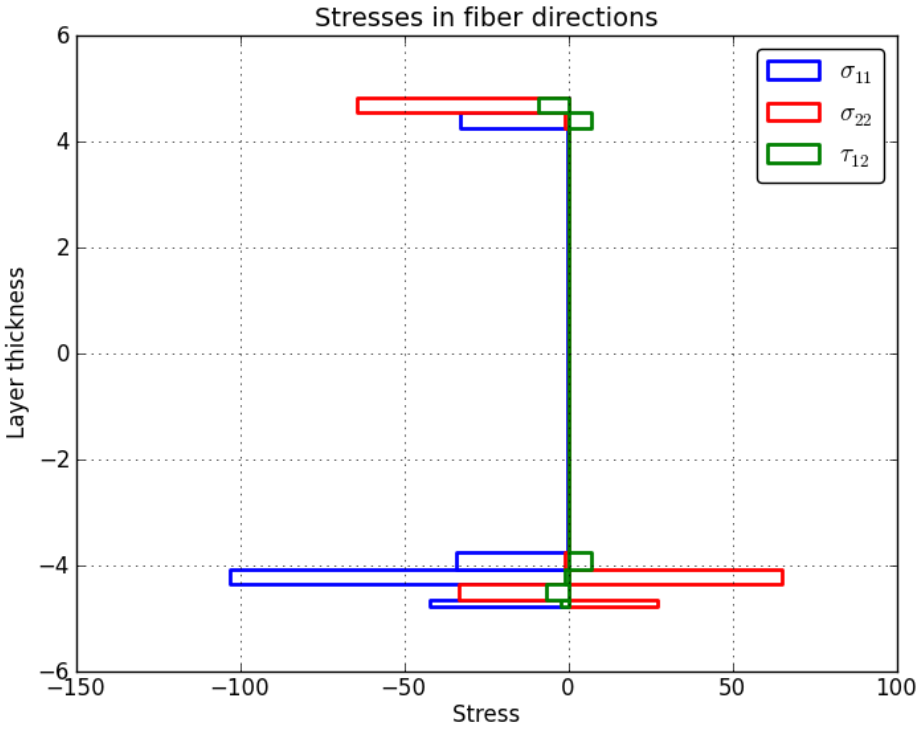
Stresses in fiber directions
Layer thickness
Stress
σ_{11}
σ_{22}
τ_{12}
6
4
2
0
−2
−4
−6
−150
−100
−50
0
50
100

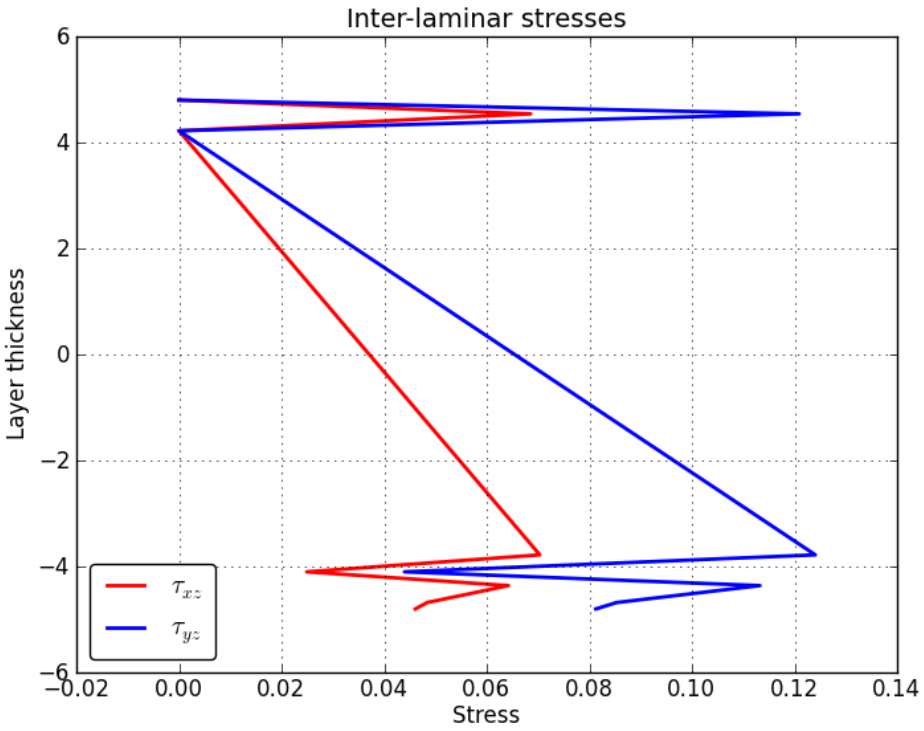
Inter-laminar stresses
Layer thickness
Stress
τ_{xz}
τ_{yz}
6
4
2
0
−2
−4
−6
−0.02
0.00
0.02
0.04
0.06
0.08
0.10
0.12
0.14

Subcase: 5

Load step:

Element ID: 4934

Stress Table :

Layer	Material	Thickness	Orientation	σ_{11}	σ_{22}	τ_{12}	τ_{xz}	τ_{yz}
1001	glass	0.1201	64.214	-42.4	27.4	-1.78	0.01	0.07
1002	carbon	0.3200	18.531	-7.0	-29.6	-7.08	0.01	0.08
1003	carbon	0.2603	64.214	-102.8	65.3	-0.83	0.02	0.10
1055	carbon	0.3201	-72.083	-29.8	-5.3	6.99	0.01	0.04
1090	herex	8.0040	64.129	-0.2	0.1	-0.03	0.02	0.12
1094	carbon	0.3201	-72.083	-28.7	-5.3	6.93	0.00	0.00
1095	carbon	0.2600	18.531	-6.1	-59.0	-8.53	0.02	0.11

Sandwich Summary

Sandwich Type: isotropic

Minimal core Thickness : 3.0

Core Shear Strength correction factor : 1.0

Wrinkling correction factor K1 : 0.63

Sandwich Failures :

Sandwich Failure	FI
Core Crushing	0.001
Core Crimpling	0.279
Core Shear Strength	0.099
Wrinkling Top side	0.123
Wrinkling Bottom side	0.135

Subcase: 5

Load step:

Element ID: 4934

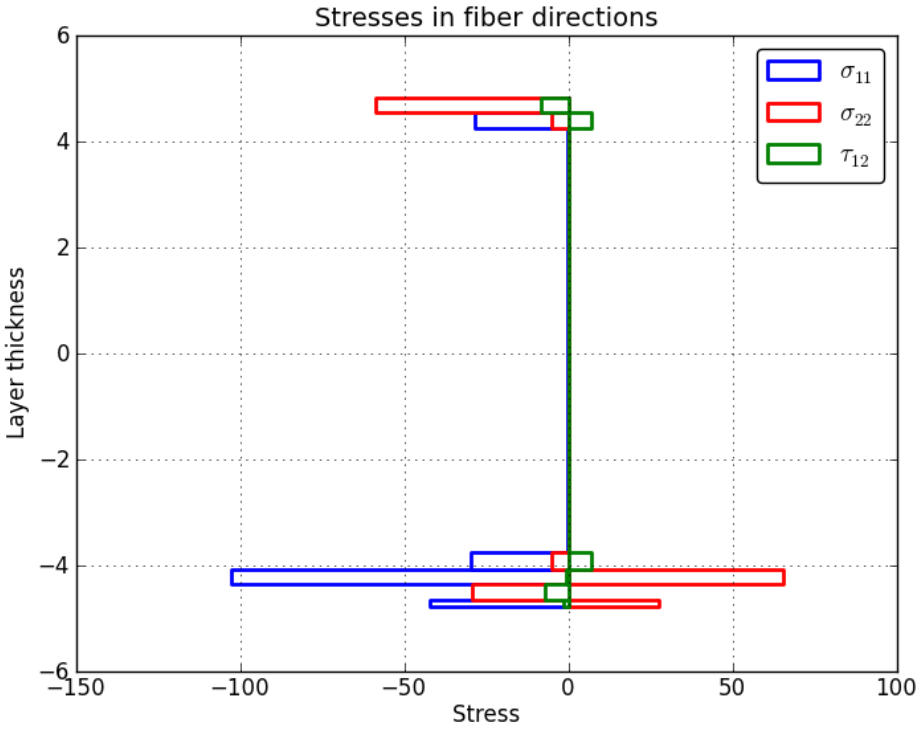
Stresses in fiber directions
Layer thickness
Stress
σ_{11}
σ_{22}
τ_{12}
6
4
2
0
−2
−4
−6
−150
−100
−50
0
50
100

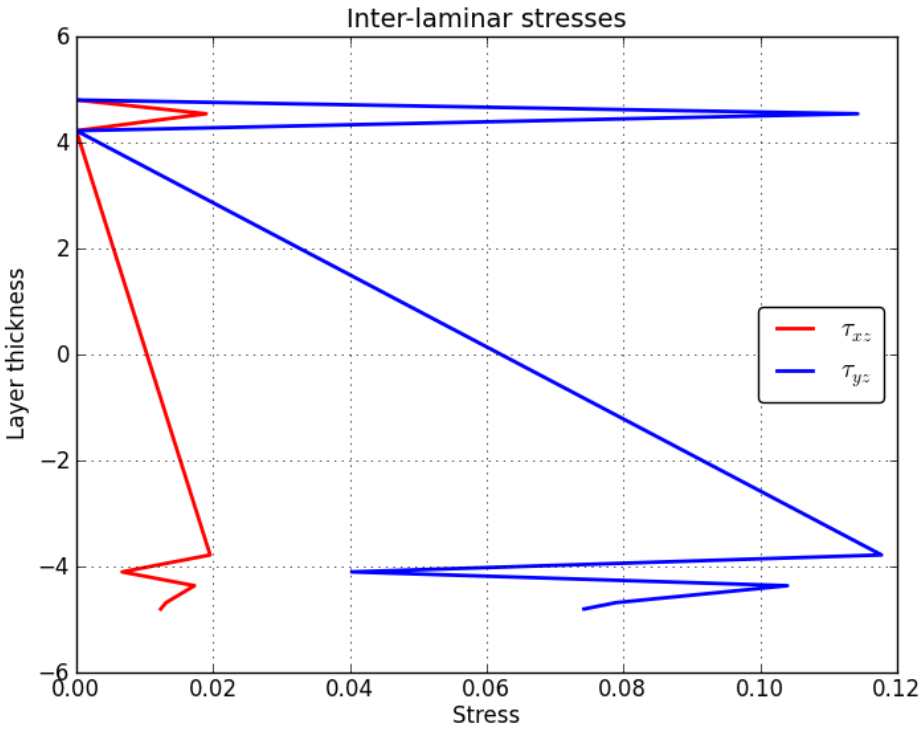
Inter-laminar stresses
Layer thickness
Stress
τ_{xz}
τ_{yz}
6
4
2
0
−2
−4
−6
0.00
0.02
0.04
0.06
0.08
0.10
0.12

Subcase: 5

Load step:

Element ID: 5928

Stress Table :

Layer	Material	Thickness	Orientation	σ_{11}	σ_{22}	τ_{12}	τ_{xz}	τ_{yz}
1001	glass	0.1200	55.119	-42.5	27.8	-0.77	-0.03	-0.25
1002	carbon	0.3215	4.828	0.4	-37.3	-6.99	-0.03	-0.25
1003	carbon	0.2601	55.119	-104.8	65.1	-0.25	-0.03	-0.24
1055	carbon	0.3215	-80.745	-23.0	-9.6	7.05	-0.03	-0.24
1060	carbon	0.3200	-79.850	-19.5	-10.0	7.00	-0.03	-0.22
1061	carbon	0.3200	-79.850	-18.5	-7.9	6.93	-0.03	-0.20
1062	carbon	0.3200	-79.850	-17.5	-5.7	6.85	-0.02	-0.16
1064	carbon	0.3200	-79.850	-16.5	-3.6	6.78	-0.02	-0.12
1065	carbon	0.3200	-79.850	-15.5	-1.5	6.71	-0.01	-0.06
1091	herex	8.0002	55.192	-0.2	0.1	0.01	-0.03	-0.23
1094	carbon	0.3215	-80.745	-17.0	3.1	6.62	0.00	0.00
1095	carbon	0.2612	4.828	-52.3	-68.0	-9.09	-0.03	-0.22

Sandwich Summary

Sandwich Type: isotropic

Minimal core Thickness : 3.0

Core Shear Strength correction factor : 1.0

Wrinkling correction factor K1 : 0.63

Sandwich Failures :

Sandwich Failure	FI
Core Crushing	0.001
Core Crimpling	0.418
Core Shear Strength	0.194
Wrinkling Top side	0.233
Wrinkling Bottom side	0.113

Subcase: 5

Load step:

Element ID: 5928

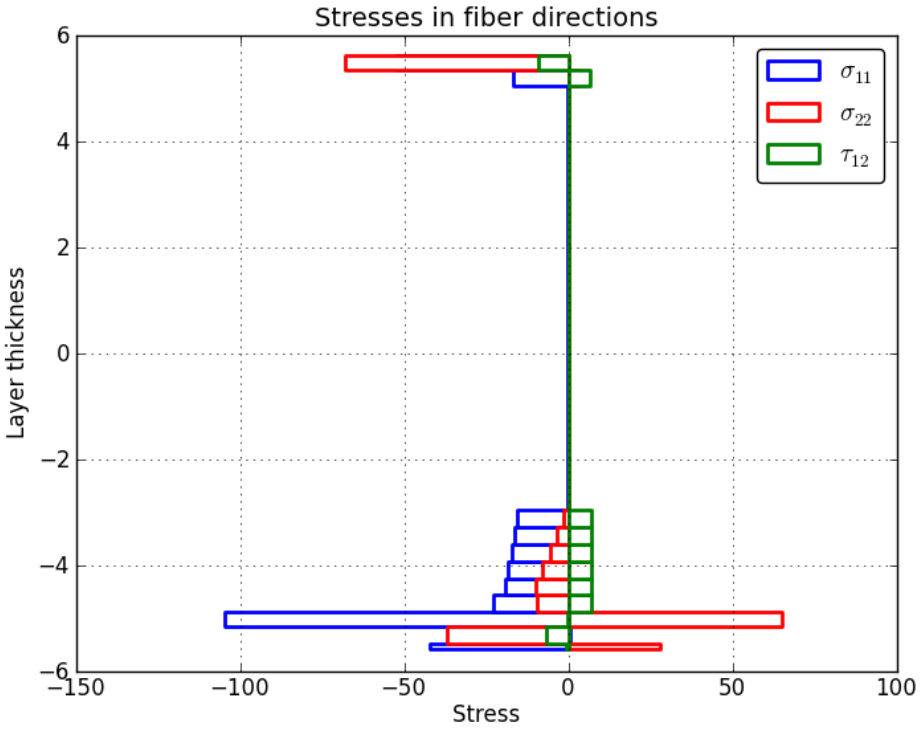
Stresses in fiber directions
Layer thickness
Stress
σ_{11}
σ_{22}
τ_{12}
6
4
2
0
−2
−4
−6
−150
−100
−50
0
50
100

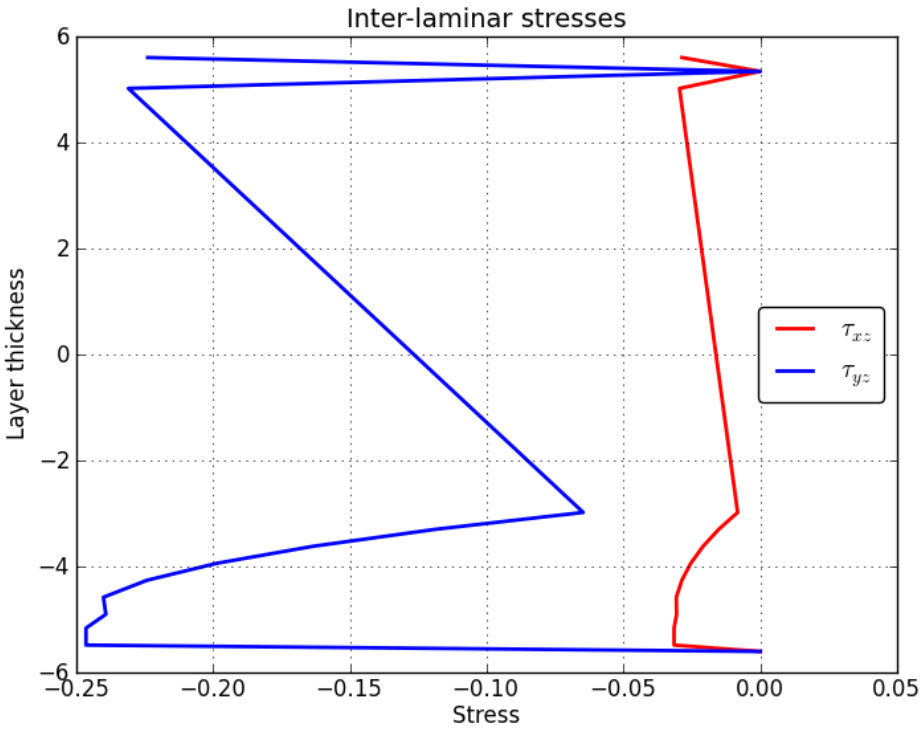
Inter-laminar stresses
Layer thickness
Stress
τ_{xz}
τ_{yz}
6
4
2
0
−2
−4
−6
−0.25
−0.20
−0.15
−0.10
−0.05
0.00
0.05

Subcase: 5

Load step:

Element ID: 6339

Stress Table :

Layer	Material	Thickness	Orientation	σ_{11}	σ_{22}	τ_{12}	τ_{xz}	τ_{yz}
1001	glass	0.1202	-86.244	0.7	-5.0	-5.64	-0.05	-0.29
1002	carbon	0.3210	43.048	24.1	-31.6	0.94	-0.05	-0.29
1003	carbon	0.2605	-86.244	1.5	-5.6	-2.66	-0.05	-0.30
1052	carbon	0.3207	-84.983	-0.0	-0.6	-2.80	-0.05	-0.29
1053	carbon	0.3207	-84.983	-0.2	3.3	-2.95	-0.04	-0.26
1055	carbon	0.3209	-43.500	-32.6	19.9	-0.87	-0.05	-0.28
1060	carbon	0.3200	-41.611	-33.3	16.8	-0.89	-0.04	-0.25
1061	carbon	0.3200	-41.611	-33.3	13.1	-1.05	-0.04	-0.22
1062	carbon	0.3200	-41.611	-33.3	9.4	-1.22	-0.03	-0.18
1064	carbon	0.3200	-41.611	-33.3	5.6	-1.39	-0.02	-0.13
1065	carbon	0.3200	-41.611	-33.3	1.9	-1.55	-0.01	-0.07
1092	herex	8.0000	-86.550	0.0	0.1	-0.09	-0.04	-0.22
1094	carbon	0.3209	-43.500	-32.0	-3.2	-1.81	0.00	0.00
1095	carbon	0.2608	43.048	140.9	-40.6	-2.93	-0.03	-0.21

Sandwich Summary

Sandwich Type: isotropic

Minimal core Thickness : 3.0

Core Shear Strength correction factor : 1.0

Wrinkling correction factor K1 : 0.63

Sandwich Failures :

Sandwich Failure	FI
Core Crushing	0.001
Core Crimpling	0.155
Core Shear Strength	0.187
Wrinkling Top side	0.132
Wrinkling Bottom side	0.095

Subcase: 5

Load step:

Element ID: 6339

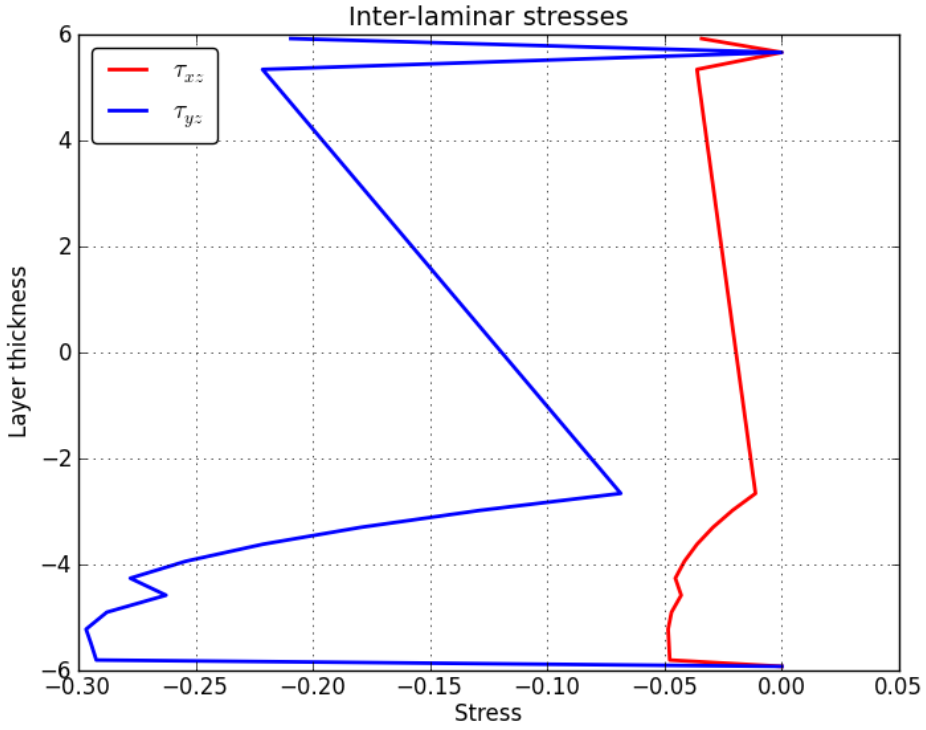

Subcase: 5

Load step:

Element ID: 6429

Stress Table :

Layer	Material	Thickness	Orientation	σ_{11}	σ_{22}	τ_{12}	τ_{xz}	τ_{yz}
1001	glass	0.1202	-86.244	-0.3	0.2	-5.36	0.04	-0.34
1002	carbon	0.3210	43.048	28.7	-26.9	0.41	0.04	-0.34
1003	carbon	0.2605	-86.244	1.2	3.4	-2.55	0.04	-0.34
1052	carbon	0.3207	-84.983	0.9	6.5	-2.69	0.04	-0.33
1053	carbon	0.3207	-84.983	2.1	8.5	-2.85	0.03	-0.30
1055	carbon	0.3209	-43.500	-26.8	24.2	-0.14	0.04	-0.32
1060	carbon	0.3200	-41.611	-26.5	20.7	-0.02	0.03	-0.29
1061	carbon	0.3200	-41.611	-26.1	17.2	-0.04	0.03	-0.26
1062	carbon	0.3200	-41.611	-25.8	13.7	-0.07	0.02	-0.21
1064	carbon	0.3200	-41.611	-25.4	10.2	-0.09	0.02	-0.15
1065	carbon	0.3200	-41.611	-25.0	6.7	-0.11	0.01	-0.08
1092	herex	8.0000	-86.550	0.0	0.1	-0.09	0.03	-0.26
1094	carbon	0.3209	-43.500	-24.5	3.1	-0.22	-0.00	0.00
1095	carbon	0.2608	43.048	129.8	-37.9	0.61	0.03	-0.24

Sandwich Summary

Sandwich Type: isotropic

Minimal core Thickness : 3.0

Core Shear Strength correction factor : 1.0

Wrinkling correction factor K1 : 0.63

Sandwich Failures :

Sandwich Failure	FI
Core Crushing	0.000
Core Crimpling	0.019
Core Shear Strength	0.215
Wrinkling Top side	0.101
Wrinkling Bottom side	0.073

Subcase: 5

Load step:

Element ID: 6429